Gearbox Reliability Collaborative Phase 3 Gearbox 2 Test Plan

H. Link, J. Keller, and Y. Guo
National Renewable Energy Laboratory

B. McNiff
McNiff Light Industry

NREL is a national laboratory of the U.S. Department of Energy, Office of Energy Efficiency & Renewable Energy, operated by the Alliance for Sustainable Energy, LLC.

Technical Report
NREL/TP-5000-58190
April 2013

Contract No. DE-AC36-08GO28308

NREL
NATIONAL RENEWABLE ENERGY LABORATORY

Gearbox Reliability Collaborative Phase 3 Gearbox 2 Test Plan

H. Link, J. Keller, and Y. Guo
National Renewable Energy Laboratory

B. McNiff
McNiff Light Industry

Prepared under Task No. WE11.0301

National Renewable Energy Laboratory
15013 Denver West Parkway
Golden, Colorado 80401
303-275-3000 • www.nrel.gov

Technical Report
NREL/TP-5000-58190
April 2013

Contract No. DE-AC36-08GO28308

NOTICE

Available electronically at http://www.osti.gov/bridge

Available for a processing fee to U.S. Department of Energy
and its contractors, in paper, from:

U.S. Department of Energy
Office of Scientific and Technical Information
P.O. Box 62
Oak Ridge, TN 37831-0062
phone: 865.576.8401
fax: 865.576.5728
email: mailto:reports@adonis.osti.gov

Available for sale to the public, in paper, from:

U.S. Department of Commerce
National Technical Information Service
5285 Port Royal Road
Springfield, VA 22161
phone: 800.553.6847
fax: 703.605.6900
email: orders@ntis.fedworld.gov
online ordering: http://www.ntis.gov/help/ordermethods.aspx

Cover Photos: (left to right) PIX 16416, PIX 17423, PIX 16560, PIX 17613, PIX 17436, PIX 17721

Printed on paper containing at least 50% wastepaper, including 10% post consumer waste.

Acknowledgments

This work was supported by the U.S. Department of Energy under Contract No. DE-AC36-08GO28308 with the National Renewable Energy Laboratory.

List of Acronyms

CM	condition monitoring
COE	cost of energy
CRB	cylindrical roller bearing
DAS	data acquisition system
DLC	design load case
DGBB	deep groove ball bearing
DOE	Department of Energy
EPO	emergency power off
FAST	Fatigue, Aerodynamics, Structures, and Turbulence
fcCRB	full complement cylindrical roller bearing
GB	gearbox
gpm	gallon per minute
GRC	Gearbox Reliability Collaborative
F_x	thrust
HS	high speed
HSS	high-speed shaft
HS-ST	high-speed stage
IEC	International Electrotechnical Commission
IS	intermediate speed
ISS	intermediate-speed shaft
IS-ST	intermediate-speed stage
kNm	kiloNewton-meter
LS	low speed
LSS	low-speed shaft
LS-ST	low-speed stage
LVDT	linear variable displacement transformer
M_{yy}	pitch moment
M_{zz}	yaw moment
NI	National Instruments
NREL	National Renewable Energy Laboratory
NTL	non-torque loads
NWTC	National Wind Technology Center
PL	Planet
PLC	planet carrier
rpm	revolutions per minute
RTD	resistance temperature detector
SRB	spherical roller bearing
TDC	top dead center (spatial reference)
TRB	tapered roller bearing
VDC	volts direct current
VFD	variable frequency drive

Table of Contents

List of Figures

List of Tables

1 Introduction and Background

Gearboxes in wind turbines have not been achieving their expected design life; however, they commonly meet and exceed the design criteria specified in current standards in the gear, bearing, and wind turbine industry as well as third-party certification criteria. The failures are widespread across manufacturers and turbine sizes, and the majority of these failures are not due to manufacturing issues. One of the basic premises put forth by the National Renewable Energy Laboratory (NREL) Gearbox Reliability Collaborative (GRC) is that this gap between design-estimated and actual gearbox reliability results from the absence of critical elements in the design process or insufficient design tools.

Key goals of the GRC are to improve design approaches and analysis tools, and to recommend practices and test methods resulting in improved design standards for wind turbine gearboxes that lower the cost of energy (COE) through improved reliability. The GRC uses a combined gearbox testing, modeling, and analysis approach, along with a database of information from gearbox failures collected from overhauls and investigation of gearbox condition monitoring (CM) techniques to improve wind turbine operations and maintenance practices.

Full-scale dynamometer testing builds an understanding of how selected loads and events translate into gear and bearing response, including reactions, load distributions, displacements, temperatures, stresses, and slip. Ideally, the knowledge gained from the GRC will result in any necessary improvements to gearbox design standards and associated modeling tools.

There are four main objectives of the GRC gearbox testing program. Testing to be conducted under this plan addresses some, but not all of these objectives.

1. Verify the gearbox operates within the basic design standards and assumptions, such as:
    - Load distribution and sharing for the gears and bearings
    - Structural deflections
    - Bearing race temperature gradients
    - Cooling capacity.
2. Assess the effect of real-world operating conditions on the as-built gearbox and potentially extend the current design standards and assumptions to consider these effects, such as:
    - Static and dynamic non-torque loading
    - High-speed shaft misalignment
    - Bearing rolling element skidding.
3. Validate key portions of drivetrain, gear, and bearing analysis tools, such as:
    - Dynamic response
    - Generator coupling stiffness
    - Bearing rolling element skidding.
4. Develop a standard dynamometer testing and acceptance process, including tests such as:
    - Non-torque loading
    - Dynamic (field representative) loading
    - Length of testing
    - Modal testing.

Testing in the GRC project has included eleven test series to date, including tests that have been grouped under the nomenclature of Phase 1 and Phase 2 tests [1]. This test plan describes the first of two test series under Phase 3. Phase 3 tests are currently planned in the National Wind Technology Center (NWTC) dynamometer as described below.

- **Phase 3a.** Test of gearbox 2 (GB2) using the two-speed turbine controller that has been used in prior testing. This test series will investigate non-torque loads, high-speed shaft misalignment, and reproduction of field conditions in the dynamometer. This test series also includes vibration testing using an eddy-current brake on the gearbox's high-speed shaft. This will permit operation at any generator speed between 100 rpm and 2,000 rpm at torque levels of about 5% of rated—sufficient to load bearings and gear mesh. Vibration testing enables the investigation of gearbox modal behavior and enhances the ability to duplicate high-frequency torque events observed in Phase 1 field testing.
- **Phase 3b.** Test of the newly designed gearbox 3 (GB3) in the NWTC dynamometer using the variable frequency drive. GB3 is a redesigned and rebuilt version of the GB1. It is expected to demonstrate a significantly better capability to withstand non-torque loads.

Other non-dynamometer tests also are planned for completion in 2013. Each of these tests is described in a separate test plan.

- **High-speed flexible coupling stiffness measurement.** The coupling is removed from the GRC drivetrain and installed in a test rig, which simulates radial (also known as parallel) misalignment conditions. A range of lateral forces is applied and the resulting deflections are measured, yielding a force-deflection curve that will most likely be non-linear. Determining the coupling stiffness enables a greater understanding of axial and bending loads induced in the high-speed shaft when the coupling is subjected to the radial misalignment. This information can be of direct use in simulating the radial misalignment tests described herein.
- **High-speed bearing stiffness measurement.** Both the cylindrical and tapered roller bearings used on the high-speed shaft are installed in a test rig, which determines the 5 x 5 stiffness matrix for each bearing. A range of radial forces is applied under different preload conditions and the resulting small deflections are measured, yielding a force-deflection curve. Once completed, the experimentally determined stiffness matrix is compared to theoretical predictions, likely resulting in a modification of GRC gearbox models.
- **Static modal test.** Accelerometers are attached to shafts inside the GRC gearbox and torsional vibration modes are excited with a hammer. Shafting is locked to prevent rotation and various torque settings are applied. This test is similar to a test previously conducted by Purdue University, but this test provides vibration data from internal components of the gearbox.
- **Lubrication flow check.** Delivery of lubrication oil to the gears and bearings has been predicted but not yet measured. This test uses several non-intrusive flow meters to measure flow through several of the branches of the lubrication system distribution tree. The flow meters are calibrated relative to a positive displacement flow meter currently used to measure total flow to the gearbox.

2 Test Article

2.1 Test Turbine

The GRC drivetrain originally was designed for a stall-controlled, three-bladed upwind turbine with a rated power of 750 kW. Figure 1 shows a field of these turbines at Xcel Energy's Ponnequin Wind Farm in northern Colorado. The turbine generates electricity at two rotor speeds, 14.7 rpm and 22.1 rpm. The gearbox ratio of 81.491 converts these mainshaft speeds to generator speeds of 1,200 rpm and 1,800 rpm.

The generator has two sets of windings that permit generation of 200 kW at 1,206 rpm and 750 kW at 1,809 rpm. The generator has 0.5% slip, which accounts for operation at speeds slightly greater than synchronous, 1,200 rpm and 1,800 rpm. Thus, online speed variation is limited to only 9 rpm when the high-speed windings are engaged. During startup, the generators are connected to the utility grid using custom soft-start electronics that soften torque spikes associated with electrical contactor closure. After the soft start establishes stable operation at synchronous speed, a bypass contact is engaged.

Figure 1. Ponnequin wind farm in northern Colorado (*NREL PIX/19258*)

The GRC turbine follows a conventional, modular configuration. In this configuration, all individual components of the drivetrain are mounted onto the bed plate or main frame. These components include the hub, main bearing, mainshaft, gearbox, brake, generator shaft, and generator as shown in Figure 2. Everything but the hub is included in the dynamometer tests.

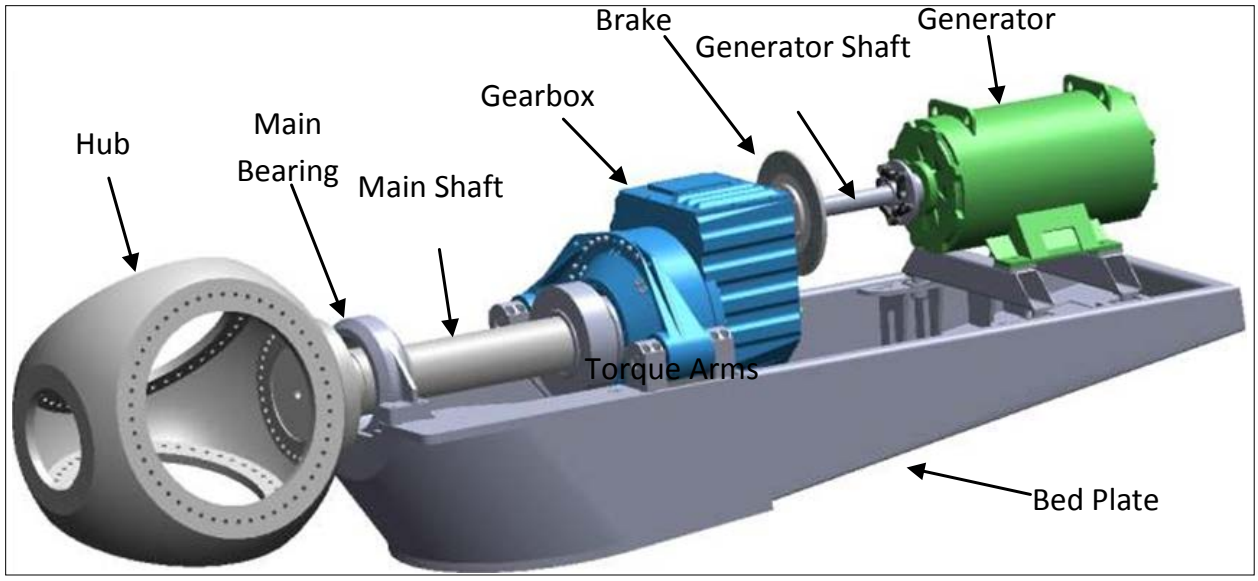

Figure 2. Gearbox Reliability Collaborative drivetrain configuration

The GRC lubrication system used in dynamometer testing consists of two circuits, the inline filter loop featuring an 8 gallon per minute (gpm) pump and two stage filters of 50 μm and 10 μm, the offline filter loop featuring a 0.65-gpm pump and a filter of 3 μm.

The GRC cooling system used in dynamometer testing features a custom glycol cooling and pumping unit. This unit provides a cool glycol/water mixture to the generator and to the lubrication system heat exchanger.

Several condition monitoring instruments will be employed in Phase 3 testing, including a Hydac CSM2000 particle counter that samples unfiltered oil from the gearbox sump. Other sensors include an inline filter loop wear debris sensor, and several offline filter loop wear debris and oil-condition sensors [2].

2.2 Test Drivetrain

2.2.1 External Gearbox Configuration

The configuration of the GRC gearbox follows the typical configuration of the megawatt-scale turbines used in the industry today. The gearbox is mounted with a three-point configuration in which torsional loads are transferred to the main frame through two torque arms, and non-torque moments and forces are reacted mostly at the main bearing. Each torque arm transfers loads by means of an elastomeric bearing supported by mounts that help isolate and reduce noise. Figure 3 shows the torque arm configuration and a cutaway view of the elastomeric mount [1].

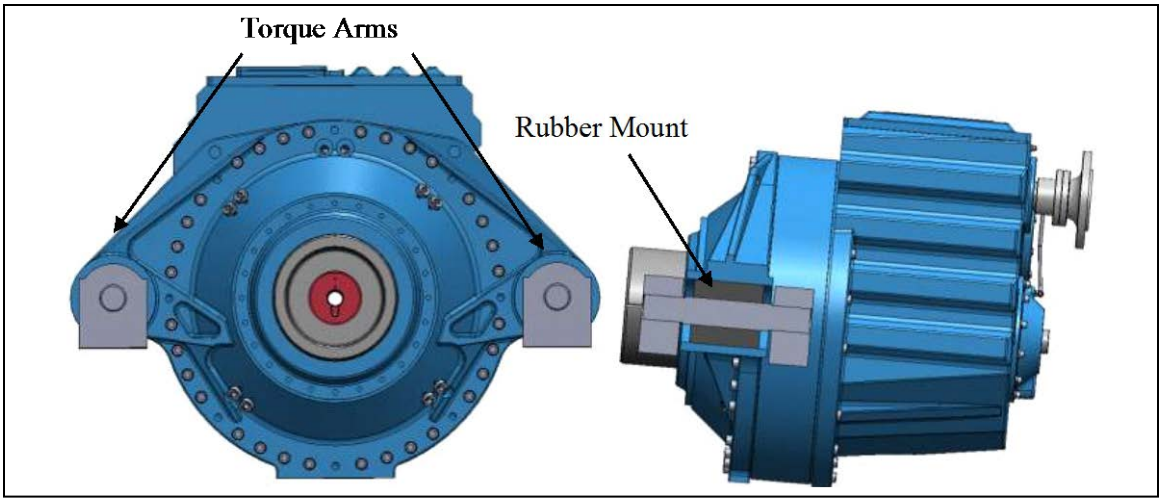

Figure 3. Torque arm and rubber mount detail

2.2.2 Internal Gearbox Configuration

The gearbox used in the GRC project has been modified from the original gearbox configuration used in the commercial versions of this wind turbine [1]. The gearbox has an overall ratio of 81.491. It is composed of one low-speed (LS) planetary stage and two parallel shaft stages. The planetary stage accommodates three planet gears. The annulus gear of this stage also serves as part of the gearbox housing. The sun gear is set in a floating configuration to equalize the load distribution among the planets. To accommodate the floating sun arrangement, the low-speed shaft (LSS) is hollow and has an internal spline that transfers the torsional loads to the parallel-shaft stages.

2.2.2.1 Gear Arrangements

The LS planetary gears have a helix angle of 7.5°, and the intermediate speed (IS) and high-speed (HS) gear sets have a helix angle of 14°. Figure 4 and Figure 5 show the internal components and their nomenclature [1]. Table 1 gives the dimensions and details of the gearing.

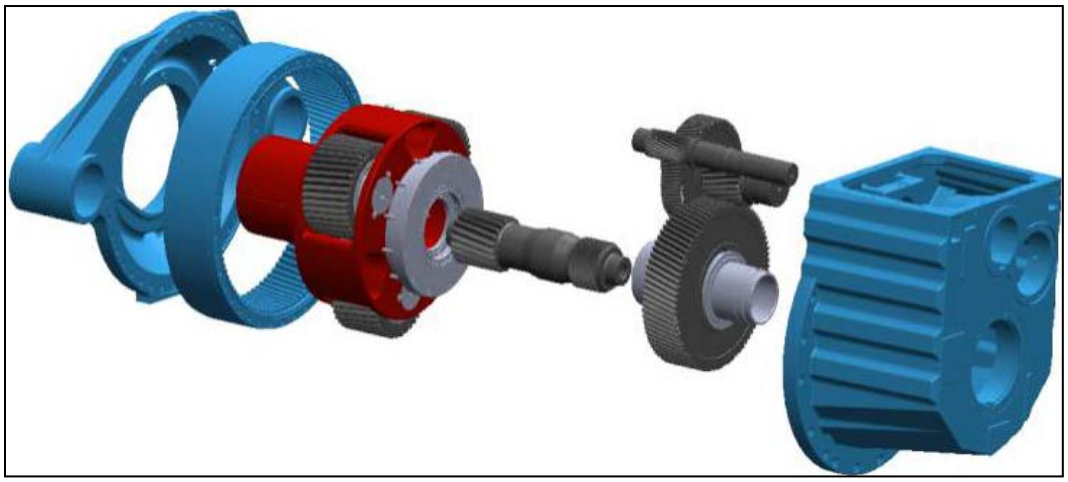

Figure 4. Gearbox Reliability Collaborative gearbox internal component view

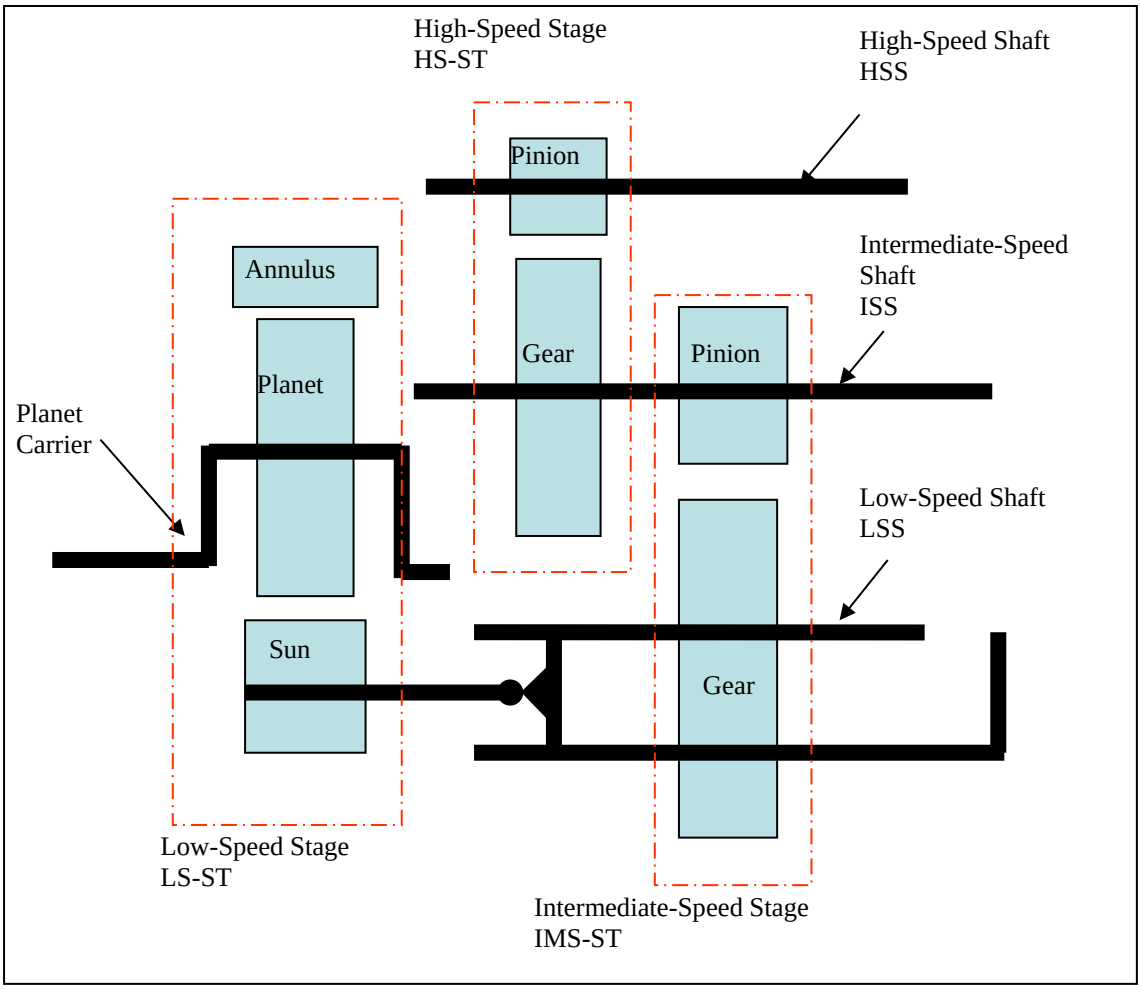

Figure 5. Gearbox Reliability Collaborative gearbox internal nomenclature and abbreviations

Table 1. Gear Dimensions and Details

Gear Element	Teeth	Mate Teeth	Root Diameter (mm)	Helix Angle	Facewidth (mm)	Speed Ratio
Planet gear	39	99	372	7.5°L	227.5	
Ring gear	99	39	1047	7.5°L	230	5.71
Sun pinion	21	39	186	7.5°R	220	
Intermediate gear	82	23	678	14°R	170	3.57
Intermediate pinion	23	82	174	14°L	186	
High-speed gear	88	22	440	14°L	110	4.00
HSS pinion	22	88	100	14°R	120	
Overall speed ratio						81.49

2.2.2.2 Bearing Arrangements

Several roller-bearing types are employed in the gearbox according to the loading conditions and gearbox-life requirements. The planet carrier is supported by two full-complement cylindrical roller bearings (fcCRBs), and each planet gear assembly is supported by two identical cylindrical

roller bearings (CRBs). Each parallel shaft in the gearbox is supported by a CRB on the upwind side of the assembly, and by two back-to-back mounted, duplex, tapered roller bearings (TRBs) on the downwind side.

Table 2 gives the location and bearing type for all bearings in the gearbox. The letter following the location abbreviation indicates the position of the bearing according to the component from upwind (A) to downwind (B, C).

Table 2. Bearing Types

Location	Type
PLC-A	fcCRB
PLC-B	fcCRB
PL-A	CRB
PL-B	CRB
LSS-A	fcCRB
LSS-B	TRB
LSS-C	TRB
ISS-A	CRB
ISS-B	TRB
ISS-C	TRB
HSS-A	CRB
HSS-B	TRB
HSS-C	TRB
Conduit	DGBB

2.3 Coordinate System

The coordinate system used in GRC testing is consistent with common wind turbine drivetrain practice as described below.

- X-axis: Aligned with the input low-speed shaft with the downwind direction being positive. In the GRC drivetrain, this axis is inclined at 5° to the horizontal. Thrust (F_x) is force acting along the positive X-axis and torque is a moment about the X-axis.
- Z-axis: Orthogonal to the X-axis with upward being positive. Vertical force acts along the Z-axis and yaw moment (M_{zz}) acts about the Z-axis. Rotor weight causes negative vertical force acting at the main bearing.
- Y-axis: Orthogonal to the X-axis and Z-axis with leftward being positive when viewing the drivetrain from upwind. Lateral force acts along the Y-axis and rotor weight causes a negative pitch moment (M_{yy}) about the Y-axis.
- Rotor azimuth angle: Increases clockwise when viewed from upwind with 0° being upward. Normal rotor rotation in the GRC drivetrain, as for most wind turbines, is positive.

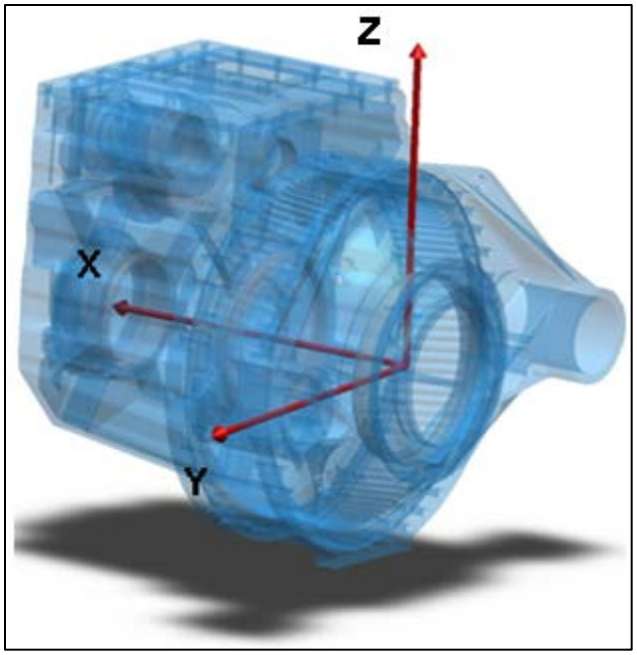

Figure 6. Gearbox coordinate system

3 Test Environment

3.1 Dynamometer Configuration

The National Wind Technology Center 2.5-MW dynamometer test facility [3] will be used for Phase 3 testing, as shown in Figure 7 and Figure 8 [1]. All references to “dynamometer” in this document mean the 2.5-MW facility, not the 225-kW or 5-MW dynamometers that also are available for drivetrain testing at the NWTC. The 2.5-MW dynamometer is essential for this project because it enables loads to be applied to the drivetrain under controlled conditions, in contrast to field testing where wind loads are not controllable. These test conditions can be steady-state conditions that are useful for simple model validation, but also can be dynamic and compare the response in the dynamometer versus the field test turbine and even more complex models. Furthermore, it is much easier to modify instrumentation, service the drivetrain, and modify the configuration in the dynamometer than it is to perform these tasks on a drivetrain installed in a turbine in the field.

Figure 7. The NWTC 2.5-MW dynamometer test facility (*NREL PIX/17398*)

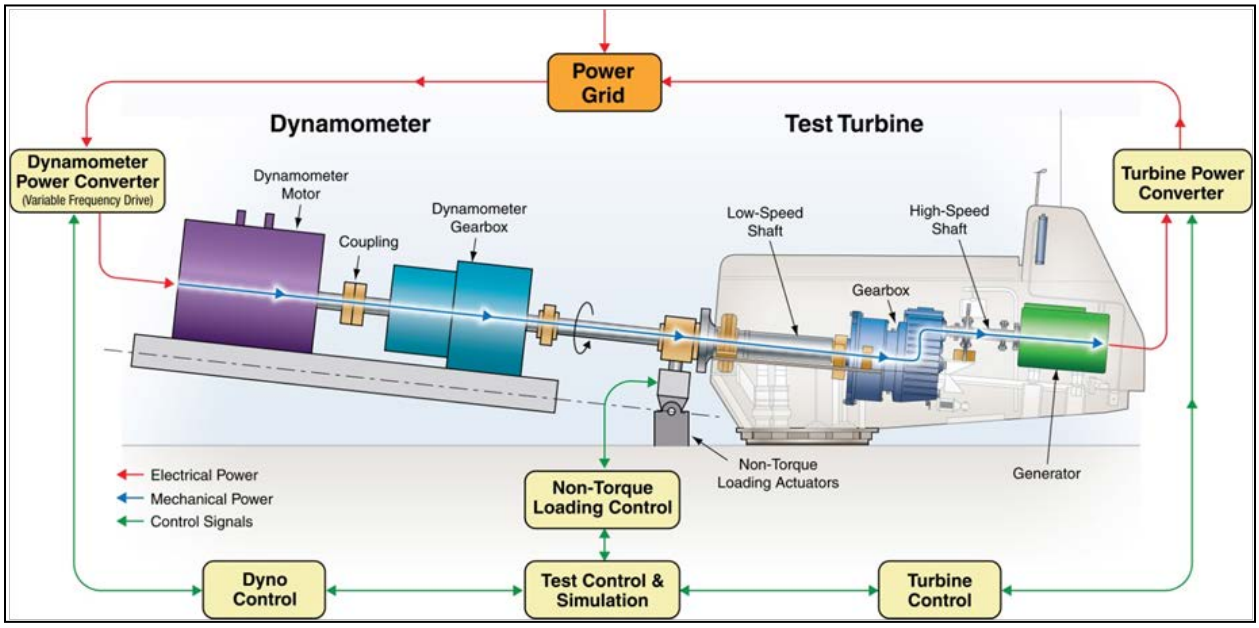

Figure 8. Schematic of NWTC 2.5-MW dynamometer test facility and control block diagram

3.2 Dynamometer Control

The dynamometer can be operated in either torque or speed control. In torque control, the operator commands a torque level that the dynamometer motor applies. The test drivetrain—in this case the GRC drivetrain—regulates speed. In speed control, the dynamometer operator commands the dynamometer motor's speed, and torque is regulated by the test drivetrain. The GRC drivetrain uses a generator that operates at two speeds. At each of those speeds, however, the generator allows only a 0.5% change from nominal, synchronous speed. It therefore is preferable to operate the dynamometer in torque-control mode. All Phase 1 and Phase 2 testing was conducted in this mode. Unfortunately, acceleration during start-up is difficult to control using torque control.

During Phase 2 testing, the dynamometer control was enhanced to provide more precise control of the start-up ramp rate and dynamometer behavior during grid connection. In this configuration, the dynamometer was started in speed-control mode at a preprogrammed rate of change (ramp rate). At generator synchronous speed, the torque set point was set to the current torque demand and the dynamometer is switched to torque control mode. Once in torque control mode, the dynamometer ramps at a specified rate to a predetermined torque value. Details of the asynchronous generator control mode are shown in Figure 9 [1].

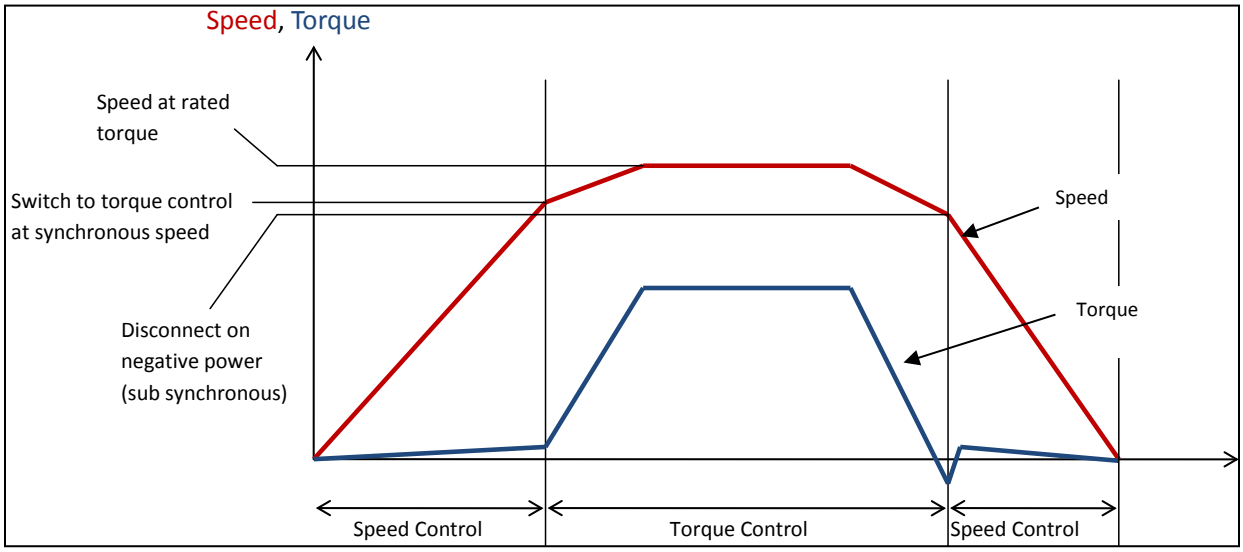

Figure 9. Asynchronous generator control mode

3.3 Non-Torque Loading System

In addition to torque and thrust, a wind turbine rotor applies loads to the drivetrain in four other degrees of freedom perpendicular to the main shaft axis: lateral force, vertical force, pitch moment, and yaw moment. These four off-axis loads are interrelated and can be simulated for testing purposes with just two actuators. During early GRC testing, the dynamometer was enhanced to provide control of these off-axis loads as well as thrust. The system used to apply these loads is called a non-torque loading (NTL) system. The NTL system used in the NWTC 2.5-MW dynamometer is shown in Figure 10 and Figure 11 [1].

The current NTL system uses three servo-hydraulic cylinders to apply thrust and the other four off-axis loads. This system can apply loads statically or dynamically over a limited frequency range.

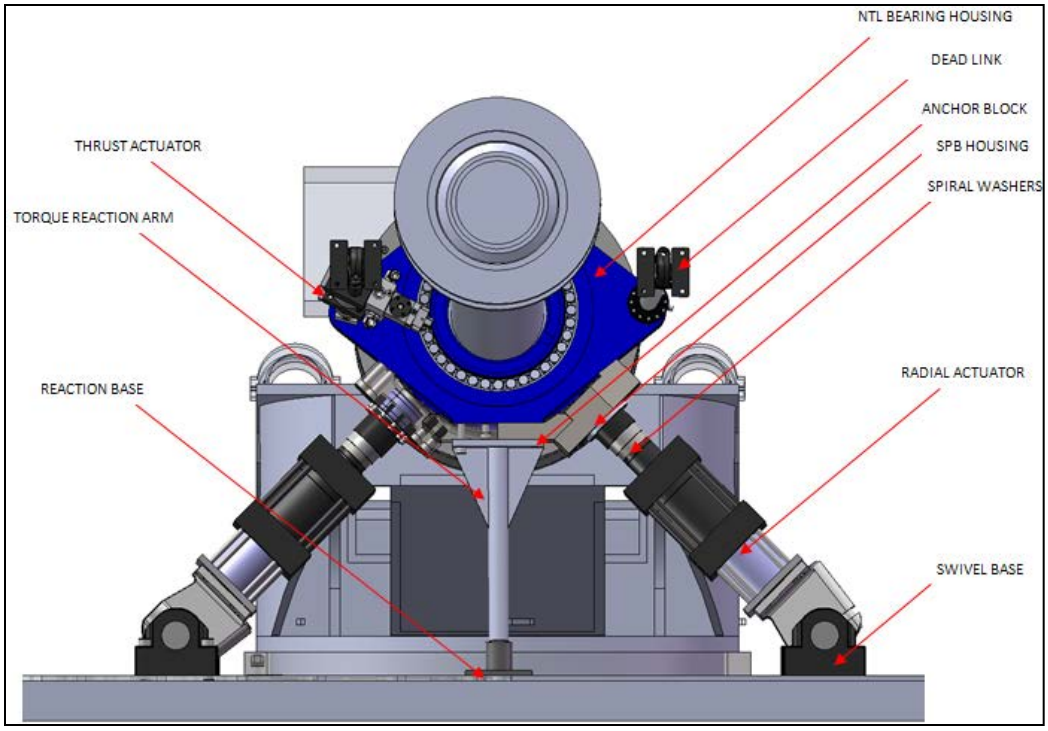

Figure 10. Upwind view of test article and NTL system components (thrust frame hidden)

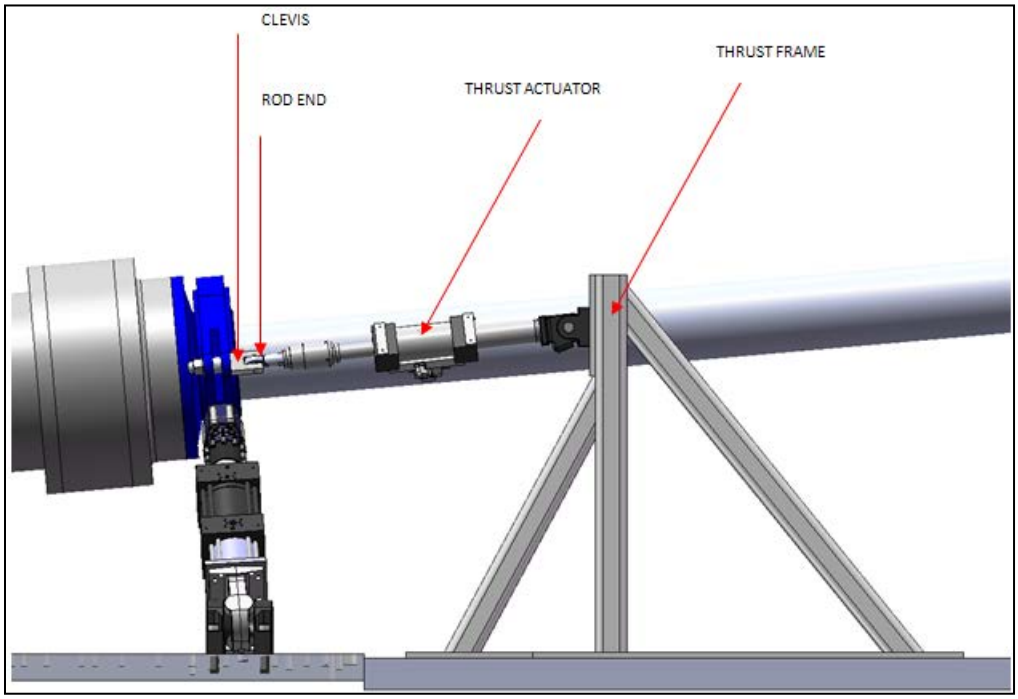

Figure 11. Side view of system showing thrust components

Given the fixed distance between the NTL bearing housing and the GRC main bearing, the relationship between the radial force and pitch or yaw moment for the system is fixed. Further, the geometry of the radial hydraulic actuators limits radial force in all directions to the maximum

vertical force. The following maximum loads are defined at the main bearing of the GRC drivetrain.

- Maximum pitch or yaw moment +/- 1,337 kNm
- Maximum radial force +/- 685 kN
- Maximum thrust force +/- 311 kN

These are “NTL-applied” loads and should not be confused with the loads applied to the drivetrain during testing. Overhanging weight of shafting and NTL components add the following loads.

- Pitch moment from overhanging weight - 14 kNm
- Vertical force from overhanging weight - 83 kN
- Thrust force from overhanging weight 7 kN

Additionally, flexible couplings between the NTL and the dynamometer gearbox impart moments during testing. These are functions of torque loads and coupling misalignment. Thus, tare loads (i.e., loads applied to the drivetrain when NTL-applied loads are zero) must be measured as part of each test condition.

In comparison to the shaft overhanging loads in the dynamometer, the turbine rotor’s weight of 12,500 kg centered at 1.291 m upwind of the main bearing applies the following loads to the mainshaft at the main bearing.

- Pitch moment from rotor weight - 158 kNm
- Vertical force from rotor weight - 122 kN
- Thrust force from rotor weight 11 kN

3.4 Data-Acquisition System

The data-acquisition system (DAS) is based on National Instruments (NI) deterministic Ethernet platform [4]. One system consisting of two backplanes is mounted to the mainshaft. The output of that system is converted to fiber optic and sent across a fiber optic rotary joint to the non-rotating frame. On top of the gearbox, a second system is mounted with two more deterministic Ethernet backplanes. The deterministic Ethernet synchronizes the different modules. Figure 12 shows a general layout of the DAS and Figure 13 shows the physical layout of the data-acquisition boxes. The two boxes mounted on top of the gearbox process fixed-frame signals. The box mounted on the mainshaft, attached with the blue safety strap, processes signals generated on the mainshaft and carrier assembly.

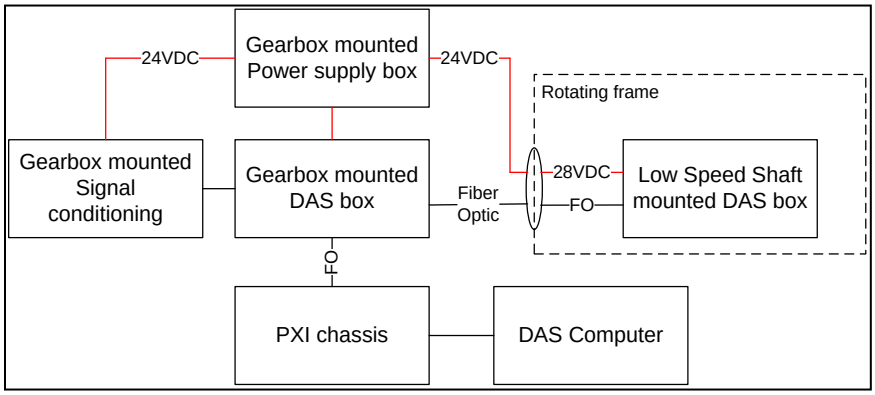

Figure 12. Schematic of GRC data acquisition system during Phase 2 testing

Figure 13. Data acquisition boxes for the GRC drivetrain (*NREL PIX/24914*)

For Phase 3 testing, the gearbox-mounted DAS and signal conditioning will be expanded to acquire additional data pertaining to dynamic high-speed shaft alignment and external ring gear stress and strain. To accommodate additional channels and signal conditioning hardware, a new enclosure will be added in the stationary frame.

For most of the testing a 100-Hz sample rate is used, unless otherwise specified in the test description. Snapshot data also can be collected in so-called burst mode at 2,000 Hz.

4 Instrumentation

Instrumentation for Phase 3 testing can be categorized by location of the sensor. General descriptions of the sensors in these areas are provided in this section. Appendix A contains a listing of all sensors and resulting signals, and Appendix B provides details on sensor installation and wiring.

- Non-torque loading system
- Mainshaft/gearbox low-speed shaft
- Gearbox housing
- Gearbox ring gear
- Low-speed stage planet carrier
- Low-speed stage planet
- Low-speed stage sun
- Intermediate stage
- High-speed stage and shaft
- Generator
- Controller
- Lubrication system

4.1 Non-Torque Loading System

The non-torque loading system has three actuators, each of which has a load cell and a displacement sensor. The thrust actuator is offset from the center of the shaft, therefore its load is balanced by a linkage which also features a load cell. Strain gages on the stabilizer link provide measurements of axial and lateral loads transmitted by that component. Hydraulic pressure to the actuators is monitored using a pressure transducer. During Phase 2 testing, the flexible couplings between the non-torque loading system and the dynamometer gearbox were determined to impart significant bending loads on the mainshaft. These loads are greatly affected by coupling misalignment. Therefore, in Phase 3 these loads will be measured using two sets of strain gages to measure bending loads at each end of the jackshaft that connects the dynamometer gearbox to the non-torque loading system. Additionally, two proximity sensors on each of the two flexible couplings indicate the magnitude and direction of coupling misalignment.

4.2 Mainshaft and Gearbox Low-Speed Shaft

The mainshaft is rigidly connected to the gearbox low-speed shaft and planet carrier and measurement of this assembly provides the critical input loads to the drivetrain. Torque is measured on the mainshaft with a full strain gage bridge, as shown in Figure B-1 in Appendix B. Mainshaft torque is also measured with a custom torque spool located upwind of the non-torque loading equipment. This measurement device is more accurately calibrated than the torque gages

on the GRC mainshaft, but it does not account for friction in the NTL bearing or the GRC main bearing.

A shaft encoder on the aft end of the signal conduit tube measures the speed and azimuth of the gearbox LSS, as shown in Figure B-2. A pulse counter/timer circuit derives the speed, giving a 0- to 5-volt DC (VDC) output proportional to speed. The azimuth angle is from a separate counter circuit using the same encoder input, generating a 0 to 4.095 VDC sawtooth output proportional to shaft position. The sawtooth is reset to 0 by the index pulse once per revolution. Resolution is about 1/4°. Zero azimuth angle is defined when Planet C is upward at "top dead center" (TDC).

Main shaft bending is measured in both directions, as shown in Figure B-3 and Figure B-4. The measured shaft azimuth is used to convert these rotating shaft-bending moments into pitch and yaw moments in the fixed frame. Additionally, a proximity sensor quantifies axial displacement of the mainshaft relative to the mainframe close to the mainshaft flange, as shown in Figure B-5.

4.3 Gearbox

4.3.1 Housing

Gearbox housing measurements provide information on the displacement of the gearbox relative to the mainframe. Motion of the gearbox relative to the mainframe in six degrees of freedom is measured using six proximity sensors, as shown in Figure B-6 to Figure B-9. These are located on the trunnion arms and on the bottom of the gearbox. A three-element strain gage set is used to validate finite element models of the gearbox, as shown in Figure B-10.

Motion of the gearbox relative to the ground is measured using low-frequency (DC – 100 Hz) accelerometers, as shown in Figure B-11. Two of these are triaxial accelerometers mounted close to the trunnion mounts. A single-axis accelerometer measures motion about the trunnion axis.

Additionally, high-frequency vibration is measured, focusing on gear mesh frequencies, bearing ball pass frequencies, and higher order drivetrain natural frequencies. This is done using CM systems with accelerometers, and stress wave microphones with analysis of notch frequencies of interest.

4.3.2 Ring Gear

Strain gages on both the inside and the outside of the gearbox ring gear indicate contact patterns between the ring gear teeth and planet teeth. Other gages quantify ring gear deformation, which occurs primarily because of loads induced by meshing with the planets.

On its inner surface, the ring gear has strain gages mounted in the root area of the internal teeth arranged to sense tooth bending strain. Experience suggests that gages in this orientation are relatively insensitive to alignment errors. These gages are distributed axially at eight locations along the root apex to measure the tooth–face width load distribution. The gages are arranged in two separate Wheatstone bridges of four gages each. This approach has several advantages, including increasing the signal-to-noise ratio and temperature compensation. It requires spacing the gages over several teeth, however, such that the gages on adjacent bridge arms are not in the contact area at the same time. If they are, the signal could be attenuated erroneously. The ring gear has a 7.5° helix angle and the contact ratio is moderately high. For these reasons, adjacent

gages were installed four teeth apart. This arrangement is repeated at three circumferential locations on the ring gear at TDC and spaced 120° apart (as shown in Figure B-12, Figure B-13, and Figure B-14), for a total of 24 internal gages.

On its external surface, the ring gear has one set of eight strain gages in an arrangement similar to the internal gages (*see* Figure B-15), to measure the tooth–face width load distribution from the exterior of the ring gear. These gages are located at approximately 65° from TDC.

Also on its external surface the ring gear has four sets of two gages, each arranged in Poisson bridges gages oriented to measure ring gear hoop strain. These gages are located 45° from TDC and are spaced 90° apart, as shown in Figure B-16. These gages help to define positions of internal components relative to the mainshaft.

The primary function of the internal gages is to determine load share between planets and characterize changes in the face width load distribution. Additionally, the external gages enable comparison to be made to investigate the accuracy of measuring face width load distribution from the exterior of the gearbox—which is significantly easier than using gages that are inside the gearbox. The external gages also can be used to investigate the effect of the stiffness of the ring gear.

4.3.3 Planet Carrier

Proximity sensors indicate the radial and axial motion of the planet carrier relative to the housing, as shown in Figure B-17 and Figure B-18. This motion is a combination of rigid body and deformation. These sensors are mounted on the upwind face and sides of the gearbox housing, using a custom fitting that bolts to the housing.

4.3.4 Planetary Gears

Planetary gear sensors include six proximity sensors which are mounted on the carrier. These measure the position of two of the planets (B and C) relative to the carrier. Each set of three is mounted identically, as shown in Figure B-19 and Figure B-20. These indicate both axial and tilting motion of the planetary gears.

4.3.5 Planetary Bearings

Thirty-six strain gages are mounted in axial grooves in the inner races of the planet bearings to provide information on planet loads and roller contact pressure distribution. Three grooves were machined into each bearing. Each groove has two strain gages—one at 25% and one at 75% of the inner ring width as shown in Figure B-21. All six bearings have a groove at top dead center which is in the direction of motion of the planet pin and close to the center of pressure between the pin and the planet. The remaining grooves on each planet are located at different azimuthal locations, as shown in Figure B-22 to Figure B-24.

This instrumentation allows measurement of the following:

- The axial and circumferential distribution of load through the load zone
- Change of load distribution during shaft and gear load fluctuations and motions
- Load sharing between planet bearings.

Thermocouples are also mounted in the axial midpoint of the each groove to measure planet bearing inner race temperatures, as shown in Figure B-25. Of the eighteen installed thermocouples, the twelve were judged to be sufficient to characterize bearing temperatures and therefore were connected to the data-acquisition system. This includes all thermocouples from planet A, as well as selected ones from the other two planets. One radiant-type non-contact temperature sensor is used to measure temperature on the outer race of Planet A to identify the temperature gradient across the bearing, as shown in Figure B-26.

An inductive proximity sensor is used to sense passage of the eighteen rivets in the roller cage of one of the planet bearings, as shown in Figure B-27. This provides a measure of the rotational speed of one of the rollers about the planet pin, and is used to detect slippage of the rollers relative to the planet bearing races. Bearing slip is suspected to play a significant role in contact damage. Slip is expected to be less than 1% of race speed at high bearing loads, but could be more than 25% in lightly loaded and transient situations.

4.3.6 Sun Gear

Two proximity sensors indicate the radial position of the sun gear relative to the planet carrier, as shown in Figure B-28. They sense the upwind end of the sun shaft in the area of the shaft that extends about 50 mm beyond the end of the sun pinion. These sensors record this motion relative to carrier in two orthogonal directions. These rotating frame internal gearbox measurements exit the gearbox through a slip ring assembly (Figure B-29).

4.3.7 Intermediate Stage

The two measurements in the intermediate stage are axial position of the intermediate shaft relative to the housing using a proximity sensor, as shown in Figure B-30, and the temperature of the rear bearing, as shown in Figure B-31.

4.3.8 High-Speed Shaft

In Phase 2, the only sensors on the high speed shaft section were two resistance temperature detectors (RTDs) measuring the outer ring temperatures of the CRB and the upwind TRB. In Phase 3, the high-speed shaft instrumentation is significantly enhanced to assess high-speed shaft, pinion, and bearing loads. Three sets of bending gages define shaft bending loads on either side of the high-speed gear mesh and downwind of the pair of TRBs as shown in Figure B-32 to Figure B-34. An additional set of gages also downwind of the pair of TRBs measures torque transmitted by the high-speed shaft. Eight gages are installed in the root of the teeth of the high-speed pinion to measure the face width load distribution as shown in Figure B-35. The shaft bending gages are not capable of distinguishing loads between the two TRBs, so additional gages are mounted in axial grooves in the outer races to measure bearing loads on the TRBs as shown in Figure B-36 and Figure B-37. Each bearing has 4 axial grooves with 2 gages per groove for a total of 16 strain gages to measure these TRB loads. Two RTDs will also measure the temperature of the outer races of the two TRBs as shown in Figure B-38.

4.4 Brake Disk

An encoder measures shaft speed and position as shown in Figure B-39. Five proximity sensors—three axial, one vertical, and one lateral—measure the brake disk position relative to the dynamometer floor, as shown in Figure B-40 and Figure B-41. These, in combination with

similar proximity sensors on the generator shaft, provide the data required to calculate alignment of the two flexible couplings in the high-speed shaft assembly.

4.5 Generator

Five proximity sensors—three axial, one vertical and one lateral—measure generator position and rotation relative to the dynamometer floor in five degrees of freedom, as shown in Figure B-42 and Figure B-43. A robust framework is needed to measure generator displacement, because the downwind portion of the mainframe is very flexible. This mainframe displacement measurement is shown in Figure B-44. In combination with measurements of gearbox housing motion, these generator measurements yield information on alignment of the high-speed shaft assembly during applications of torque and non-torque load to the main shaft.

An encoder on the aft end of the generator measures the generator shaft speed and azimuth as shown in Figure B-45 and Figure B-46. An RTD measures the temperature of the downwind bearing, which previously has run hotter than the upwind bearing.

4.6 Additional Measurements

Relays indicate the status of the generator's electrical connection to the grid; one relay for the high-power generator windings, one for the low-power generator windings, and one to indicate when the soft-start components are bypassed. A power meter indicates real and reactive power at the connection of the generator to the grid.

The gearbox lubrication system is monitored using a temperature and pressure sensor at the distribution manifold, a temperature sensor at the outlet of the sump (Figure B-47), and a displacement-type flow meter to measure total oil flow to the gearbox. An optical particle sensor measures metallic and non-metallic particles in the sump oil. The entire drivetrain (i.e., main bearing, gearbox, and generator) is instrumented with various condition monitoring systems (e.g., vibration and oil debris analysis packages).

5 Test Sequence

5.1 Test Overview

Testing in Phase 3a consists of the following major activities:

- Drivetrain recommissioning
- Effect of non-torque loads
- Radial misalignment of high-speed shaft
- Reproduction of field conditions
- Campbell diagram measurement.

The first test sequence in the dynamometer verifies that the drivetrain operates normally and that all controls and data systems perform as desired. The GRC drivetrain has not been operated for several years and a number of sensors have been added to the instrumentation suite since Phase 2 testing concluded. Recommissioning tests are used to gradually increase speed, torque, and non-

torque loads, with frequent checks to ensure acceptable control and data-acquisition performance.

Non-torque loading effects were investigated in Phase 2 tests. Analysis of test data after testing was completed, however, indicated that the test series was not as comprehensive as desired. In Phase 3 tests the range of non-torque loads is expanded, simple dynamic non-torque load events are applied, and the response of the gearbox and other drivetrain components are measured more completely.

In Phase 2 tests the high-speed shaft was purposefully misaligned. The high-speed shaft, pinion, and bearing were not instrumented, however, so it was not possible to measure misalignment effects. By outfitting the high-speed shaft with improved instrumentation, Phase 3 tests will clarify what conditions, if any, impart excessive loads onto the HSS bearings. Phase 3 tests investigate radial misalignment of the generator, non-torque loading of the mainshaft, and brake application as possible contributors to HSS bearing loads.

Reproduction of field conditions in the dynamometer was attempted in Phase 2 testing. A key shortfall in the NWTC 2.5-MW dynamometer is the limited control bandwidth of the variable frequency drive. The bandwidth of the 15-year-old drive limits the frequency with which torque can be applied to the test drivetrain. NREL is in the process of replacing the drive with a more modern and more reliable drive which will be available in time for GRC Phase 3 testing. This new drive should permit more accurate reproduction of field loading in the dynamometer.

Several tests have been conducted on the GRC gearbox to determine vibration characteristics. However, NREL has not been able to conduct a test that would describe both excitation and resonant frequency characteristics under torque and over a broad speed range. This is because the only method of resisting torque applied by the dynamometer is the two-speed GRC generator and generator controller. In Phase 3, NREL plans to procure either a variable frequency drive (VFD) or an eddy-current brake. Either device will permit operation over a range of speeds and torques. The VFD is the preferred device that would permit operation at torque ranging from zero to rated and at speeds from 50 rpm to 2,000 rpm. An eddy-current brake would enable operation over a similar speed range. But torque would be limited to approximately 5% of rated. This plan will describe the full range of testing desired. The test will be conducted over as broad a range as possible depending upon the equipment obtained.

5.2 General Dynamometer Test Procedures

In Phase 3 testing, NREL will verify operation of data acquisition signals before each dynamometer run. This allows the test operator to fix signals critical to the test before the test begins. In general each run should be preceded with the slow roll checks described in step 4 of the recommissioning test in section 5.3. Because some signals only show a response under load, it is essential to look at data sets shortly after they are collected to judge whether critical signals are still functioning. Automatic indicators should be in place to alert the user to issues such as signal railing.

Building on knowledge from Phase 1 testing, it has become clear that to maximize the effectiveness of individual data sets, it is necessary to implement data standards. Because the

GRC is focused on elucidating response to static and dynamic loading conditions, finding the response against background noise can be vastly improved by following a few simple steps.

1. **Acquire data while stopped, before operation.** In doing this, it ensures that the data will capture movement from rest for solid body motion. This is *very useful* for seeing gearbox response to non-torque loads. At least 60 seconds of data are necessary to complete this section.
2. **If possible, perform unloaded (torque and non-torque) slow rolls before accelerating.** These provide response to rotation and might contain misalignment caused by rotation. Around 60 seconds of data will be sufficient.
3. **Take a snapshot of desired data when the generator comes online.** Transient events, which frequently occur at start-up, are aliased by the standard data sampling rate.
4. **Take a snapshot of data when the test article goes offline.** This helps characterize the generator response.
5. **Acquire data while stopped, after operation.** It has been found that the gearbox does not settle in the same position after each run.

5.3 Recommissioning Test

Prior to the first start of the dynamometer NREL will verify control and instrumentation as much as possible.

1. Prior to connection of the dynamometer low-speed shaft to the GRC drivetrain.
    A. With the dynamometer drive off, check Emergency Power Off (EPO) buttons to ensure that the EPO relay in the Vista Switch operates properly.
    B. Exercise each fault sensor to ensure that the fault is detected at the dynamometer control panel and that the dynamometer drive shuts down.
        i. Dynamometer motor overspeed
        ii. Dynamometer lube oil pressure
        iii. GRC controller fault
    C. Verify dynamometer motor and drive controls are operating properly.
    D. Get zero position on proximity sensor by hand rotation of brake in both directions and unloading.
    E. For each proximity sensor the signal will be calibrated by moving the proximity sensor closer or further from its actual target by either turning the proximity sensor in the threaded hole it is mounted in or by turning the locking nuts holding the sensor in an unthreaded hole. The thread pitch is known, therefore the increase or decrease in distance will be known. The initial distance is measured with feeler gages or gage block depending on the gap size.
    F. For all strain gage channels, shunt calibrations are performed.

G. For each Linear Variable Displacement Transformer (LVDT), gage blocks or feeler gages are used to calibrate the sensor. The LVDT's are used only in locations where the change in distance is important.

H. Check other data-acquisition channel to ensure that nominal values are reported.

2. Check GRC mainshaft bending moments.

   A. Check other data acquisition channel to ensure that nominal values are reported.

   B. With no shaft adapters attached, slow roll the GRC main shaft. Bending moments should be less than 1 kNm.

   C. With the 5,100-lb white coupling (cylinder and upwind flange) attached to the GRC mainshaft, slow roll. Bending moments should be about 8 kNm.

3. Connect the dynamometer shaft to the GRC drivetrain.

   A. Verify that the NTL actuator tuning parameters are set up properly; that load cell and LVDT signals are nominal; and that the mechanical system is set up, torqued, and adjusted. Refer to the document used to commission the NTL equipment and to the readiness verification checklist for these verifications.

   B. Place the NTL radial actuators in force feedback and command oscillations at a force value of +/- 5 kN and a frequency of less than 0.3 Hz. Using the force feedback signal, adjust the swivel ends so the there is no backlash in the system and low friction in the swivels.

4. Conduct a slow roll with no GRC-generator connection to the grid.

   A. Listen for unusual sounds or vibrations in the dynamometer and GRC drivetrain.

   B. Check each data acquisition channel to ensure that nominal values are reported.

   C. Verify that data are recorded in both slow and fast recording modes.

   D. Check GRC main shaft bending. With shaft overhanging weight, it should be about 65 kNm.

   E. Check NTL vertical load required to zero mainshaft bending. This should be approximately 65 kN.

5. Accelerate to synchronous speed and connect the high-power generator windings. Command 5% rated torque.

   A. Listen for unusual sounds or vibrations in the dynamometer and GRC drivetrain.

   B. Check each data acquisition channel to ensure that nominal values are reported.

6. Gradually increase torque to 100% of rated.

   A. Listen for unusual sounds or vibrations in the dynamometer and GRC drivetrain.

   B. Check each data-acquisition channel to ensure that reasonable responses are reported.

7. Reduce torque to 5% of rated and gradually apply F_x to 50 kN.

   A. Listen for unusual sounds or vibrations in the dynamometer and GRC drivetrain.

B. Check each data-acquisition channel to ensure that reasonable responses are reported.

8. At 5% of rated torque and 0 kN F_x, gradually apply M_{yy} to -50 kNm and then from -50 kNm to +50 kNm.
    A. Listen for unusual sounds or vibrations in the dynamometer and GRC drivetrain.
    B. Check each data-acquisition channel to ensure that reasonable responses are reported.
9. At 5% of rated torque, with 0 kN F_x, and 0 kNm applied M_{yy}, gradually apply M_{zz} to -50 kNm and then from -50 kNm to +50 kNm.
    A. Listen for unusual sounds or vibrations in the dynamometer and GRC drivetrain.
    B. Check each data-acquisition channel to ensure that reasonable responses are reported.

5.4 Non-Torque Load Test

The primary objective of the non-torque load test is to quantify the effects of non-torque loads (thrust, pitch, and yaw) on both internal and external features of the gearbox. This test also will help define how flexible couplings—typically used in dynamometer drivetrains—add to the loads applied by non-torque loading devices. Primary measurements include gearbox solid body motion, main shaft to gearbox alignment, and planet to ring tooth contact changes. Secondary measurements include HSS alignment, HSS bearing loads, dynamometer flexible coupling alignment, and loads. NREL staff also will monitor planet bearing roller behavior to determine whether skidding occurs when the roller moves into the load zone. Although non-torque loads might not affect the intermediate- and high-speed stages, data will be obtained to assess this possibility.

5.4.1 Static Bending Moment Test

The static bending moment test is a continued test from Phase 2. A major finding from Phase 2 testing is that pitch and yaw moments affect tooth contact in the planetary gear stage, as shown in Figure 14 [5]. These effects were seen when moments were varied from zero to approximately 170 kNm. In this test, moments are increased to 300 kNm, a level approached during limited field testing, as shown in Figure 15.

Tests also are conducted over a range of torques. It is possible that torque will change the effect of non-torque loads on bearing loads and tooth-contact patterns. This phenomenon is investigated by applying bending moments at essentially zero torque (when the generator is off-line) as well as at greater torque levels.

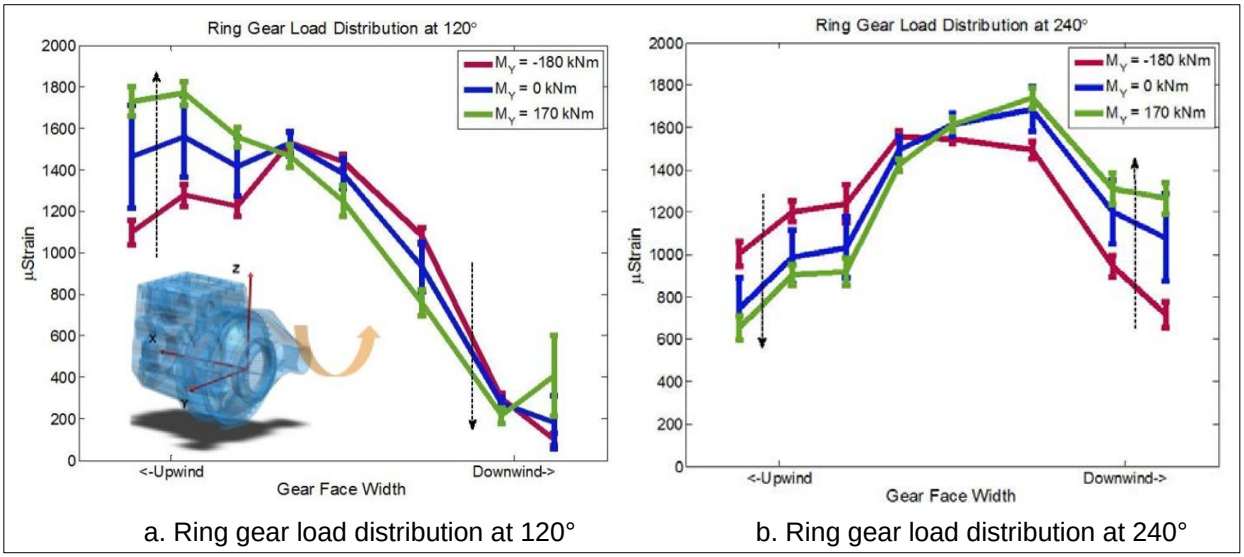

a. Ring gear load distribution at 120° b. Ring gear load distribution at 240°

Figure 14. Effect of pitching moment (M_{yy}) on ring gear load distributions

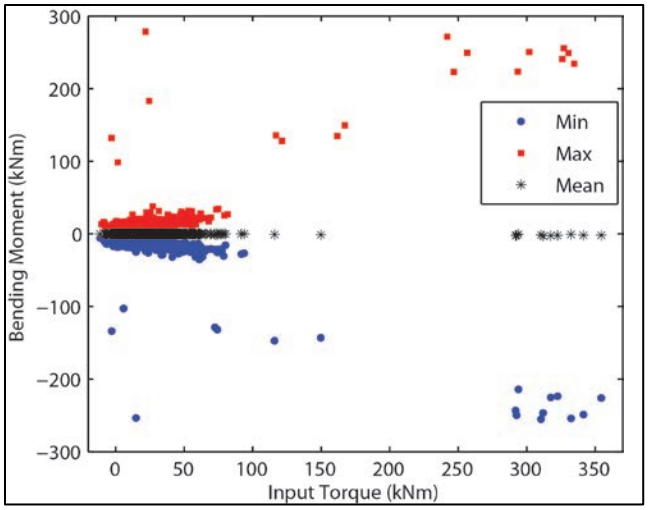

Figure 15. Torque and bending moment distribution measured during the GRC field test

As non-torque loads are introduced, changes in critical measurements for the gearbox and turbine nacelle are expected. The following parameters should be observed carefully to assure that the system is behaving as expected.

- **Shaft Bending:** Calculate the bending measured by the gages on the LSS in terms of magnitude and direction to verify that they are within limits.
- **Misalignment:** Use the information from proximity sensors to verify that displacements of the high-speed shaft and generator are logical.
- **Load Share:** Verify that loads in the actuator load cells, dead-link, and torque reaction arm are within limits.
- **Temperature:** Look for any adverse or unusual temperature increases of the bearings.

5.4.1.1 Test Procedure

Apply torque and non-torque bending moments as follows. At each test condition, record 1 minute of 100 Hz data. At all test conditions where torque is applied, record 10 seconds of 5 kHz data to capture HSS measurements.

5.4.1.2 Torque and Non-Torque Bending Moments

1. Off-line, 100 rpm, normal direction
    A. Applied M_{zz} zero, M_{yy} -300 to +300 in 50 kNm steps
    B. Applied M_{zz} -100 kNm, M_{yy} -200 to +200 in 100 kNm steps
    C. Applied M_{zz} -200 kNm, M_{yy} -200 to +300 in 100 kNm steps
    D. Applied M_{zz} +100 kNm, M_{yy} -300 to +300 in 100 kNm steps
    E. Applied M_{zz} +200 kNm, M_{yy} +200 to +300 in 100 kNm steps
    F. Applied M_{yy} zero, M_{zz} -300 to +300 in 50 kNm steps
    G. Applied M_{yy} -100 kNm, M_{zz} -200 to +200 in 100 kNm steps
    H. Applied M_{yy} -200 kNm, M_{zz} -200 to +300 in 100 kNm steps
    I. Applied M_{yy} +100 kNm, M_{zz} -300 to +300 in 100 kNm steps
    J. Applied M_{yy} +200 kNm, M_{zz} +200 to +300 in 100 kNm steps
2. Off-line, 100 rpm, reverse direction
    A. Applied M_{zz} zero, M_{yy} -300 to +300 in 50 kNm steps
    B. Applied M_{yy} zero, M_{zz} -300 to +300 in 50 kNm steps
3. Off-line, 1,800 rpm
    A. Applied M_{zz} zero, M_{yy} -300 to +300 in 50 kNm steps
    B. Applied M_{yy} zero, M_{zz} -300 to +300 in 50 kNm steps
4. Online, 25% rated torque
    A. Applied M_{zz} zero, M_{yy} -300 to +300 in 50 kNm steps
    B. Applied M_{zz} -100 kNm, M_{yy} -200 to +200 in 100 kNm steps
    C. Applied M_{zz} -200 kNm, M_{yy} -200 to +300 in 100 kNm steps
    D. Applied M_{zz} +100 kNm, M_{yy} -300 to +300 in 100 kNm steps
    E. Applied M_{zz} +200 kNm, M_{yy} +200 to +300 in 100 kNm steps
    F. Applied M_{yy} zero, M_{zz} -300 to +300 in 50 kNm steps
    G. Applied M_{yy} -100 kNm, M_{zz} -200 to +200 in 100 kNm steps
    H. Applied M_{yy} -200 kNm, M_{zz} -200 to +300 in 100 kNm steps
    I. Applied M_{yy} +100 kNm, M_{zz} -300 to +300 in 100 kNm steps
    J. Applied M_{yy} +200 kNm, M_{zz} +200 to +300 in 100 kNm steps.

5. Online, 50% rated torque
    A. Applied M_{zz} zero, M_{yy} -300 to +300 in 50 kNm steps
    B. Applied M_{zz} -100 kNm, M_{yy} -200 to +200 in 100 kNm steps
    C. Applied M_{zz} -200 kNm, M_{yy} -200 to +300 in 100 kNm steps
    D. Applied M_{zz} +100 kNm, M_{yy} -300 to +300 in 100 kNm steps
    E. Applied M_{zz} +200 kNm, M_{yy} +200 to +300 in 100 kNm steps
    F. Applied M_{yy} zero, M_{zz} -300 to +300 in 50 kNm steps
    G. Applied M_{yy} -100 kNm, M_{zz} -200 to +200 in 100 kNm steps
    H. Applied M_{yy} -200 kNm, M_{zz} -200 to +300 in 100 kNm steps
    I. Applied M_{yy} +100 kNm, M_{zz} -300 to +300 in 100 kNm steps
    J. Applied M_{yy} +200 kNm, M_{zz} +200 to +300 in 100 kNm steps
6. Online, 75% rated torque
    A. Applied M_{zz} zero, M_{yy} -300 to +300 in 50 kNm steps
    B. Applied M_{zz} -100 kNm, M_{yy} -200 to +200 in 100 kNm steps
    C. Applied M_{zz} -200 kNm, M_{yy} -200 to +300 in 100 kNm steps
    D. Applied M_{zz} +100 kNm, M_{yy} -300 to +300 in 100 kNm steps
    E. Applied M_{zz} +200 kNm, M_{yy} +200 to +300 in 100 kNm steps
    F. Applied M_{yy} zero, M_{zz} -300 to +300 in 50 kNm steps
    G. Applied M_{yy} -100 kNm, M_{zz} -200 to +200 in 100 kNm steps
    H. Applied M_{yy} -200 kNm, M_{zz} -200 to +300 in 100 kNm steps
    I. Applied M_{yy} +100 kNm, M_{zz} -300 to +300 in 100 kNm steps
    J. Applied M_{yy} +200 kNm, M_{zz} +200 to +300 in 100 kNm steps
7. Online, 100% rated torque
    A. Applied M_{zz} zero, M_{yy} -300 to +300 in 50 kNm steps
    B. Applied M_{zz} -100 kNm, M_{yy} -200 to +200 in 100 kNm steps
    C. Applied M_{zz} -200 kNm, M_{yy} -200 to +300 in 100 kNm steps
    D. Applied M_{zz} +100 kNm, M_{yy} -300 to +300 in 100 kNm steps
    E. Applied M_{zz} +200 kNm, M_{yy} +200 to +300 in 100 kNm steps
    F. Applied M_{yy} zero, M_{zz} -300 to +300 in 50 kNm steps
    G. Applied M_{yy} -100 kNm, M_{zz} -200 to +200 in 100 kNm steps
    H. Applied M_{yy} -200 kNm, M_{zz} -200 to +300 in 100 kNm steps
    I. Applied M_{yy} +100 kNm, M_{zz} -300 to +300 in 100 kNm steps
    J. Applied M_{yy} +200 kNm, M_{zz} +200 to +300 in 100 kNm steps

8. Off-line, 100 rpm
    A. Applied M_{zz} zero, M_{yy} -300 to +300 in 50 kNm steps
    B. Applied M_{yy} zero, M_{zz} -300 to +300 in 50 kNm steps

5.4.2 Dynamic Bending Moment Test

Some GRC participants have suggested that quickly changing bending moments might affect bearings and teeth mesh in ways not seen under steady-state conditions. This test explores that possibility by using the NTL device to apply sinusoidal pitch and yaw moments of varying magnitude and frequency.

5.4.2.1 Test Procedure

Apply torque and non-torque bending moments as follows. At each test condition, record 1 minute of 100 Hz data. During each frequency sweep every 30 seconds, record 10 seconds of 5 kHz data to capture HSS measurements.

5.4.2.2 Torque and Non-Torque Bending Moments

1. Off-line, 1,800 rpm, normal direction
    A. Applied M_{zz} 0, vary M_{yy} from 0 to -50 kNm at 0.30 Hz
    B. Increase frequency from 0.30 Hz to 2 Hz over a period of 5 minutes
    C. Stop cycling M_{yy} and set M_{yy} to equal 0
    D. Begin another frequency sweep by varying M_{yy} from 0 to -200 kNm at 0.3 Hz
    E. Increase frequency from 0.30 Hz to 2 Hz over a period of 5 minutes
    F. Stop cycling M_{yy} and set M_{yy} to equal 0
    G. Applied M_{yy} 0, vary M_{zz} from 0 kNm to 50 kNm at 0.30 Hz
    H. Increase frequency from 0.30 Hz to 2 Hz over a period of 5 minutes
    I. Stop cycling M_{zz} and set M_{zz} to equal 0
    J. Begin another frequency sweep by varying M_{zz} from 0 kNm to 200 kNm at 0.3 Hz
    K. Increase frequency from 0.30 Hz to 2 Hz over a period of 5 minutes
    L. Stop cycling M_{zz} and set M_{zz} to equal 0
    M. Begin another frequency sweep by varying M_{zz} from -200 kNm to 200 kNm at 0.3 Hz
    N. Increase frequency from 0.30 Hz to 2 Hz over a period of 5 minutes
    O. Stop cycling M_{zz} and set M_{zz} to equal 0
2. Online, 25% rated torque
    A. Applied M_{zz} 0, vary M_{yy} from 0 kNm to -50 kNm at 0.30 Hz
    B. Increase frequency from 0.30 Hz to 2 Hz over a period of 5 minutes
    C. Stop cycling M_{yy} and set M_{yy} to equal 0

D. Begin another frequency sweep by varying M_{yy} from 0 kNm to -200 kNm at 0.3 Hz

E. Increase frequency from 0.30 Hz to 2 Hz over a period of 5 minutes

F. Stop cycling M_{yy} and set M_{yy} to equal 0

G. Applied M_{yy} 0, vary M_{zz} from 0 kNm to 50 kNm at 0.30 Hz

H. Increase frequency from 0.30 Hz to 2 Hz over a period of 5 minutes

I. Stop cycling M_{zz} and set M_{zz} to equal 0

J. Begin another frequency sweep by varying M_{zz} from 0 kNm to 200 kNm at 0.3 Hz

K. Increase frequency from 0.30 Hz to 2 Hz over a period of 5 minutes

L. Stop cycling M_{zz} and set M_{zz} to equal 0

M. Begin another frequency sweep by varying M_{zz} from -200 kNm to 200 kNm at 0.3 Hz

N. Increase frequency from 0.30 Hz to 2 Hz over a period of 5 minutes

O. Stop cycling M_{zz} and set M_{zz} to equal 0

3. Online, 100% rated torque

A. Applied M_{zz} 0, vary M_{yy} from 0 kNm to -50 kNm at 0.30 Hz

B. Increase frequency from 0.30 Hz to 2 Hz over a period of 5 minutes

C. Stop cycling M_{yy} moment and set M_{yy} to equal 0

D. Begin another frequency sweep by varying M_{yy} from 0 kNm to -200 kNm at 0.3 Hz

E. Increase frequency from 0.30 Hz to 2 Hz over a period of 5 minutes

F. Stop cycling M_{yy} moment and set M_{yy} to equal 0

G. Applied M_{yy} 0, vary M_{zz} from 0 kNm to 50 kNm at 0.30 Hz

H. Increase frequency from 0.30 Hz to 2 Hz over a period of 5 minutes

I. Stop cycling M_{zz} and set M_{zz} to equal 0

J. Begin another frequency sweep by varying M_{zz} from 0 kNm to 200 kNm at 0.3 Hz

K. Increase frequency from 0.30 Hz to 2 Hz over a period of 5 minutes

L. Stop cycling M_{zz} and set M_{zz} to equal 0

M. Begin another frequency sweep by varying M_{zz} from -200 to 200 kNm at 0.3 Hz

N. Increase frequency from 0.30 Hz to 2 Hz over a period of 5 minutes

O. Stop cycling M_{zz} and set M_{zz} to equal 0

5.4.3 Static Thrust Test

Phase 2 GRC tests explored the response of the drivetrain to thrust loads over a range of -20 kN to 100 kN. This range is reasonably representative of thrust loads during normal operating

conditions in the field. There is some potential for larger negative thrust loads in the field, however, which could have deleterious effects on the gearbox. Figure 16 shows that, under a sufficiently large negative thrust load, the mainshaft is expected to move upwind. If the gearbox motion does not follow the mainshaft exactly, the relative motion will change mesh patterns in the planetary stage. In Phase 3 tests, thrust is varied between -100 kN and +100 kN.

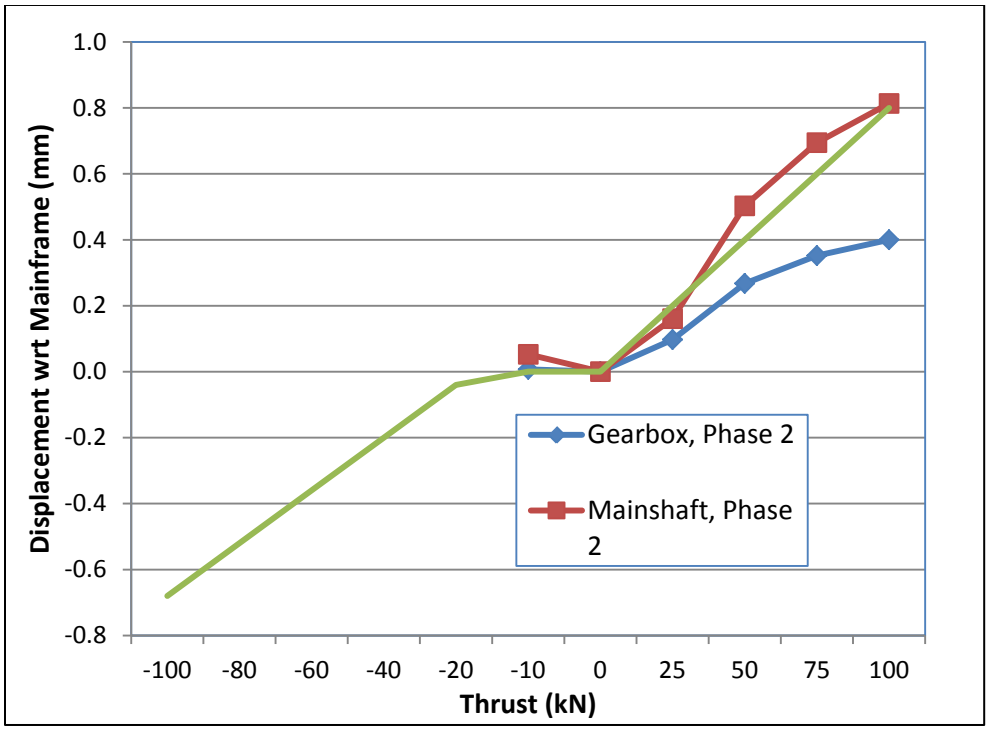

Figure 16. Response of GRC mainshaft and gearbox to thrust load

5.4.3.1 Test Procedure

Apply torque, bending moments, and thrust as follows. At each test condition, record 1 minute of 100 Hz data. At all test conditions where torque is applied, record 10 seconds of 5 kHz data to capture HSS measurements.

5.4.3.2 Torque, Bending Moments, and Thrust

1. Off-line, 100 rpm, normal direction, with zero applied moment
    A. Apply F_x from 0 to +100 in 20 kN steps
    B. Apply F_x from +100 to -100 in 20 kN steps
    C. Apply F_x from -100 to +100 in 20 kN steps
    D. Apply F_x from +100 to -100 in 20 kN steps
    E. Apply F_x from -100 to 0 in 20 kN steps
2. Off-line, 100 rpm, normal direction, with applied moments to zero mainshaft bending
    A. Apply F_x from 0 to -100 in 20 kN steps

B. Apply F_x from -100 to +100 in 20 kN steps

C. Apply F_x from +100 to 0 in 20 kN steps

3. Online, 25% rated torque, with M_{yy} zero
   A. Apply F_x from 0 to -100 in 20 kN steps
   B. Apply F_x from -100 to +100 in 20 kN steps
   C. Apply F_x from +100 to 0 in 20 kN steps
4. Online, 50% rated torque, with M_{yy} zero
   A. Apply F_x from 0 to -100 in 20 kN steps
   B. Apply F_x from -100 to +100 in 20 kN steps
   C. Apply F_x from +100 to 0 in 20 kN steps
5. Online, 75% rated torque, with M_{yy} zero
   A. Apply F_x from 0 to -100 in 20 kN steps
   B. Apply F_x from -100 to +100 in 20 kN steps
   C. Apply F_x from +100 to 0 in 20 kN steps
6. Online, 100% rated torque, with M_{yy} zero
   A. Apply F_x from 0 to -100 in 20 kN steps
   B. Apply F_x from -100 to +100 in 20 kN steps
   C. Apply F_x from +100 to 0 in 20 kN steps
7. Online, 100% rated torque, with applied moments to zero mainshaft bending
   A. Apply F_x from 0 to -100 in 20 kN steps
   B. Apply F_x from -100 to +100 in 20 kN steps
   C. Apply F_x from +100 to 0 in 20 kN steps

5.4.4 Trunnion Mount Axial Locking Test

Figure 16 shows that the gearbox moved in response to thrust loading, but not as much as the mainshaft moved. This is expected because the gearbox position relative to the mainshaft is constrained by friction in the planetary stage mesh when torque is applied and by shoulders on the carrier cylindrical roller bearings when no torque is present. For the gearbox to move, these internal forces must overcome the friction between the trunnion pins and the trunnion blocks, which resists gearbox motion. The extent of gearbox motion, however, can be limited by eventual contact between a steel sleeve on the trunnion pin and the inner surfaces of the trunnion blocks or can be constrained entirely by the trunnion pins if they become corroded and effectively “lock” the gearbox in place. Should either of these conditions occur, thrust loads will likely cause greater displacements of the mainshaft relative to the gearbox housing and greater displacements of the carrier relative to the ring gear.

This test explores the effects of this “locked” condition. Specifically, the loads in the ring gear teeth could increase or the load distribution might shift to an edge-loading condition. Similarly,

the loads in the planet bearings could increase or become more unevenly distributed among the planets or between the upwind and downwind bearings.

In the first part of this test, the gearbox housing is pulled upwind with moderate force to load the carrier bearing and main bearing. Shims then are installed between the trunnion sleeves and the downwind trunnion blocks. Then the NTL applies positive (downwind) thrust to measure the effects when the gearbox is prevented from following the mainshaft as it moves downwind.

Next the constraint is reversed. After removal of the shims, the housing is pushed downwind. Shims then are installed between the trunnion sleeves and the upwind trunnion blocks. Then negative (upwind) thrust is applied. Torque is limited to 50% of rated and test duration is limited to minimize damage in case the carrier bearings are adversely loaded.

5.4.4.1 Test Procedure

Apply torque, bending moments, and thrust as follows. At each test condition, record 1 minute of 100 Hz data. At all test conditions where torque is applied, record 10 seconds of 5 kHz data to capture HSS measurements.

5.4.4.2 Torque, Bending Moments, and Thrust

1. Off-line, 1,800 rpm, normal direction, with M_{yy} and M_{zz} zero
    A. Apply -100 kN F_x
    B. Stop rotation and lock out drive
    C. Install shims between the trunnion pin sleeves and the downwind trunnion blocks
    D. Resume rotation at 1,800 rpm
    E. Apply F_x from -100 to +100 in 20 kN steps
    F. Apply F_x from +100 to -100 in 20 kN steps
2. Online, 50% rated torque, with M_{yy} and M_{zz} zero
    A. Apply F_x from -100 to +100 in 20 kN steps
    B. Apply F_x from +100 to -100 in 20 kN steps
    C. Stop rotation and lock out drive
    D. Remove shims
3. Off-line, 1,800 rpm, normal direction, with M_{yy} and M_{zz} zero
    A. Apply +100 kN F_x
    B. Stop rotation and lock out drive
    C. Install shims between the trunnion pin sleeves and the upwind trunnion blocks
    D. Resume rotation at 1,800 rpm
    E. Apply F_x from +100 to -100 in 20 kN steps
    F. Apply F_x from -100 to +100 in 20 kN steps

4. Online, 50% rated torque, with M_{yy} and M_{zz} zero
    A. Apply F_x from +100 to -100 in 20 kN steps
    B. Apply F_x from -100 to +100 in 20 kN steps
    C. Stop rotation and lock out drive
    D. Remove shims

5.4.5 Dynamic Thrust Test

Some GRC participants have suggested that quickly changing thrust forces could affect bearings and teeth mesh in ways not seen under steady-state conditions. This test explores that possibility by using the NTL device to apply sinusoidal thrust forces of varying magnitude and frequency.

5.4.5.1 Test Procedure

Apply torque and non-torque bending moments as follows. At each test condition, record 1 minute of 100 Hz data. During each frequency sweep every 30 seconds, record 10 seconds of 5 kHz data to capture HSS measurements.

5.4.5.2 Torque and Non-Torque Bending Moments

1. Off-line, 1,800 rpm, normal direction
    A. Applied M_{yy} and M_{zz} 0, vary F_x from 0 kN to +50 kN at 0.30 Hz
    B. Increase frequency from 0.30 Hz to 2 Hz over a period of 5 minutes
    C. Stop cycling F_x
    D. Begin another frequency sweep by varying F_x from -50 kN to +50 kN at 0.3 Hz
    E. Increase frequency from 0.30 Hz to 2 Hz over a period of 5 minutes
    F. Stop cycling F_x
2. Online, 25% rated torque
    A. Applied M_{yy} and M_{zz} 0, vary F_x from 0 kN to +50 kN at 0.30 Hz
    B. Increase frequency from 0.30 Hz to 2 Hz over a period of 5 minutes
    C. Stop cycling F_x
    D. Begin another frequency sweep by varying F_x from -50 kN to +50 kN at 0.3 Hz
    E. Increase frequency from 0.30 Hz to 2 Hz over a period of 5 minutes
    F. Stop cycling F_x
3. On-line, 100% rated torque
    A. Applied M_{yy} and M_{zz} 0, vary F_x from 0 kN to +50 kN at 0.30 Hz
    B. Increase frequency from 0.30 Hz to 2 Hz over a period of 5 minutes
    C. Stop cycling F_x
    D. Begin another frequency sweep by varying F_x from -50 kN to +50 kN at 0.3 Hz

E. Increase frequency from 0.30 Hz to 2 Hz over a period of 5 minutes

F. Stop cycling F_x

5.5 HSS Radial Misalignment Test

A significant number of failures of wind turbine gearboxes occur in the high-speed shaft bearings. Overload of these bearings is a possible cause of bearing-life reduction, and additional studies have examined the potential for gearbox-generator misalignment as a potential contributor [6] [7]. This test series investigates the potential for radial (also called parallel) misalignment of the generator relative to the gearbox to contribute to the high frequency of these failures by measuring the loads on the HSS TRBs in both aligned and radial misalignment conditions.

Figure 17 shows the commonly used arrangement on the GRC drivetrain. The low-speed stage, with a planet carrier (red), is partially visible on the right side of the semitransparent gearbox. The high-speed gear mesh is visible at the top of the gearbox, with the large-diameter gear on the intermediate shaft closest to the front and the smaller-diameter pinion on the high-speed shaft immediately behind it. The high-speed shaft extends to the left out of the gearbox and ends with a flange that supports the brake disk. In this picture, the generator (blue) is located to the left. The high-speed coupling is mounted between the brake disk and the generator. The high-speed coupling uses flexible, “dog-bone”–style links to allow axial, angular, and radial misalignment of the gearbox high-speed shaft relative to the generator shaft.

Three factors might contribute increased bearing loads leading to these bearing failures. The three factors are:

- An excessive misalignment of the gearbox high-speed and generator shafts, which would impart additional loads due to the coupling link stiffness
- A mass imbalance of the brake disk, which would impart additional radial loads
- The nature of the current brake disk, which is located on only one side of the brake disk rather than both sides imparting additional radial loads.

In Phase 2, tests were conducted in which the generator was purposely misaligned with the gearbox. The instrumentation that was installed to measure reaction on the gearbox HSS did not perform as planned, however, so new sensors and new components of the data-acquisition system are being installed for Phase 3 testing.

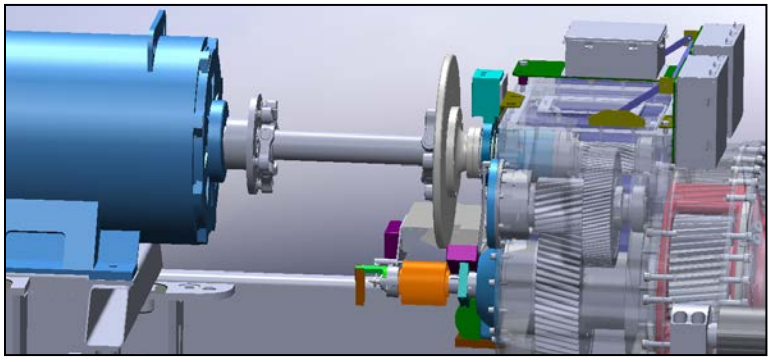

Figure 17. High-speed coupling with flexible “dog bone” links

The test matrix for this study includes the baseline and misaligned conditions listed below. These cases exercise the flexible links in the high-speed coupling to their intermittent load limit and to increase the loads on the HSS TRBs. The allowable angular misalignment conditions listed below are from published values for the CENTALINK CL-60 series coupling [8].

- Generator aligned at no-load conditions
- Generator vertically offset by 5 mm (coupling misalignment = ½°)
- Generator vertically offset by 11 mm (coupling misalignment = 1°)
- Generator vertically offset by 33 mm (coupling misalignment = 3°)

Note that each case is a radial misalignment condition. Additionally, 1° angular misalignment is the maximum allowed for continuous operation by the coupling manufacturer, and 3° angular misalignment is the maximum allowed for transient operation. These load cases should apply 24% and 73%, respectively, of the combined radial load from the HSS-ISS gear mesh on the HSS TRBs.

Prior to the start of this test series, all applied loads to the gearbox are removed and the HSS brake is rotated to unload the GRC mainshaft. Then the generator is carefully aligned with the HSS. A newly purchased laser alignment tool will be used for this purpose. After alignment, all proximity sensors on the generator and high-speed shaft are set to midrange, and their offsets are set to zero. All generator and HSS motion is relative to this position. After placing shims for each test case, the generator alignment is checked and recorded with the laser alignment tool.

5.5.1.1 Test Procedure

Apply torque and non-torque bending moments as follows. At each test condition, record 1 minute of 100 Hz data and record 10 seconds of 5 kHz data to capture HSS measurements.

5.5.1.2 Torque and Non-Torque Bending Moments

1. Generator aligned
    A. At 100 rpm, off-line, take one data set
    B. At 1,800 rpm and no applied NTL, step torque from 25% to 100% rated torque in 25% rated torque steps
    C. At 100% rated torque, apply M_{yy} of -200 and +200 kNm
    D. At 100% rated torque, apply M_{zz} of -200 and +200 kNm
    E. Take generator off-line and slow to 100 rpm for a second, slow-roll data set
2. Generator vertically offset by 5 mm (coupling misalignment = ½°)
    A. At 100 rpm, off-line, take one data set
    B. At 1,800 rpm and no applied NTL, step torque from 25% to 100% rated torque in 25% rated torque steps
    C. At 100% rated torque, apply M_{yy} of -200 and +200 kNm
    D. At 100% rated torque, apply M_{zz} of -200 and +200 kNm

3. Generator vertically offset by 11 mm (coupling misalignment = 1°)
    A. At 100 rpm, offline, take one data set
    B. At 1,800 rpm and no applied NTL, step torque from 25% to 100% rated torque in 25% rated torque steps
    C. At 100% rated torque, apply M_{yy} of -200 and +200 kNm
    D. At 100% rated torque, apply M_{zz} of -200 and +200 kNm
4. Generator vertically offset by 33 mm (coupling misalignment = 3°)
    A. At 100 rpm, offline, take one data set
    B. At 1,800 rpm and no applied NTL, step torque from 25% to 100% rated torque in 25% rated torque steps
    C. At 100% rated torque, apply M_{yy} of -200 and +200 kNm
    D. At 100% rated torque, apply M_{zz} of -200 and +200 kNm

5.6 Field Representative Test: Dynamic Torque and Non-Torque Loads

Wind turbine drivetrain loads vary in response to turbulent winds passing through the rotor and as a function of the operating state of the wind turbine. It is possible that, within these variations, some events cause damage to the drivetrain beyond that predicted by standard models. It would be beneficial if these events could be identified in dynamometer testing, assuming that the dynamometer can be operated in a manner that truly duplicates conditions in the field. In this test series, the ability of the dynamometer to accurately duplicate field loads on the GRC drivetrain is examined. Importantly, during testing some events can cause unexpected responses within the gearbox.

It is expected that the dynamometer's capability to duplicate dynamic oscillations in torque loading will be enhanced by a new variable frequency drive for the dynamometer motor. The new VFD is capable of accepting torque commands at frequencies as high as 400 Hz. The old VFD was limited to frequencies below about 2 Hz. During this test, this new capability should be sufficient to reproduce all the frequencies of interest and to counteract test-specific driveline resonances.

Common wind turbine design methods investigate many design load cases (DLCs). These represent the variety of wind and turbine state conditions likely to be encountered during the turbine's lifetime. The International Electrotechnical Commission (IEC) wind turbine design standard (61400-1) lists a variety of DLCs that should be analyzed during the design of a wind turbine. Field loads tests are used to verify that the turbine operates as designed for some of the load cases [9]. Similarly, dynamometer tests can be conducted to verify the design. In GRC Phase 3 testing, we have selected a subset of the DLCs for investigation, as shown in Table 3. NREL plans to determine how well the dynamometer can reproduce the input speed, torque, and non-torque load inputs to the drivetrain. Example time series are provided in Appendix C.

Table 3. Field Conditions to be Simulated in the Dynamometer

Situation	Load Case	Condition	Dynamometer Tests
Power production	DLC 1.1	NTW, $V_{wind,average}$ = 5 m/s	2
	DLC 1.1	NTW, $V_{wind,average}$ = 10 m/s	2
	DLC 1.1	NTW, $V_{wind,average}$ = 15 m/s	2
	DLC 1.1	NTW, $V_{wind,average}$ = 20 m/s	2
	DLC 1.1	NTW, $V_{wind,average}$ = 25 m/s	2
Start up	DLC 3.1	NWP, Rotor acceleration = 2.5 rpm/min	2
	DLC 3.1	NWP, Rotor acceleration = 5 rpm/min	2
	DLC 3.1	NWP, Rotor acceleration = 10 rpm/min	2
Normal shut down, tip brakes only	DLC 4.1	NWP	2
Emergency shutdown,	DLC 5.1	NTW	2
tip brakes and HSS brake	DLC 5.1	NTW	2
Generator shift up	Non DLC	NWP, Rotor acceleration = 2.5 rpm/min	2
Generator shift down	Non DLC	NWP, Rotor acceleration = 2.5 rpm/min	2

For each test condition identify a field-test dataset. Extract a time-series file of speed, torque, pitch, and yaw. Use this time-series file as input to the VFD and NTL controller. Program transitions between VFD torque control and speed control as required. Program an “apply-brake” signal as required for emergency-stop simulations.

Apply torque and non-torque bending moments per the time-series input file. For each power-production test, record 1 minute of 100 Hz data and record 10 seconds of 5 kHz data to capture HSS measurements. For startup and generator shift tests, record 100 Hz data for the duration of the test and record 5 kHz data starting just prior to cut-in of the generator. For normal shutdown tests, record 5 kHz data starting just before issuing the shutdown command and ending after disconnect oscillations dissipate. For emergency shutdown tests, record 5 kHz data starting just before issuing the shutdown command and ending after stopping oscillations dissipate.

5.7 Campbell Diagram Measurement Test

This test series is intended to build upon the results obtained to date by collecting vibration data while operating at various speeds and torque levels. Vibration data are often shown as a spectrum which presents the energy as a function of frequency, as seen in Figure 18. In these plots, peaks are of special interest and can be the result of a resonance or forced excitation.

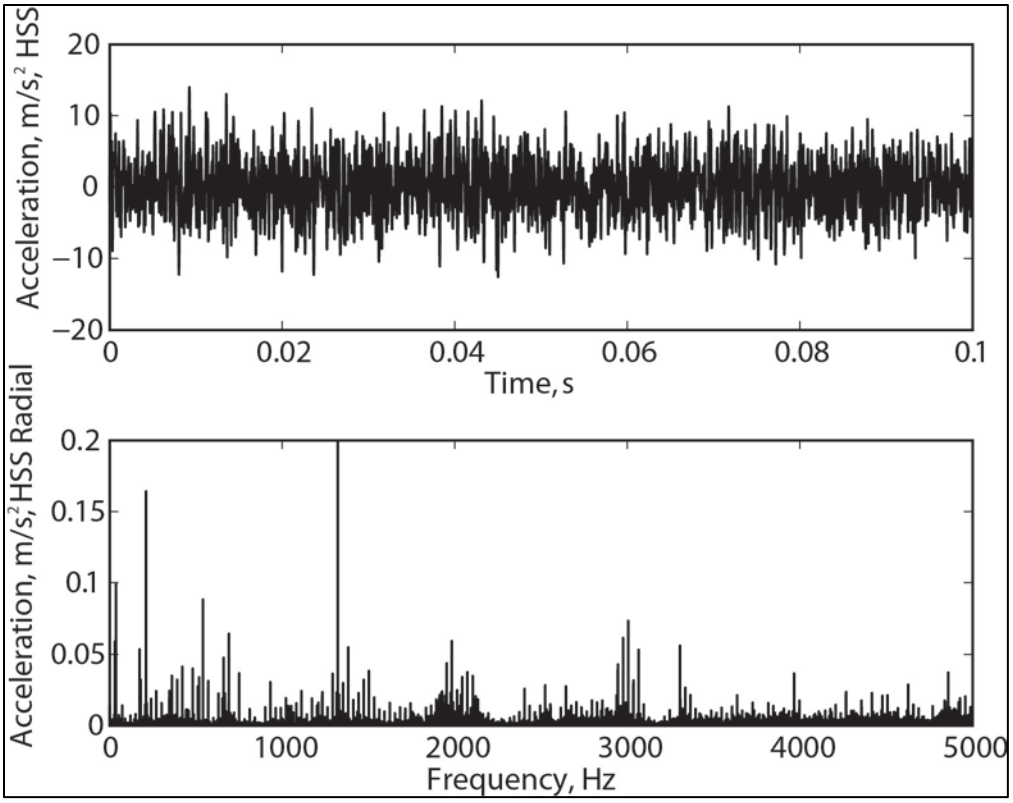

Figure 18. Sample time series and vibration spectrum
(***Reproduced from http://en.wikipedia.org/wiki/File:Voice_waveform_and_spectrum.png***)

In rotating equipment such as the GRC drivetrain, the excitations change with rotational speed [10]. This relationship can be shown in waterfall plots or in Campbell diagrams, such as that in Figure 19. A Campbell diagram plots frequency peaks against rotational frequency. In a Campbell diagram, excitation frequencies such as gear meshing orders can be identified as diagonal lines intersecting the origin and resonances generally are horizontal lines at a fixed frequency. Intersections of excitation lines with resonance lines typically indicate speeds to be avoided during normal operation. In this test, however, they represent an opportunity to identify phenomena which otherwise might be lost in the spectrum plot acquired at a given speed.

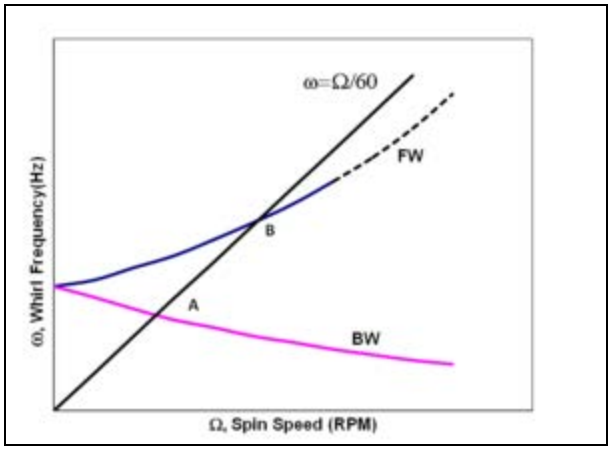

Figure 19. Example of a Campbell diagram; BW and FW represent resonances that are slightly dependent upon spin speed and the origin-intersecting line represents frequencies at 1P. (*Reproduced from http://en.wikipedia.org/wiki/File:Campbelldiagram.png*)

In this test, excitations are expected at 1P (1 times rotational frequency of LSS) and higher due to rotational frequencies of the planets, sun, intermediate- , and high-speed shafts. Higher frequency excitations are expected due to transmission error in tooth meshing and other phenomena. Inasmuch as torque should affect resonance frequencies, this test is preferably conducted at several torque levels. Because of equipment limitations, however, the test currently is planned for only low-torque (~5% rated) using an eddy-current brake on the high-speed shaft.

Tests conducted in Phase 2 showed significant energy peaks up to 2,800 Hz. Therefore accelerometers must have a frequency range of 6 kHz or higher. Six accelerometers are used, as indicated in Table 4. They are positioned as shown in Figure 20.

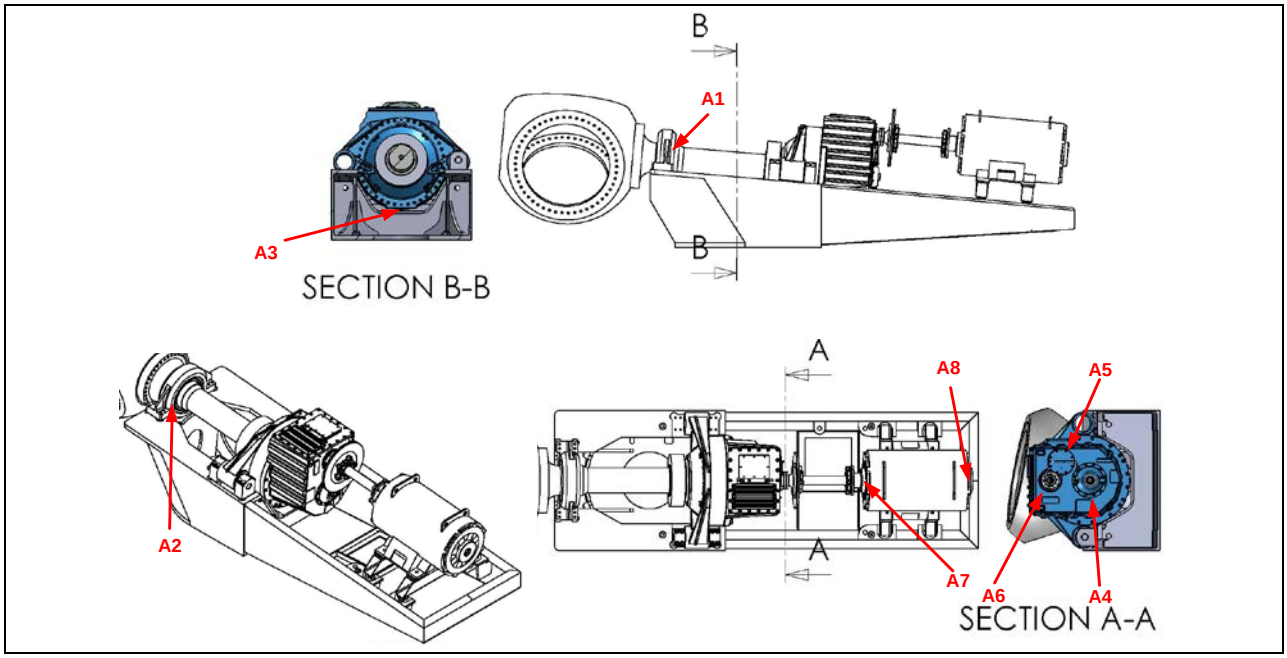

Figure 20. Accelerometer locations for Phase 3 vibration testing

Table 4. List of Accelerometers for Vibration Testing

Sensor Notation	Description
A3	Planet gear radial
A4	LSS radial
A5	ISS radial
A6	HSS radial
A7	Generator DE radial
A8	Generator NDE radial

No non-torque loads are applied in this test series. The dynamometer is operated in speed-control mode with torque controlled by setting the eddy-current brake.

1. Install and verify operation of accelerometers
2. Install and verify operation of eddy-current brake
3. Set dynamometer speed ramp to 360 rpm per minute on HSS
4. Set DAS to sample and record drivetrain operating conditions at 100 Hz
5. Set accelerometer DAS to sample and record at 40 kHz
6. Conduct the test as follows:
    A. Start DAS
    B. Start dynamometer motor and ramp to 2,000 rpm
    C. Shut down
    D. Repeat test once

6 References

1. Link, H.; LaCava, W.; van Dam, J.; McNiff, B.; Sheng, S.; Wallen, R.; McDade, M.; Lambert, S.; Butterfield, S.; Oyague, F. *Gearbox Reliability Collaborative Project Report: Findings from Phase 1 and Phase 2 Testing.* NREL/TP-5000-51885. Golden, CO: National Renewable Energy Laboratory, 2011.

2. Sheng, S.; Link, H.; LaCava, W.; van Dam, J.; McNiff, B.; Veers, P.; Keller, J. *Wind Turbine Drivetrain Condition Monitoring During GRC Phase 1 and Phase 2 Testing*. NREL/TP-5000-52748. Golden, CO: National Renewable Energy Laboratory, 2011.

3. "Dynamometer Testing (Fact Sheet), National Wind Technology Center (NWTC)." National Renewable Energy Laboratory, 2010. Accessed Nov. 20, 2012: http://www.nrel.gov/docs/fy11osti/45649.pdf.

4. McNiff, B.; van Dam, J.; Oyague, F.; Wallen, R.; Sheng, S.; Lambert, S.; Link, H. *Gearbox Reliability Collaborative Phase 2 Test Plan.* National Renewable Energy Laboratory, 2010. (internal only).

5. Keller, J.; Guo, Y.; McNiff, B.; LaCava, W.; Link, H. "Gearbox Reliability Collaborative Phase 1 and 2: Testing and Modeling Results." *International Conference on Noise and Vibration Engineering*; September 17–19, 2012, Leuven, Belgium.

6. Malkin, M.; Byme, A. "Torque-Induced Shaft Misalignment as a Potential Source of Gearbox High-Speed Bearing Failure." *American Wind Energy Conference & Exhibition*; June 3–6, 2012, Atlanta, Georgia.

7. Whittle, M.; Shin, W.; Trevelyan, J.; Wu, J. "A Parametric Study of the Effect of Generator Misalignment on Bearing Fatigue Life in Wind Turbines." *European Wind Energy Conference & Exhibition*; March 14–17, 2011, Brussels, Belgium.

8. "Product Catalog CL-07-08." CENTA. Accessed Feb. 21, 2013: http://www.centa.info/data/products/43/int/cl-07-08_01.pdf.

9. International Electrotechnical Commission. *61400-4:2012(E) Wind Turbines—Part 4: Design Requirements for Wind Turbine Gearboxes*. Geneva, Switzerland : International Organization for Standardization, 2012.

10. Helsen, J. *The Dynamics of High Power Density Gear Units with Focus on the Wind Turbine Application*. Leuven, Belgium: Katholieke Universiteit Leuven, 2012.

Appendix A. Signal List

Location	Nomenclature	Expanded Nomenclature	Sensor
Mainshaft	LSS_TQ	Torque	Strain gage
Mainshaft	MSBM_YY	Bending Z-axis	Strain gage
Mainshaft	MSBM_ZZ	Bending Y-axis	Strain gage
Mainshaft	LSS_Az	Azimuth	Encoder
Mainshaft	LSS_Speed	Speed	Encoder
Mainshaft	LSS_AZ_synch	Azimuth synch	Encoder
Mainshaft	Main_Shaft_Axial	Displacement X	Proximity
Housing	Trunion_Z_stbd	Displacement Z starboard	Proximity
Housing	Trunion_Z_port	Displacement Z port	Proximity
Housing	Trunion_My_bottom	Displacement X bottom	Proximity
Housing	Trunion_Y_port	Displacement Y port	Proximity
Housing	Trunion_X_stbd	Displacement X starboard	Proximity
Housing	Trunion_X_port	Displacement X port	Proximity
Housing	Case_A_XX	Strain X, A	Strain gage
Housing	Case_A_YY	Strain Y, A	Strain gage
Housing	Case_A_45	Strain 45°, A	Strain gage
Housing	ACC_TopX	Acceleration, X top	Accelerometer
Housing	ACC_PortX	Acceleration, X port	Accelerometer
Housing	ACC_PortY	Acceleration, Y port	Accelerometer
Housing	ACC_PortZ	Acceleration, Z port	Accelerometer
Housing	ACC_StbdX	Acceleration, X starboard	Accelerometer
Housing	ACC_StbdY	Acceleration, Y starboard	Accelerometer
Housing	ACC_StbdZ	Acceleration, Z starboard	Accelerometer
Ring	Ring_0	Strain, ring gear teeth, 0°, 1st set	Strain gage
Ring	Ring_0a	Strain, ring gear teeth, 0°, 2nd set	Strain gage
Ring	Ring_120	Strain, ring gear teeth, 120°, 1st set	Strain gage
Ring	Ring_120a	Strain, ring gear teeth, 120°, 2nd set	Strain gage
Ring	Ring_240	Strain, ring gear teeth, 240°, 1st set	Strain gage
Ring	Ring_240a	Strain, ring gear teeth, 240° 2nd set	Strain gage
Ring	EXT_KHB_23	Strain, external, 23°	Strain gage
Ring	EXT_KHB_46	Strain, external, 46°	Strain gage
Ring	EXT_KHB_69	Strain, external, 69°	Strain gage
Ring	EXT_KHB_92	Strain, external, 92°	Strain gage
Ring	EXT_KHB_115	Strain, external, 115°	Strain gage
Ring	EXT_KHB_149	Strain, external, 149°	Strain gage
Ring	EXT_KHB_184	Strain, external,184°	Strain gage
Ring	EXT_KHB_207	Strain, external, 207°	Strain gage
Ring	Ring_Local_45	Strain, circumferential, 45°	Strain gage

Location	Nomenclature	Expanded Nomenclature	Sensor
Ring	Ring_Local_135	Strain, circumferential, 135°	Strain gage
Ring	Ring_Local_225	Strain, circumferential, 225°	Strain gage
Ring	Ring_Local_315	Strain, circumferential, 315°	Strain gage
Carrier	Carrier_317	Displacement X 317°	Proximity
Carrier	Carrier_047	Displacement X 047°	Proximity
Carrier	Radial_310	Displacement Radial 310°	Proximity
Carrier	Radial_040	Displacement Radial 40°	Proximity
Carrier	Carrier_137	Displacement, X 137°	Proximity
Carrier	Carrier_227	Displacement, X 227°	Proximity
Planet	PlanetB_RIM_0	Displacement, X, B, 0°	Proximity
Planet	PlanetB_RIM_90	Displacement, X, B, 90°	Proximity
Planet	PlanetB_RIM_180	Displacement, X, B, 180°	Proximity
Planet	PlanetC_RIM_0	Displacement, X, C, 0°	Proximity
Planet	PlanetC_RIM_90	Displacement, X, C, 90°	Proximity
Planet	PlanetC_RIM_180	Displacement, X, C, 180°	Proximity
Planet	PlanetA_Bearing_slip	Slip, Planet A, cage	Proximity
Planet	AU_Kb00_25	Strain, Planet A, upwind, 0°, 25%	Strain gage
Planet	AU_Kb00_75	Strain, Planet A, upwind, 0°, 75%	Strain gage
Planet	AD_Kb00_25	Strain, Planet A, downwind, 0°, 25%	Strain gage
Planet	AD_Kb00_75	Strain, Planet A, downwind, 0°, 75%	Strain gage
Planet	AU_Kb86_25	Strain, Planet A, upwind, 86°, 25%	Strain gage
Planet	AU_Kb86_75	Strain, Planet A, upwind, 86°, 75%	Strain gage
Planet	AD_Kb86_25	Strain, Planet A, downwind, 86°, 25%	Strain gage
Planet	AD_Kb86_75	Strain, Planet A, downwind, 86°, 75%	Strain gage
Planet	AU_Kb274_25	Strain, Planet A, upwind, 274°, 25%	Strain gage
Planet	AU_Kb274_75	Strain, Planet A, upwind, 274°, 75%	Strain gage
Planet	AD_Kb274_25	Strain, Planet A, downwind, 274°, 25%	Strain gage
Planet	AD_Kb274_75	Strain, Planet A, downwind, 274°, 75%	Strain gage
Planet	BU_Kb00_25	Strain, Planet B, upwind, 0°, 25%	Strain gage
Planet	BU_Kb00_75	Strain, Planet B, upwind, 0°, 75%	Strain gage
Planet	BD_Kb00_25	Strain, Planet B, downwind, 0°, 25%	Strain gage
Planet	BD_Kb00_75	Strain, Planet B, downwind, 0°, 75%	Strain gage
Planet	BU_Kb256_25	Strain, Planet B, upwind, 256°, 25%	Strain gage
Planet	BU_Kb256_75	Strain, Planet B, upwind, 256°, 75%	Strain gage
Planet	BD_Kb256_25	Strain, Planet B, downwind, 256°, 25%	Strain gage
Planet	BD_Kb256_75	Strain, Planet B, downwind, 256°, 75%	Strain gage
Planet	BU_Kb308_25	Strain, Planet B, upwind, 308°, 25%	Strain gage
Planet	BU_Kb308_75	Strain, Planet B, upwind, 308°, 75%	Strain gage
Planet	BD_Kb308_25	Strain, Planet B, downwind, 308°, 25%	Strain gage
Planet	BD_Kb308_75	Strain, Planet B, downwind, 308°, 75%	Strain gage

Location	Nomenclature	Expanded Nomenclature	Sensor
Planet	CU_Kb00_25	Strain, Planet C, upwind, 0°, 25%	Strain gage
Planet	CU_Kb00_75	Strain, Planet C, upwind, 0°, 75%	Strain gage
Planet	CD_Kb00_25	Strain, Planet C, downwind, 0°, 25%	Strain gage
Planet	CD_Kb00_75	Strain, Planet C, downwind, 0°, 75%	Strain gage
Planet	CU_Kb290_25	Strain, Planet C, upwind, 290°, 25%	Strain gage
Planet	CU_Kb290_75	Strain, Planet C, upwind, 290°, 75%	Strain gage
Planet	CD_Kb290_25	Strain, Planet C, downwind, 290°, 25%	Strain gage
Planet	CD_Kb290_75	Strain, Planet C, downwind, 290°, 75%	Strain gage
Planet	CU_Kb334_25	Strain, Planet C, upwind, 334°, 25%	Strain gage
Planet	CU_Kb334_75	Strain, Planet C, upwind, 334°, 75%	Strain gage
Planet	CD_Kb334_25	Strain, Planet C, downwind, 334°, 25%	Strain gage
Planet	CD_Kb334_75	Strain, Planet C, downwind, 334°, 75%	Strain gage
Planet	AU_temp0	Temperature, Planet A, upwind, 0°	Thermocouple
Planet	AD_temp86	Temperature, Planet A, downwind, 86°	Thermocouple
Planet	AU_temp86	Temperature, Planet A, upwind, 86°	Thermocouple
Planet	AD_temp274	Temperature, Planet A, downwind, 274°	Thermocouple
Planet	BU_temp0	Temperature, Planet B, upwind, 0°	Thermocouple
Planet	BD_temp0	Temperature, Planet B, downwind, 0°	Thermocouple
Planet	BU_temp256	Temperature, Planet B, upwind, 256°	Thermocouple
Planet	BD_temp256	Temperature, Planet B, downwind, 256°	Thermocouple
Planet	CU_temp0	Temperature, Planet C, upwind, 0°	Thermocouple
Planet	CD_temp0	Temperature, Planet C, downwind, 0°	Thermocouple
Planet	CU_temp290	Temperature, Planet C, upwind, 290°	Thermocouple
Planet	CD_temp290	Temperature, Planet C, downwind, 290°	Thermocouple
Planet	PlanetA_OR_temp	Temperature, Planet A, outer race	Thermocouple
Sun	SUN_radial_ZZ	Displacement, radial, Z	Proximity
Sun	SUN_radial_YY	Displacement, radial, Y	Proximity
ISS	ISS_Axial	Displacement, X	Proximity
ISS	ISS_aft_roller_temp	Temperature	IR sensor
HSS	HSS_UY_BM	Bending, upwind, YY	Strain gage
HSS	HSS_UZ_BM	Bending, upwind, ZZ	Strain gage
HSS	HSS_DY_BM	Bending, downwind, YY	Strain gage
HSS	HSS_DZ_BM	Bending, downwind, ZZ	Strain gage
HSS	HSS_exY_BM	Bending, External, YY	Strain gage
HSS	HSS_exZ_BM	Bending, External, ZZ	Strain gage
HSS	HSS_TQ	Torque	Strain gage
HSS	TRB_Up_00_A	Strain, upwind TRB, 0°, thin end	Strain gage
HSS	TRB_Up_00_B	Strain, upwind TRB, 0°, thick end	Strain gage

Location	Nomenclature	Expanded Nomenclature	Sensor
HSS	TRB_Up_90_A	Strain, upwind TRB, 90°, thin end	Strain gage
HSS	TRB_Up_90_B	Strain, upwind TRB, 90°, thick end	Strain gage
HSS	TRB_Up_180_A	Strain, upwind TRB, 180°, thin end	Strain gage
HSS	TRB_Up_180_B	Strain, upwind TRB, 180°, thick end	Strain gage
HSS	TRB_Up_270_A	Strain, upwind TRB, 270°, thin end	Strain gage
HSS	TRB_Up_270_B	Strain, upwind TRB, 270°, thick end	Strain gage
HSS	TRB_Dwn_00_D	Strain, downwind TRB, 0°, thin end	Strain gage
HSS	TRB_Dwn_00_C	Strain, downwind TRB, 0°, thick end	Strain gage
HSS	TRB_Dwn_90_D	Strain, downwind TRB, 90°, thin end	Strain gage
HSS	TRB_Dwn_90_C	Strain, downwind TRB, 90°, thick end	Strain gage
HSS	TRB_Dwn_180_D	Strain, downwind TRB, 180°, thin end	Strain gage
HSS	TRB_Dwn_180_C	Strain, downwind TRB, 180°, thick end	Strain gage
HSS	TRB_Dwn_270_D	Strain, downwind TRB, 270°, thin end	Strain gage
HSS	TRB_Dwn_270_C	Strain, downwind TRB, 270°, thick end	Strain gage
HSS	TEMP_TRB_Up	Temperature, upwind TRB	RTD
HSS	TEMP_TRB_Dwn	Temperature, downwind TRB	RTD
HSS	HSP_K1234	Strain, HSS pinion teeth, 1st set	Strain gage
HSS	HSP_Kabcd	Strain, HSS pinion teeth, 2nd set	Strain gage
Brake	BRK_azimuth	Azimuth	Encoder
Brake	BRK_speed	Speed	Encoder
Brake	BRK_X_225	Displacement, X, 225°	Proximity
Brake	BRK_X_315	Displacement, X, 315°	Proximity
Brake	BRK_X_45	Displacement, X, 45°	Proximity
Brake	BRK_YY	Displacement, Y	Proximity
Brake	BRK_ZZ	Displacement, Z	Proximity
Generator	GEN_X_45	Displacement, X, 45°	Proximity
Generator	GEN_X_225	Displacement, X, 225°	Proximity
Generator	GEN_X_315	Displacement, X, 315°	Proximity
Generator	GEN_YY	Displacement, Y	Proximity
Generator	GEN_ZZ	Displacement, Z	Proximity
Generator	Gen_Temp	Temperature, generator downwind bearing	RTD
Generator	HSS_Speed	Speed	Encoder
Generator	HSS_Az	Azimuth	Encoder
Mainframe	Frame_Z_stbd	Displacement, Z, starboard, in-line with generator flange	Proximity
Mainframe	Frame_Z_port	Displacement, Z, port, in-line with generator flange	Proximity
Controller	G_Contactor	Closed, large generator contactor	Relay
Controller	gg_Contactor	Closed, small generator contactor	Relay
Controller	Bypass_Contactor	Closed, soft-start bypass contactor	Relay

Location	Nomenclature	Expanded Nomenclature	Sensor
Controller	KW_electrical	Power, real	Potential Transformer / Current Transformer
Controller	KVAR_electrical	Power, reactive	Potential Transformer / Current Transformer
Lube system	Lube_Manifold_Temp	Temperature, distribution manifold	RTD
Lube system	Lube_Manifold_Pressure	Pressure, distribution manifold	Pressure
Lube system	Sump_Temp	Temperature, sump	RTD
Lube system	Lube_Flow_Dist	Flow rate, to distribution manifold	Flow
Lube system	Lube_Flow_Br_1	Flow rate, branch 1	Flow
Lube system	Lube_Flow_Br_2	Flow rate, branch 2	Flow
Lube system	Lube_Flow_Br_3	Flow rate, branch 3	Flow
Lube system	Lube_Particles	Particle counts	Particle counter
Dyno	TQ_Applied_Force	Force, torque arm 1	Load cell
Dyno	TQ_Applied_Force2	Force, torque arm 2	Load cell
Dyno	Dyno_Torque	Torque, torque spool	Strain gage
NTL	NTL_Port_displ	Displacement, port cylinder	Proximity
NTL	NTL_Port_force	Force, port cylinder	Load cell
NTL	NTL_Star_displ	Displacement, starboard cylinder	Proximity
NTL	NTL_Star_force	Force, starboard cylinder	Load cell
NTL	NTL_thrust_displ	Displacement, thrust	Proximity
NTL	NTL_thrust_star_force	Force, thrust starboard	Load cell
NTL	NTL_thrust_port_force	Force, thrust, port	Load cell
NTL	NTL_stab_link_eX	Strain, stabilizer link, X	Strain gage
NTL	NTL_stab_link_eY	Strain, stabilizer link, Y	Strain gage
NTL	Static_Loading_System_Force	Pressure, hydraulic	Pressure
NTL	NTL_DW_BM_Y	Mainshaft bending, downwind, Y	Strain gage
NTL	NTL_DW_BM_Z	Mainshaft bending, downwind, Z	Strain gage
NTL	NTL_UW_BM_Y	Mainshaft bending, upwind, Y	Strain gage
NTL	NTL_UW_BM_Z	Mainshaft bending, upwind, Z	Strain gage
NTL	NTL_DW_BM_X_Y	Flex coupling displacement, downwind, Y	Proximity
NTL	NTL_DW_BM_X_Z	Flex coupling displacement, downwind, Z	Proximity
NTL	NTL_UW_BM_X_Y	Flex coupling displacement, upwind, Y	Proximity
NTL	NTL_UW_BM_X_Z	Flex coupling displacement, upwind, Z	Proximity

Appendix B. Instrumentation Details

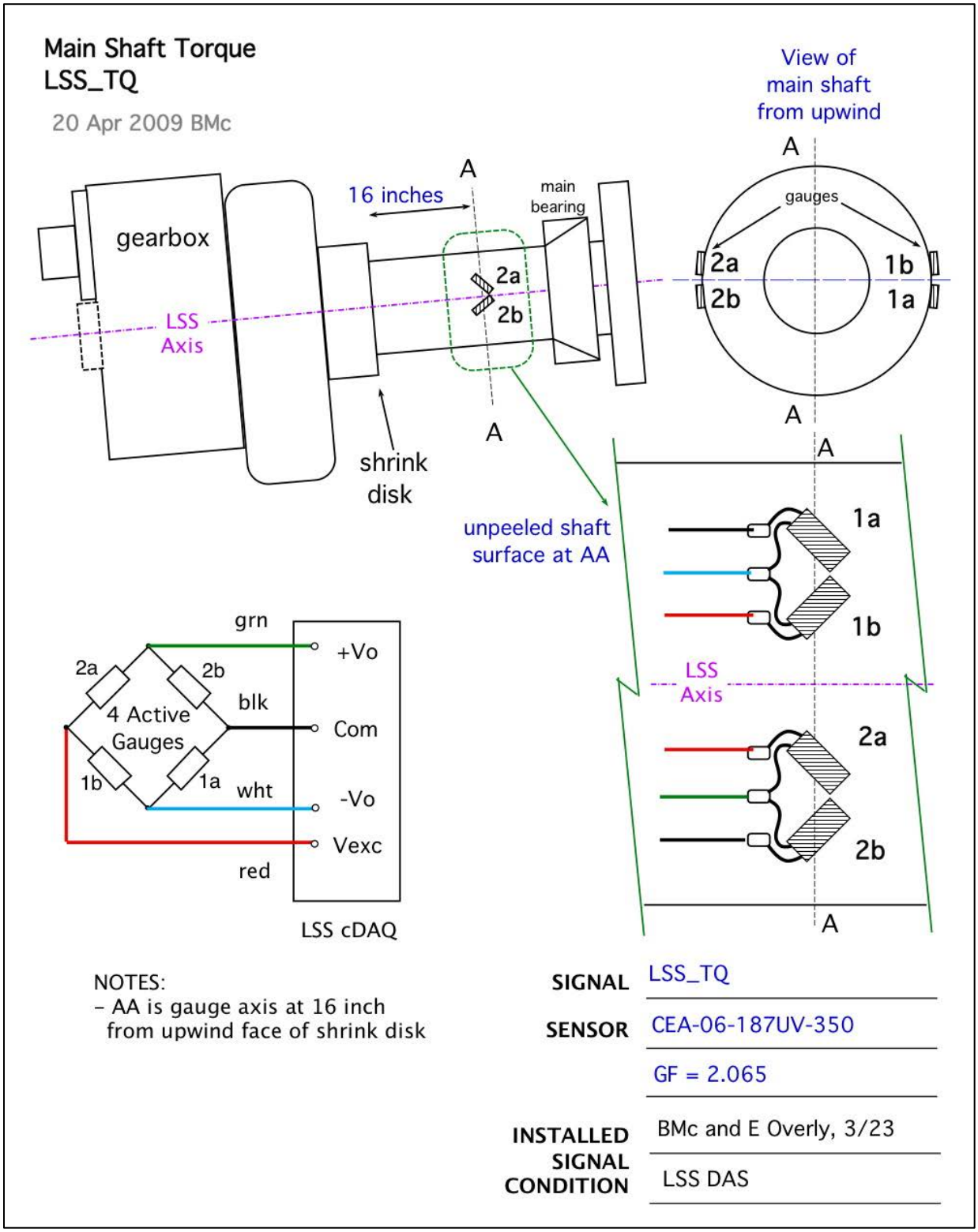

Figure B-1. Mainshaft torque

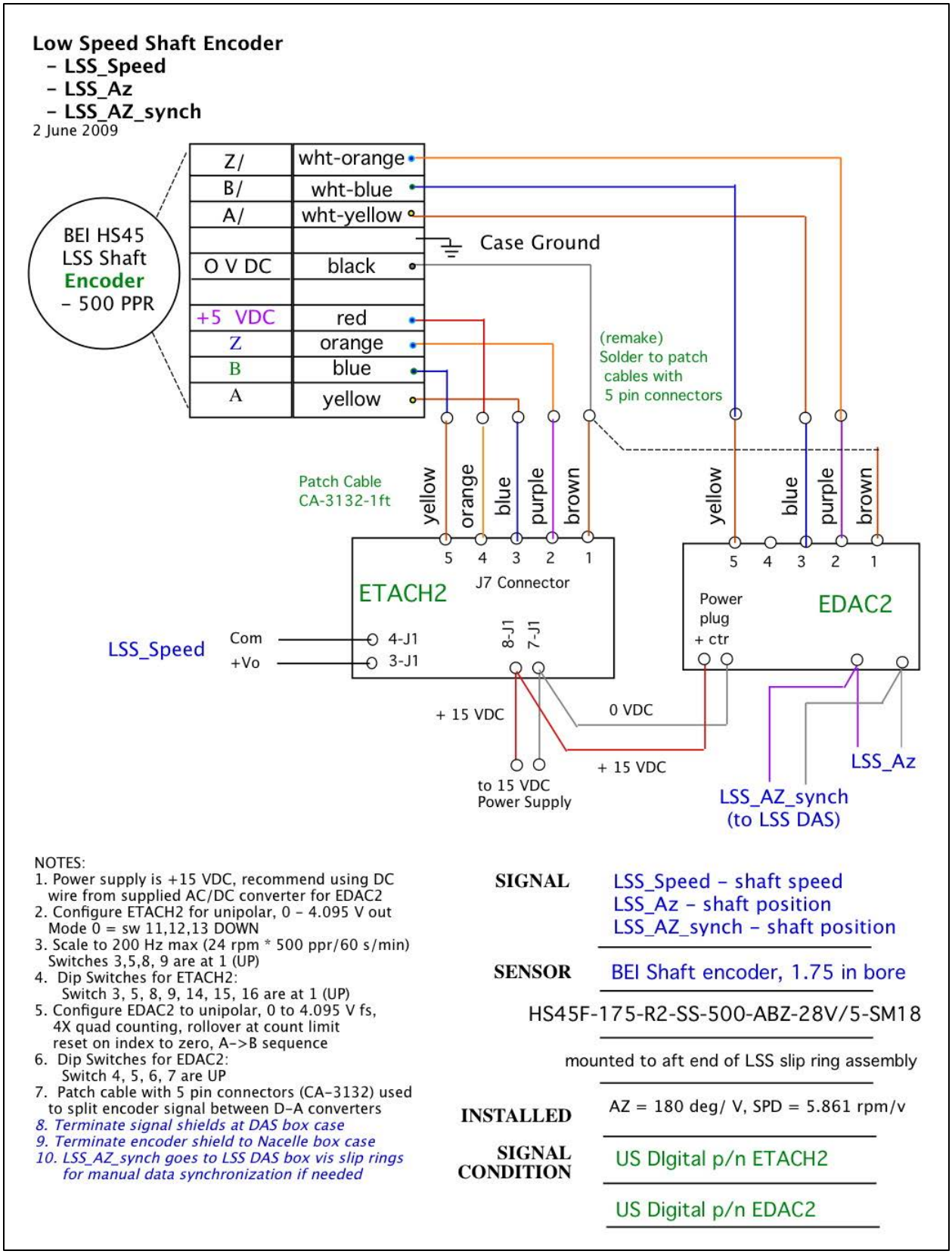

NOTES:
1. Power supply is +15 VDC, recommend using DC wire from supplied AC/DC converter for EDAC2
2. Configure ETACH2 for unipolar, 0 – 4.095 V out
   Mode 0 = sw 11,12,13 DOWN
3. Scale to 200 Hz max (24 rpm * 500 ppr/60 s/min)
   Switches 3,5,8, 9 are at 1 (UP)
4. Dip Switches for ETACH2:
   Switch 3, 5, 8, 9, 14, 15, 16 are at 1 (UP)
5. Configure EDAC2 to unipolar, 0 to 4.095 V fs, 4X quad counting, rollover at count limit reset on index to zero, A->B sequence
6. Dip Switches for EDAC2:
   Switch 4, 5, 6, 7 are UP
7. Patch cable with 5 pin connectors (CA-3132) used to split encoder signal between D-A converters
8. Terminate signal shields at DAS box case
9. Terminate encoder shield to Nacelle box case
10. LSS_AZ_synch goes to LSS DAS box vis slip rings for manual data synchronization if needed

SIGNAL	LSS_Speed – shaft speed LSS_Az – shaft position LSS_AZ_synch – shaft position
SENSOR	BEI Shaft encoder, 1.75 in bore
	HS45F-175-R2-SS-500-ABZ-28V/5-SM18
	mounted to aft end of LSS slip ring assembly
INSTALLED	AZ = 180 deg/ V, SPD = 5.861 rpm/v
SIGNAL CONDITION	US DIgital p/n ETACH2
	US Digital p/n EDAC2

Figure B-2. Mainshaft speed and azimuth

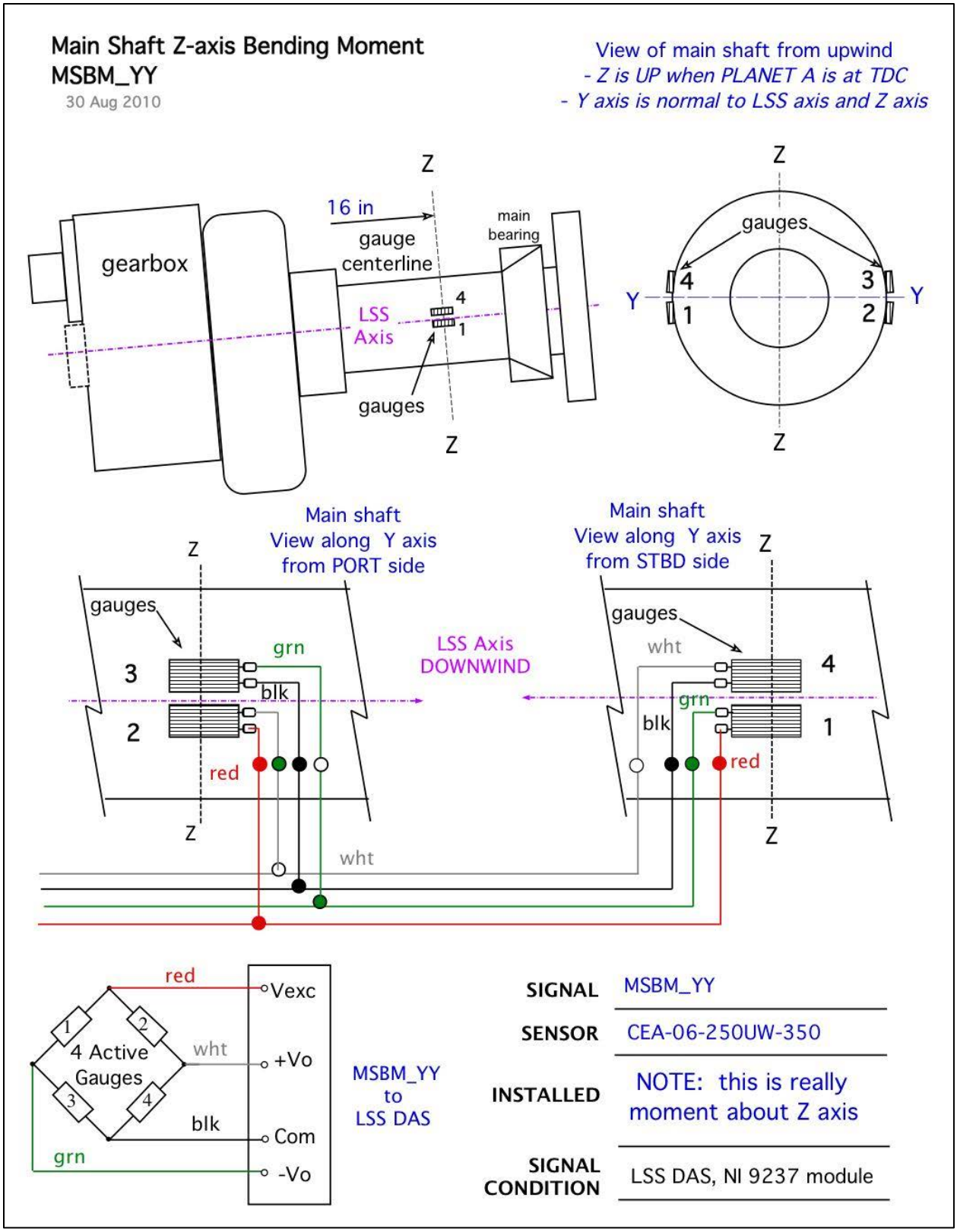

Figure B-3. Mainshaft Bending Z-axis

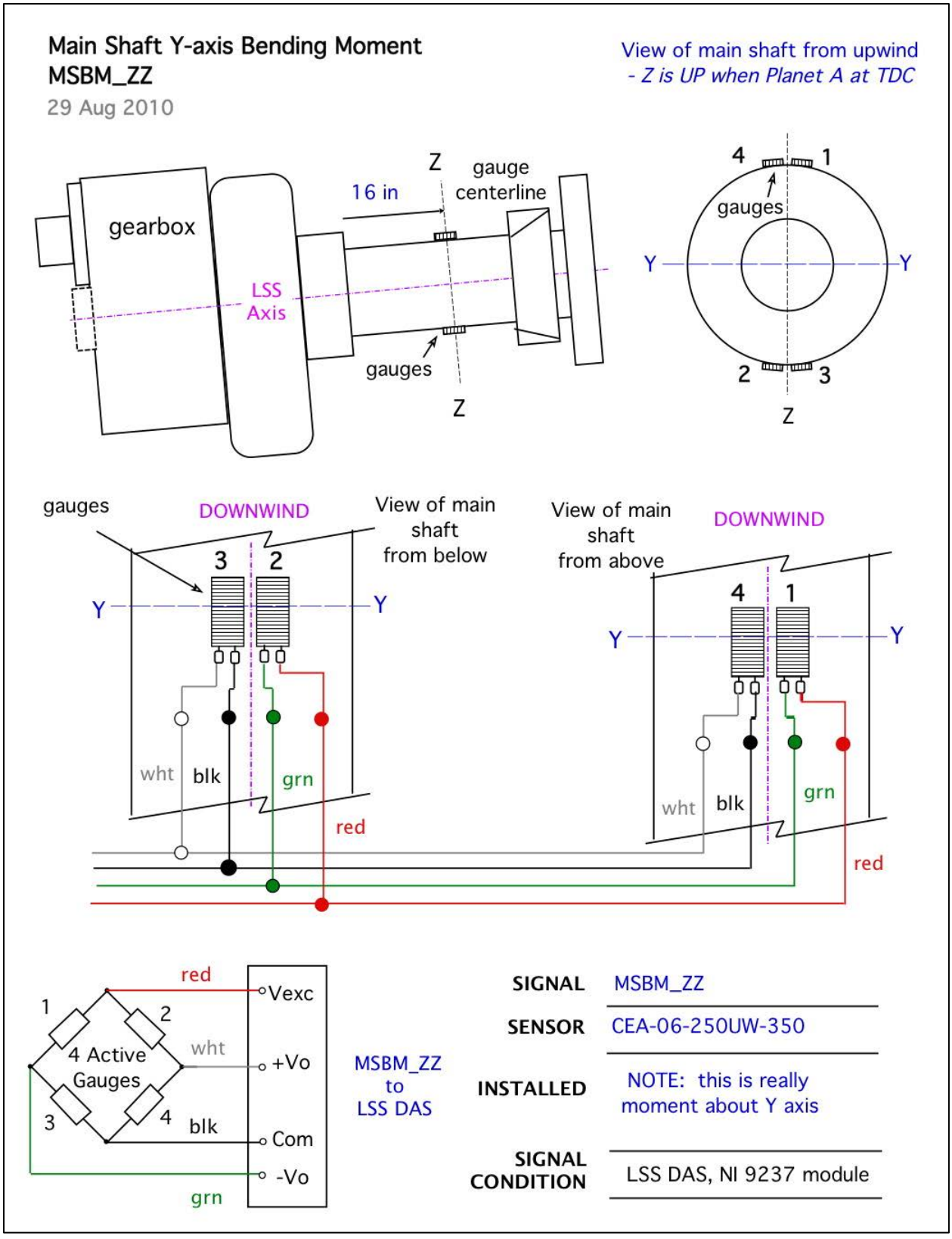

Figure B-4. Mainshaft Bending Y-axis

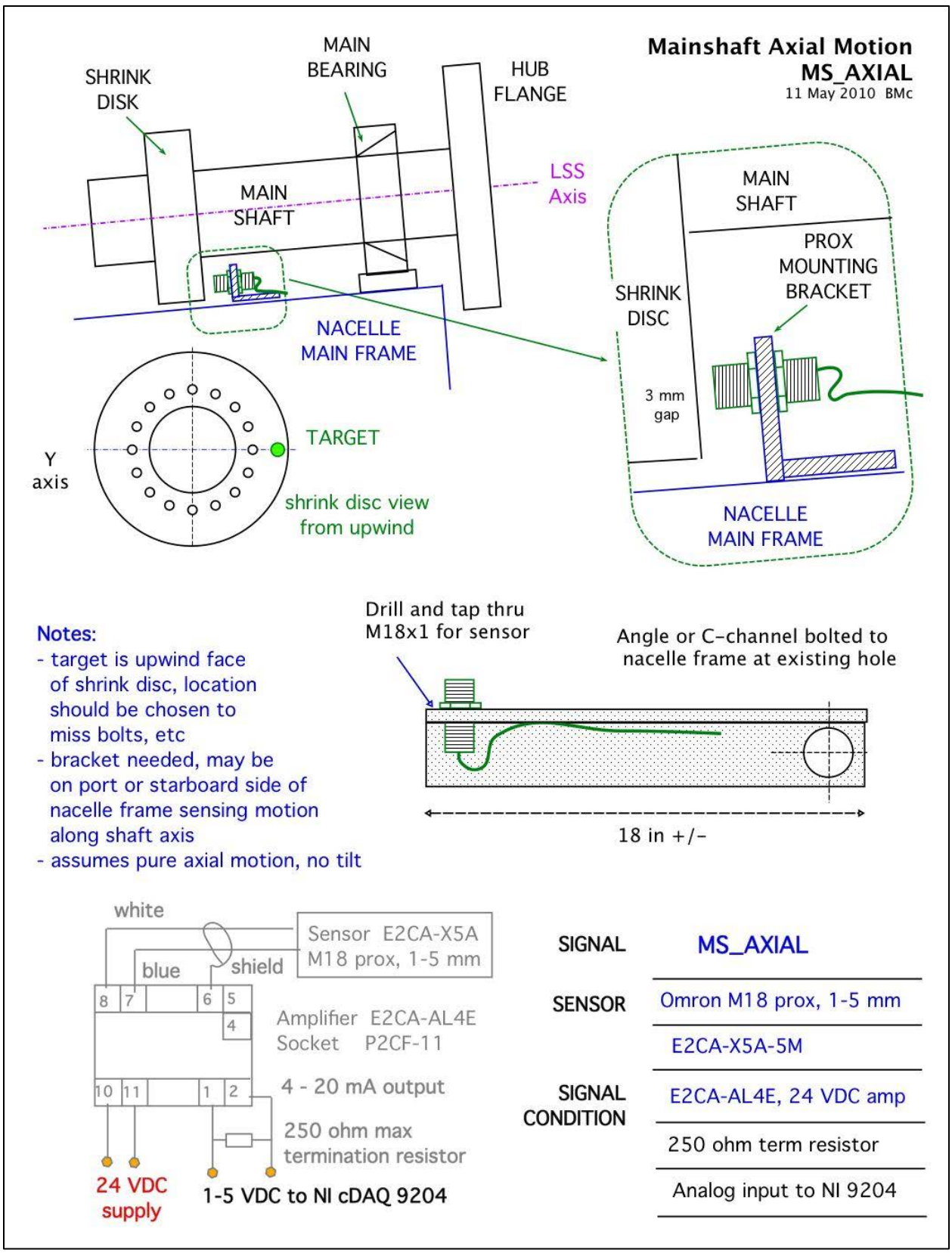

Figure B-5. Mainshaft axial motion

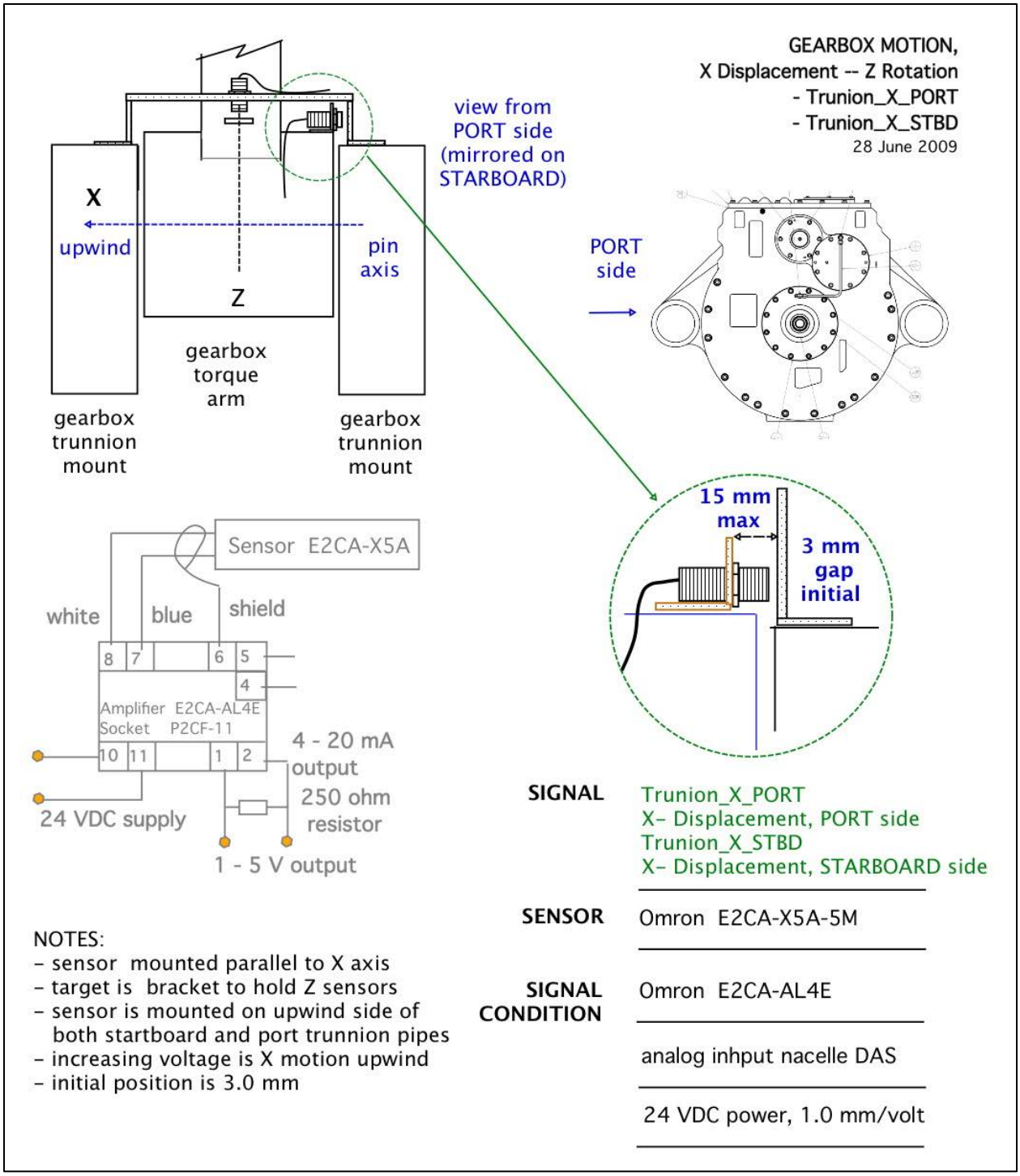

Figure B-6. Gearbox motion, XX at trunnion

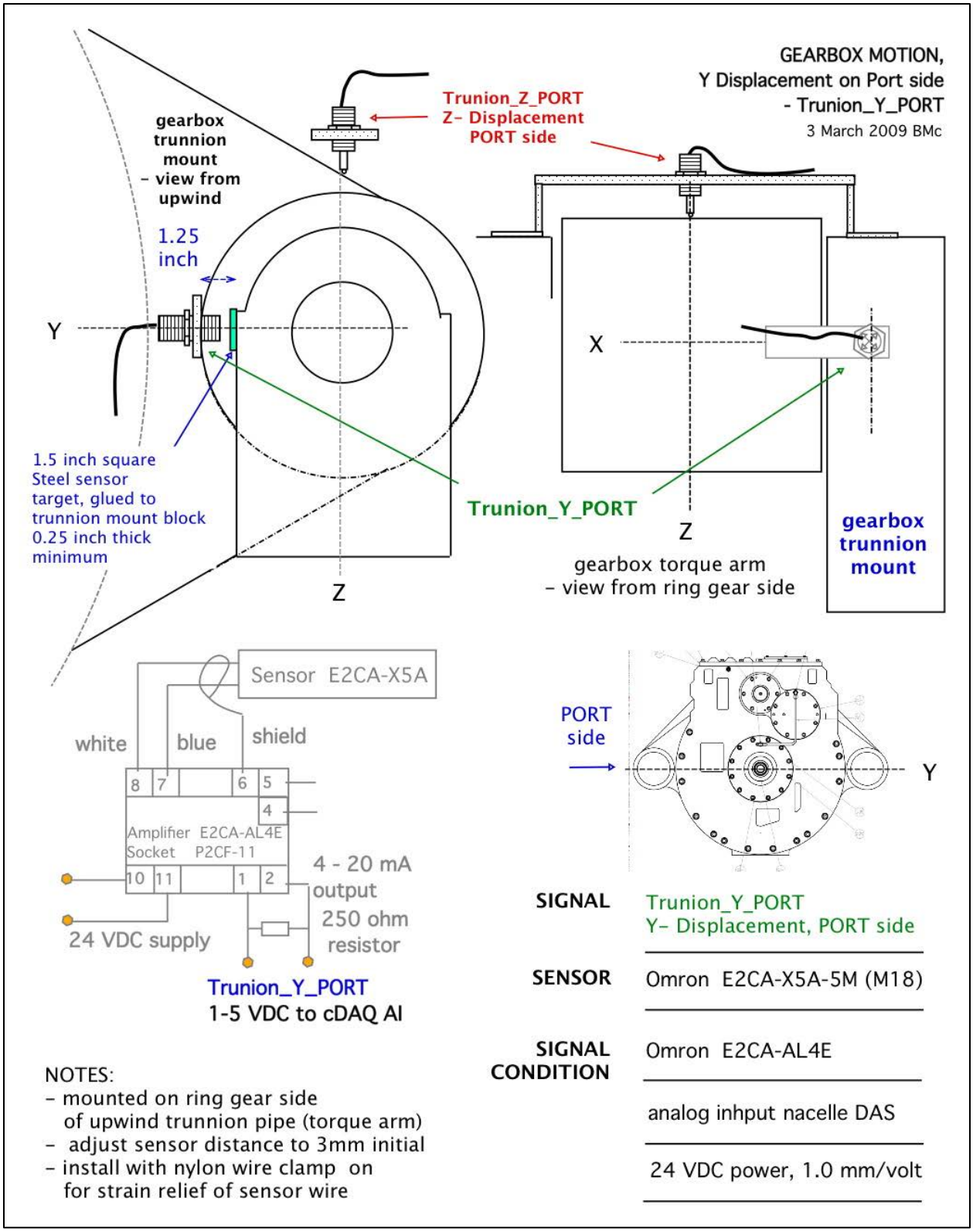

Figure B-7. Gearbox motion, YY at trunnion

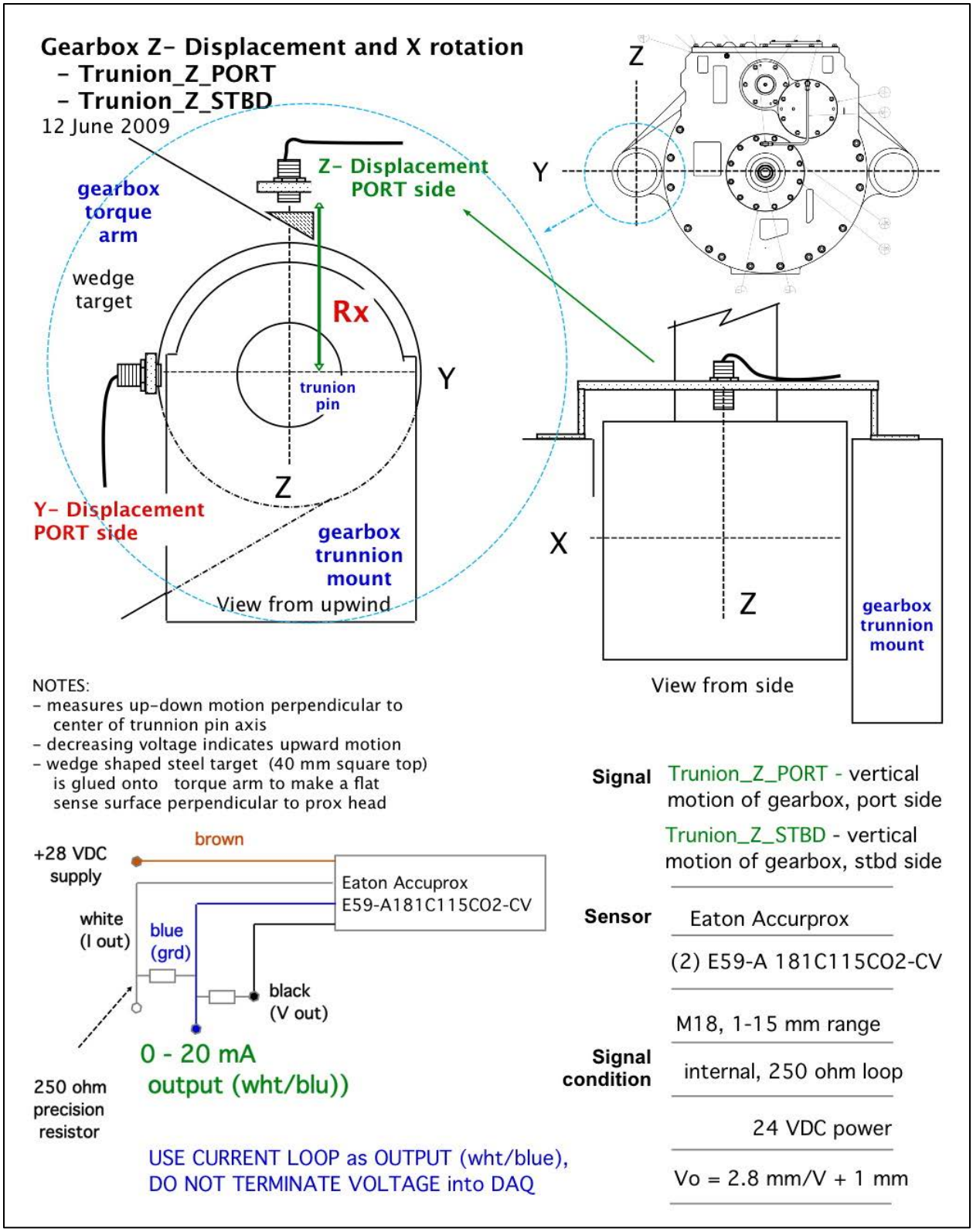

Figure B-8. Gearbox motion, ZZ, at trunnion

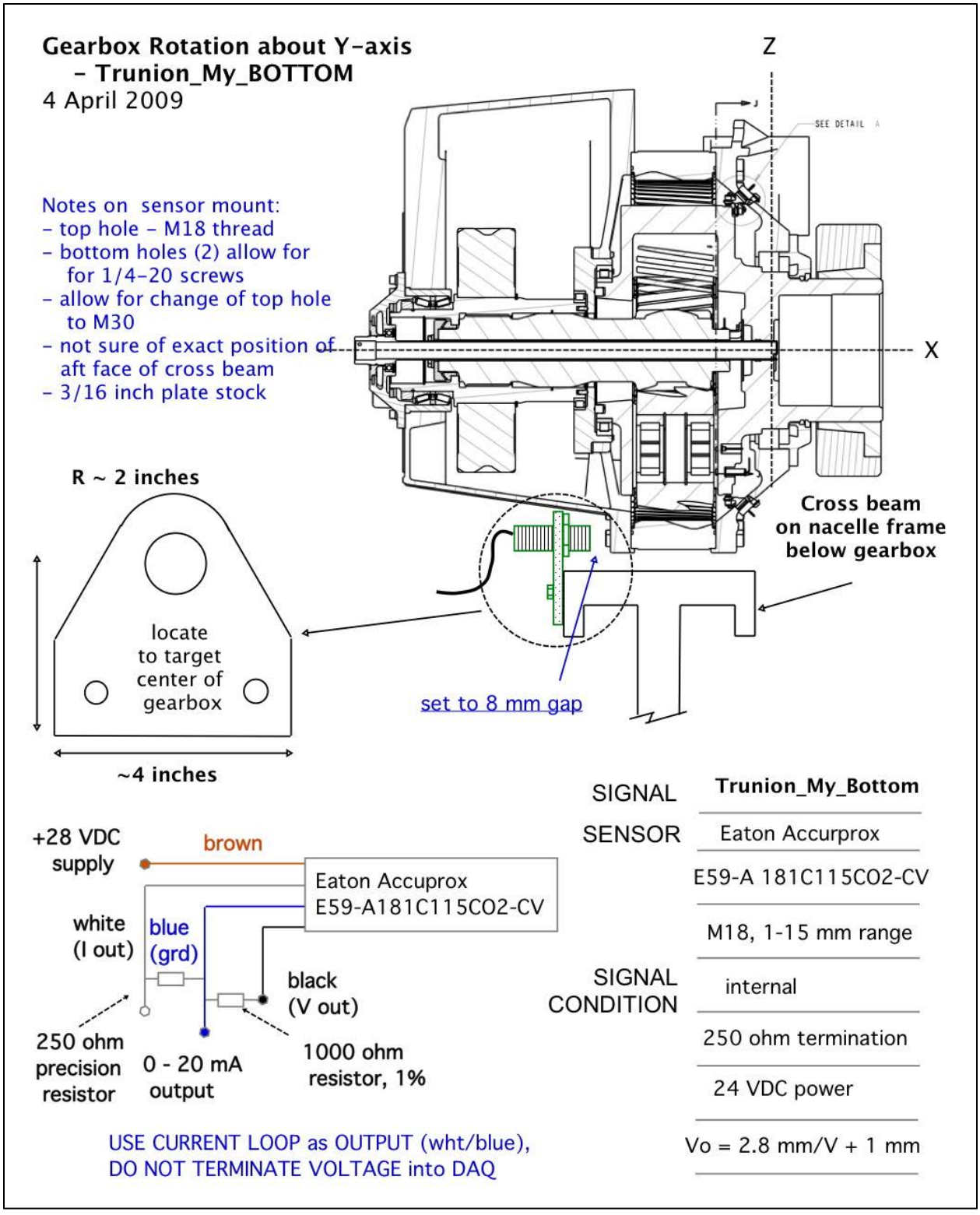

Figure B-9. Gearbox motion, YY bottom rotation

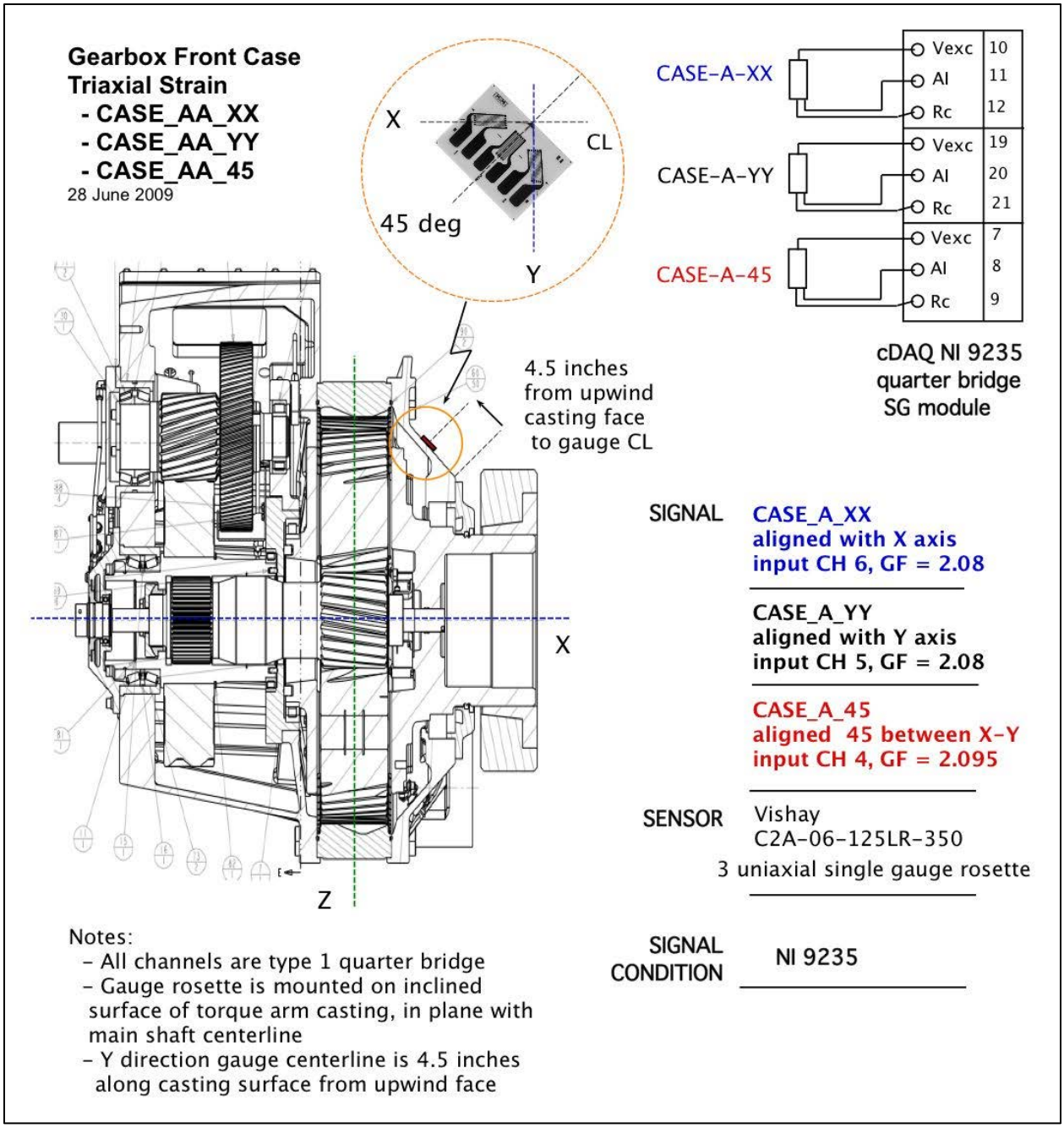

Figure B-10. Gearbox case triaxial strain, AA location

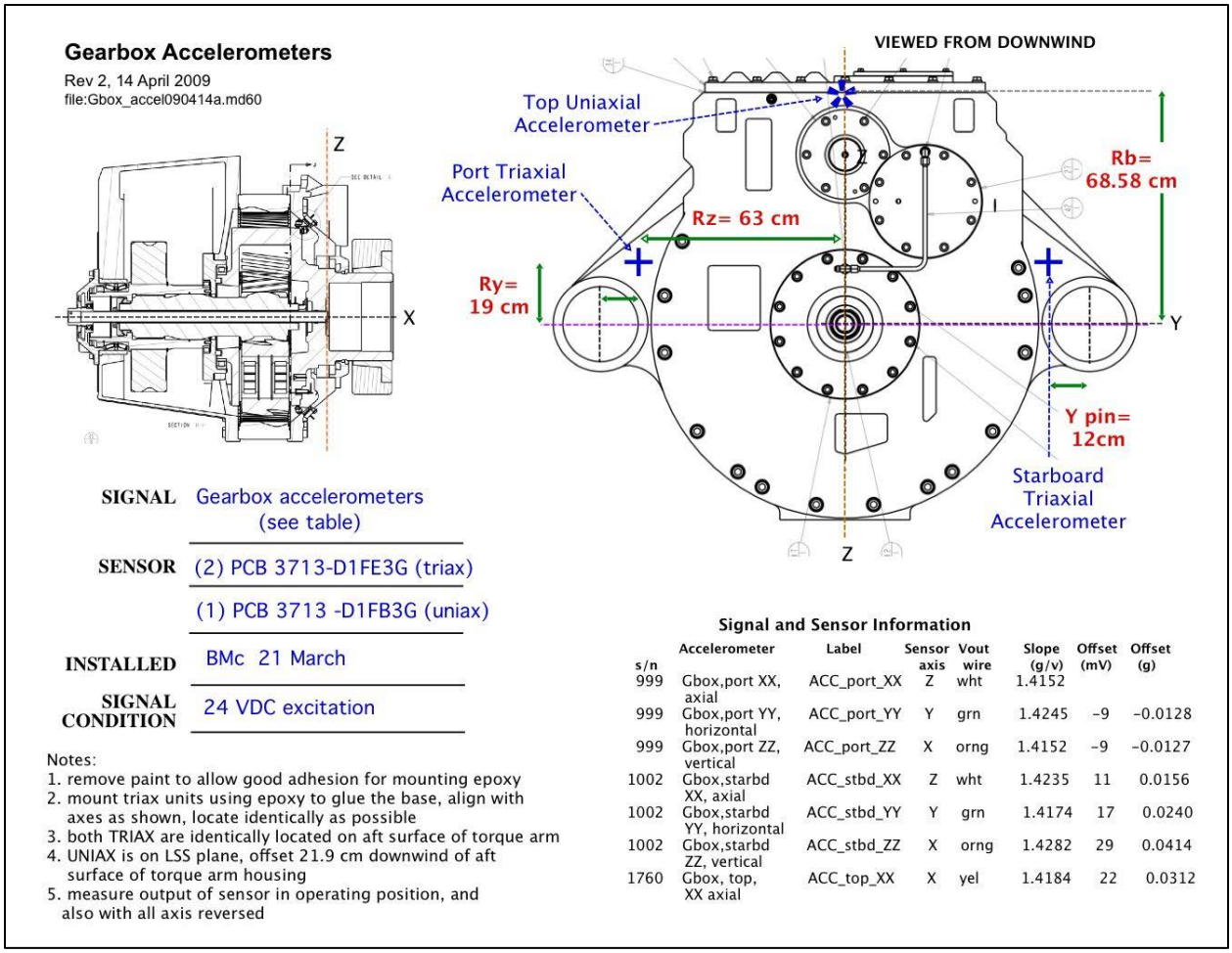

Figure B-11. Gearbox accelerometers

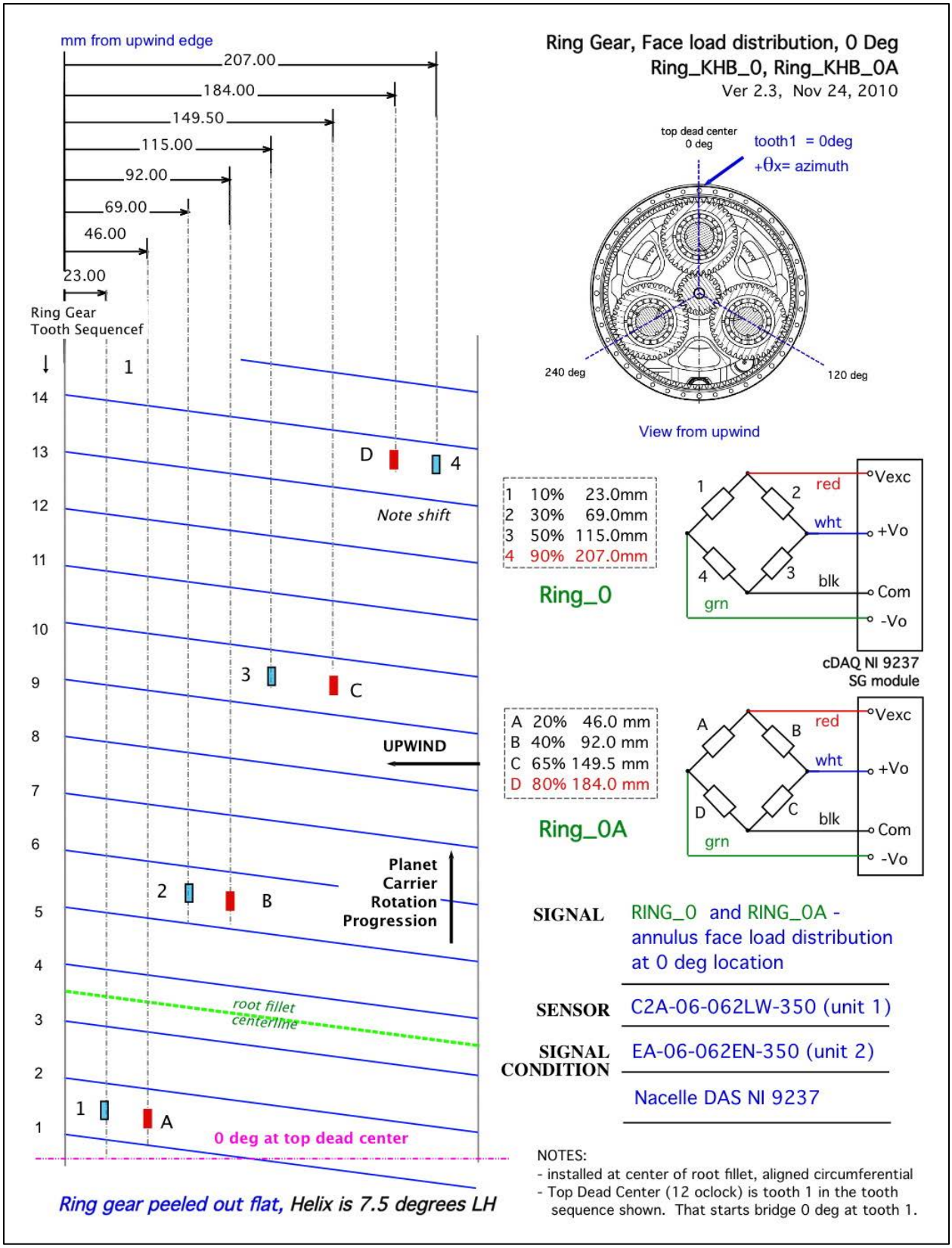

Figure B-12. Ring gear 0° face width load distribution

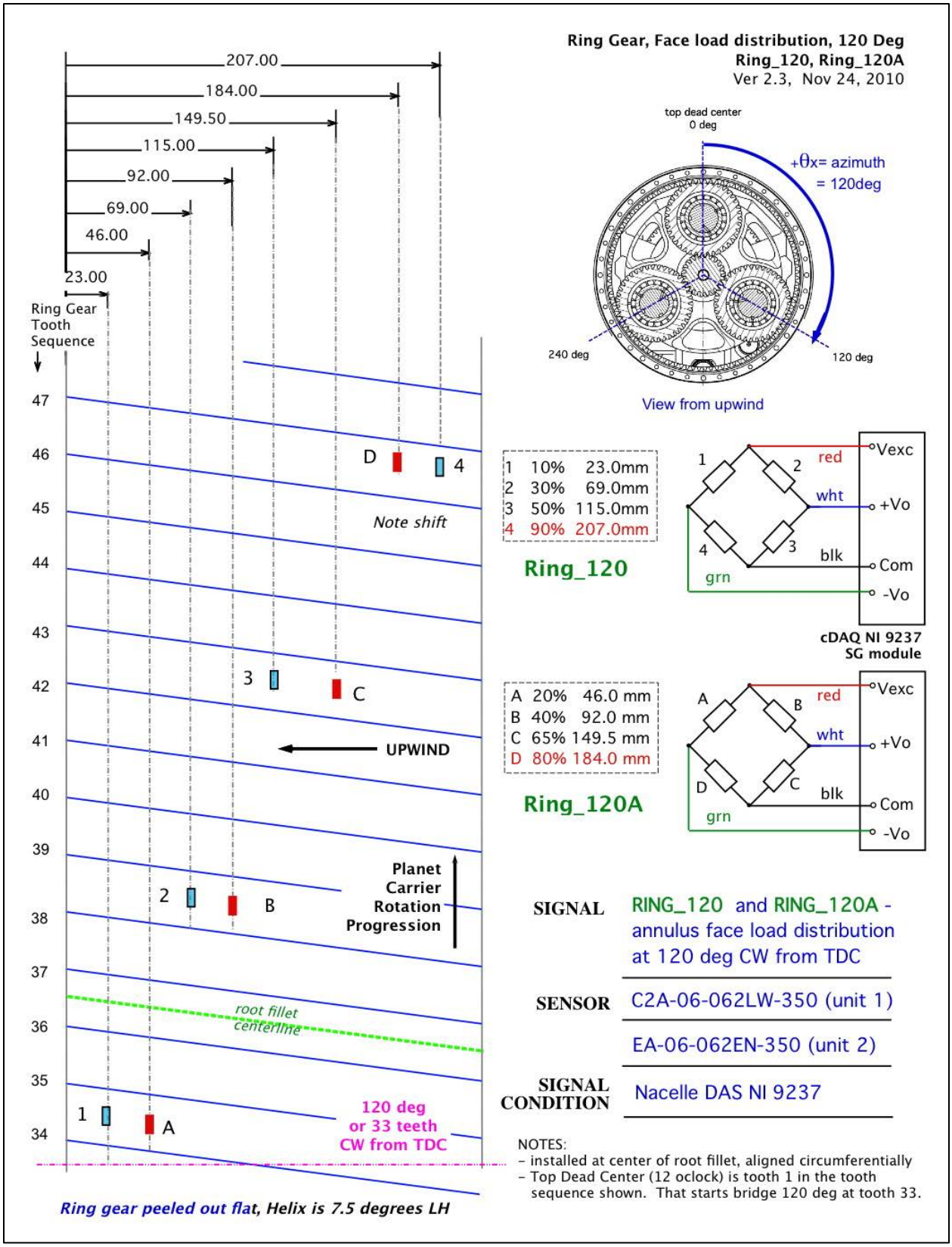

Figure B-13. Ring gear 120° face width load distribution

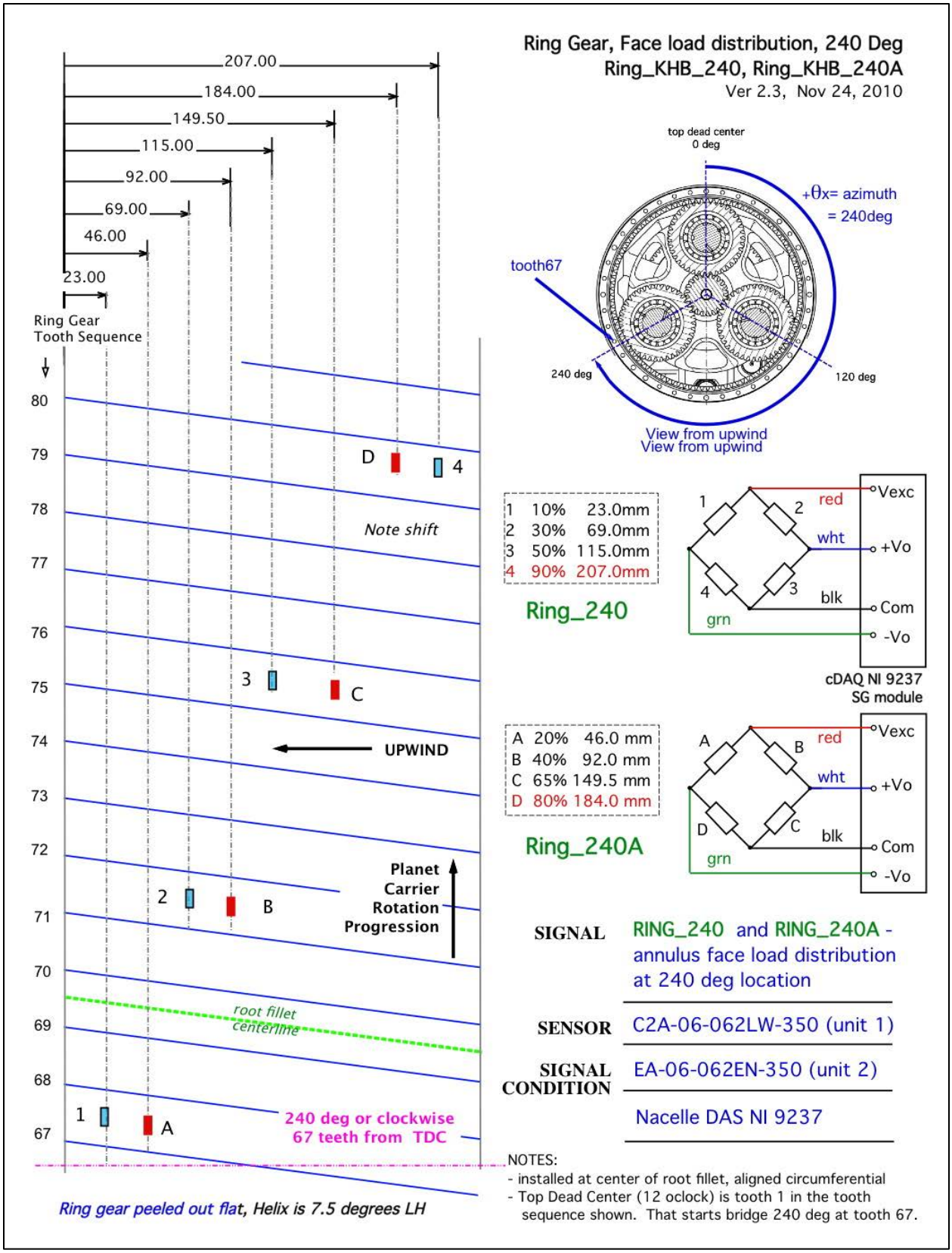

Figure B-14. Ring gear 240° face width load distribution

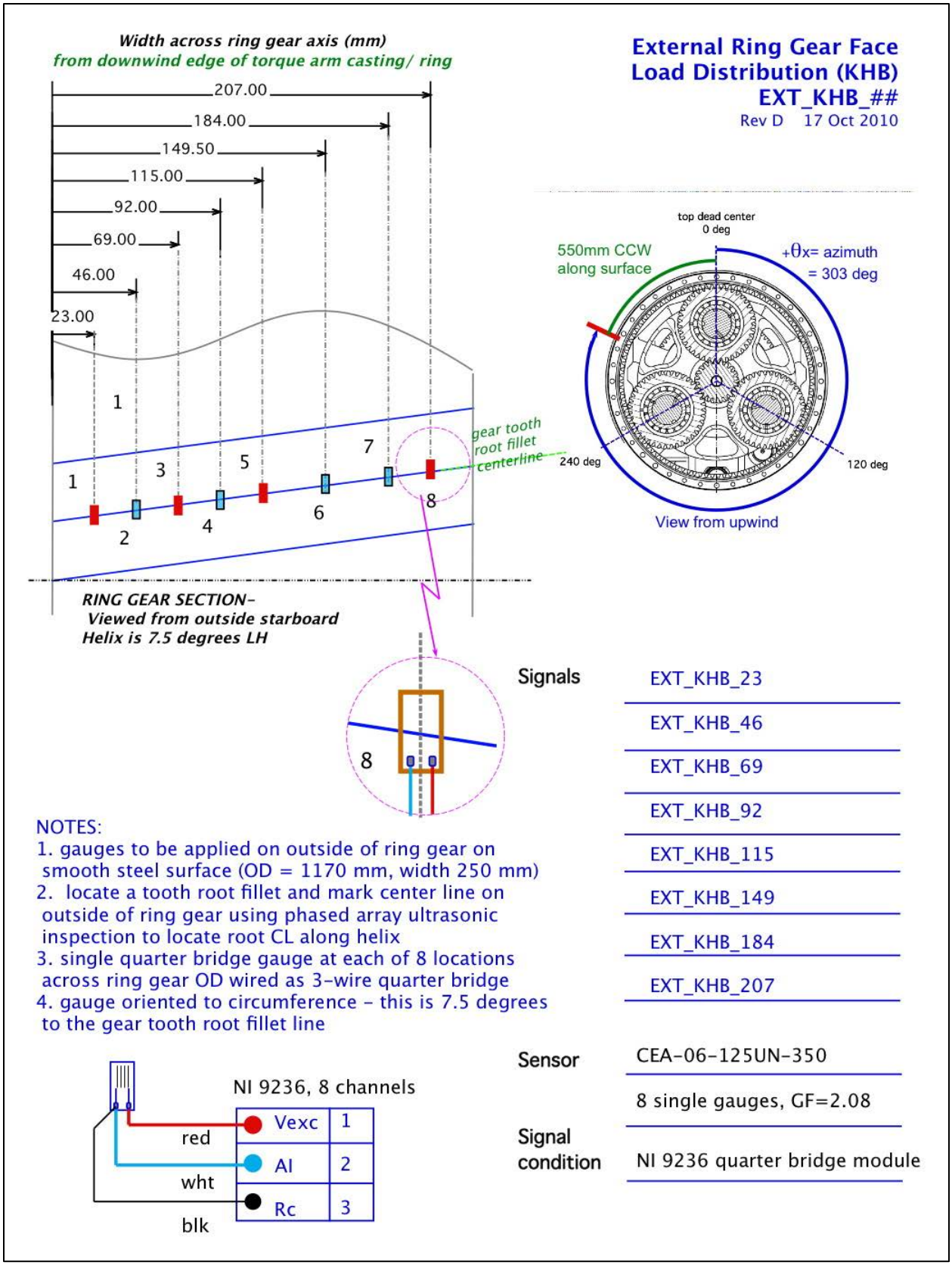

Figure B-15. Ring gear external face width load distribution

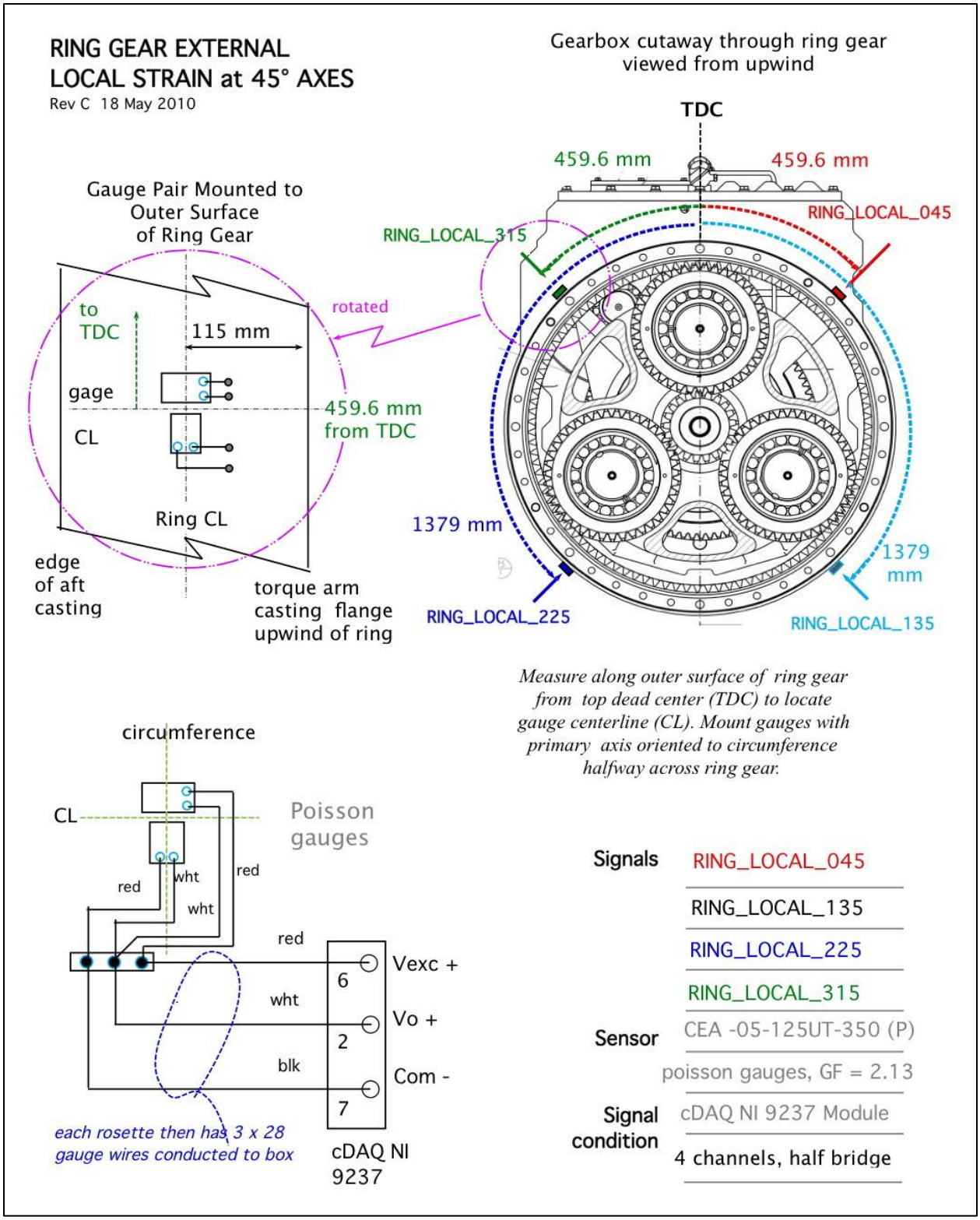

Figure B-16. Ring gear local distortion strain

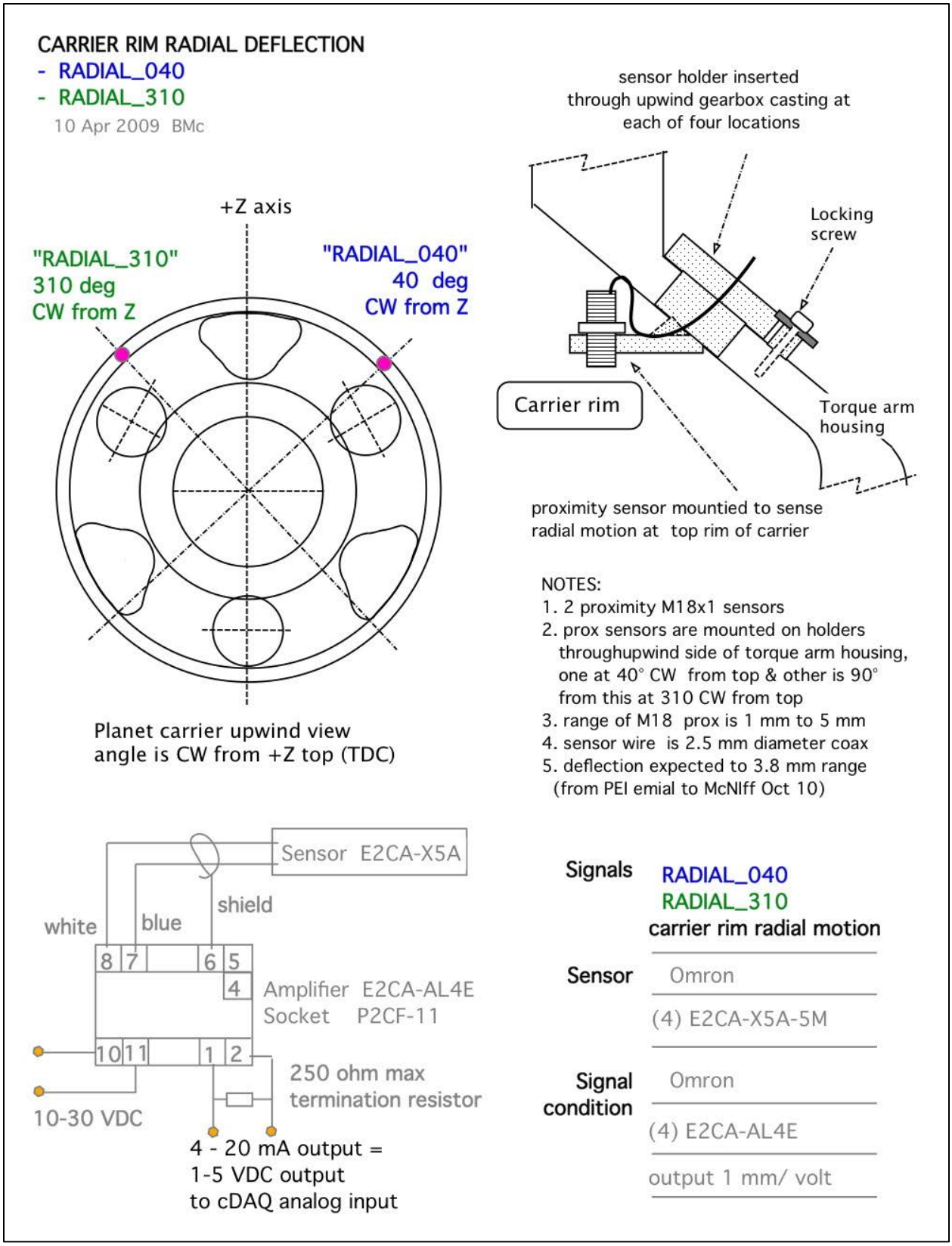

Figure B-17. Carrier-rim radial displacement

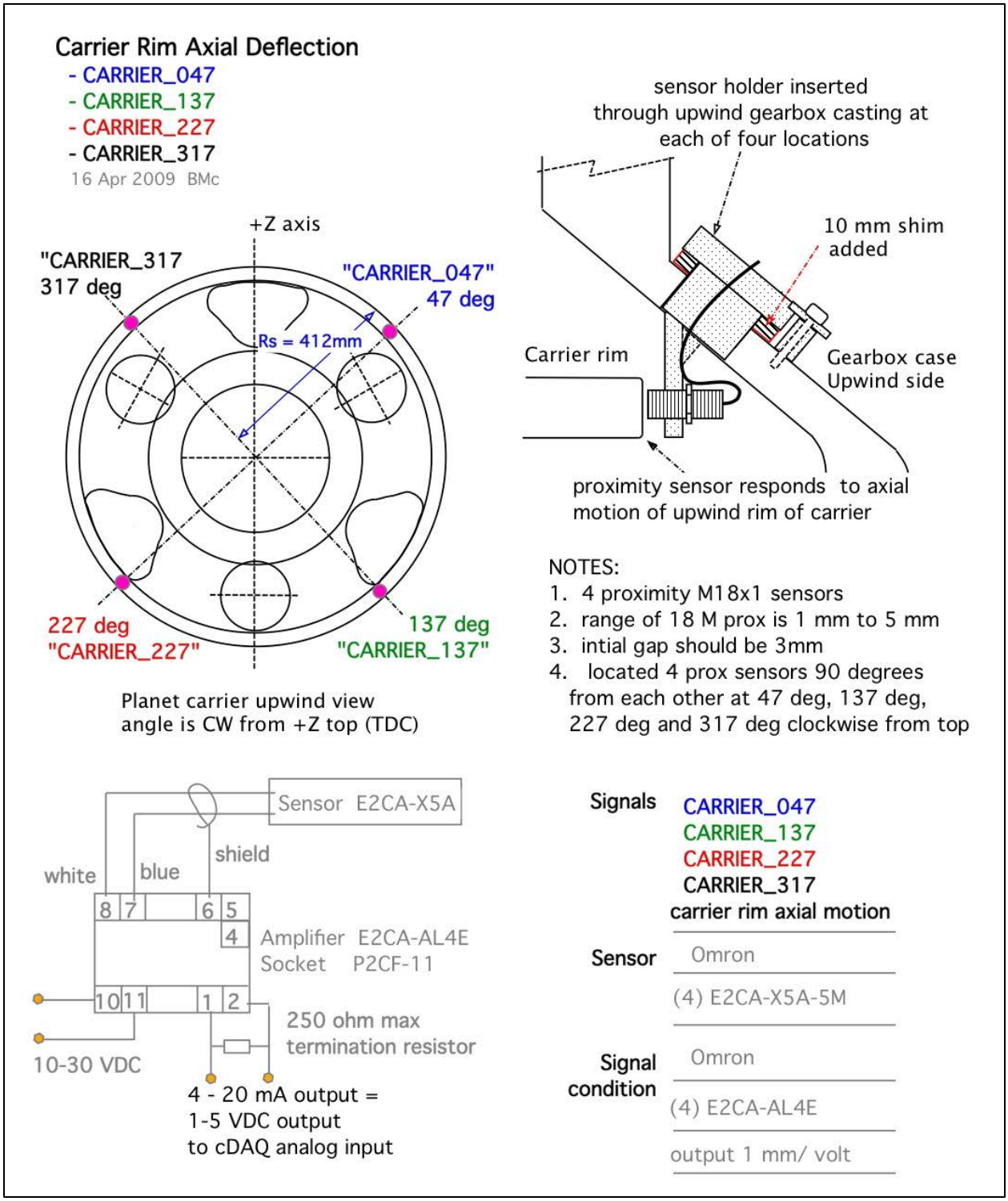

Figure B-18. Carrier-rim axial displacement

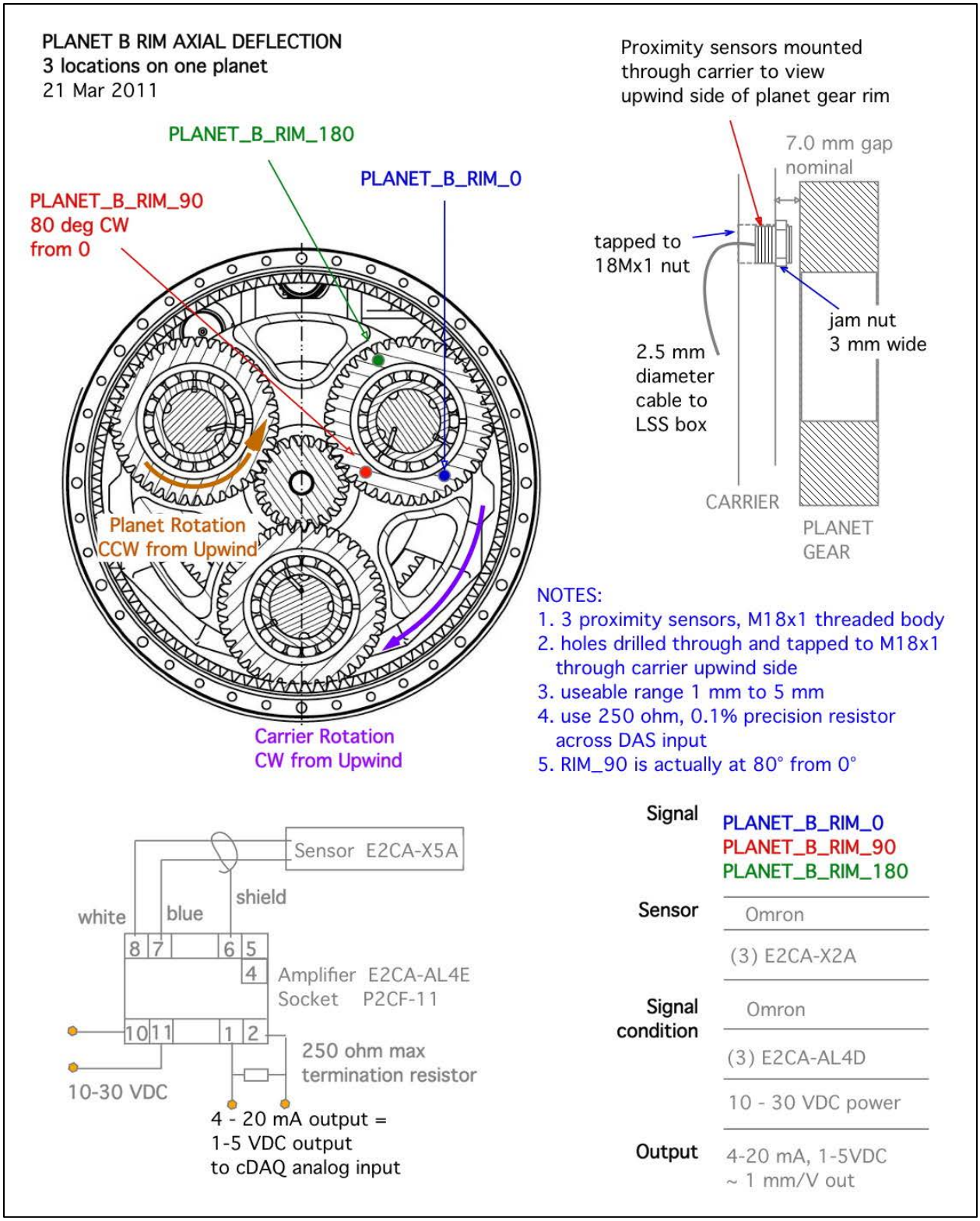

Figure B-19. Planet gear B rim deflection

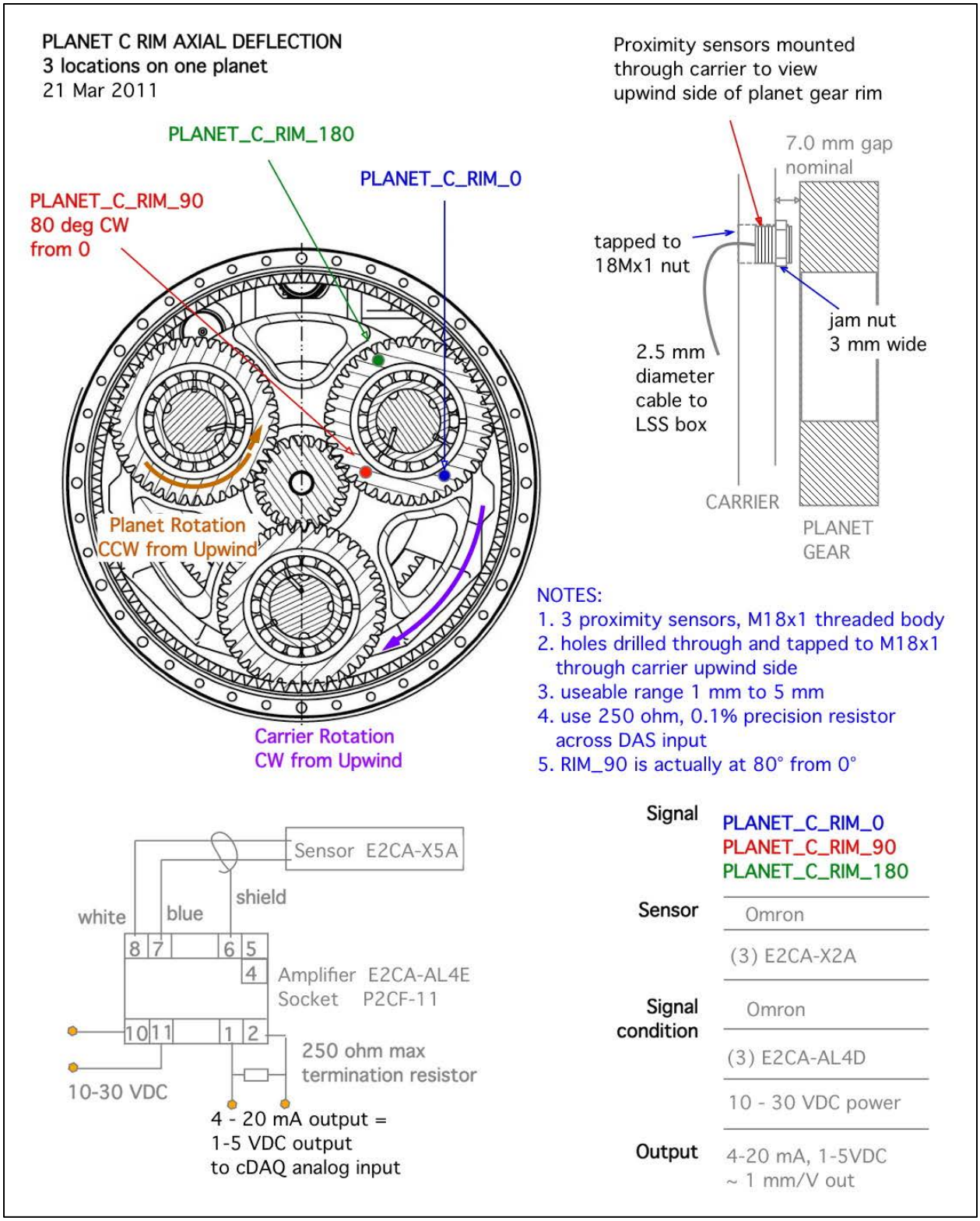

Figure B-20. Planet gear C rim deflection

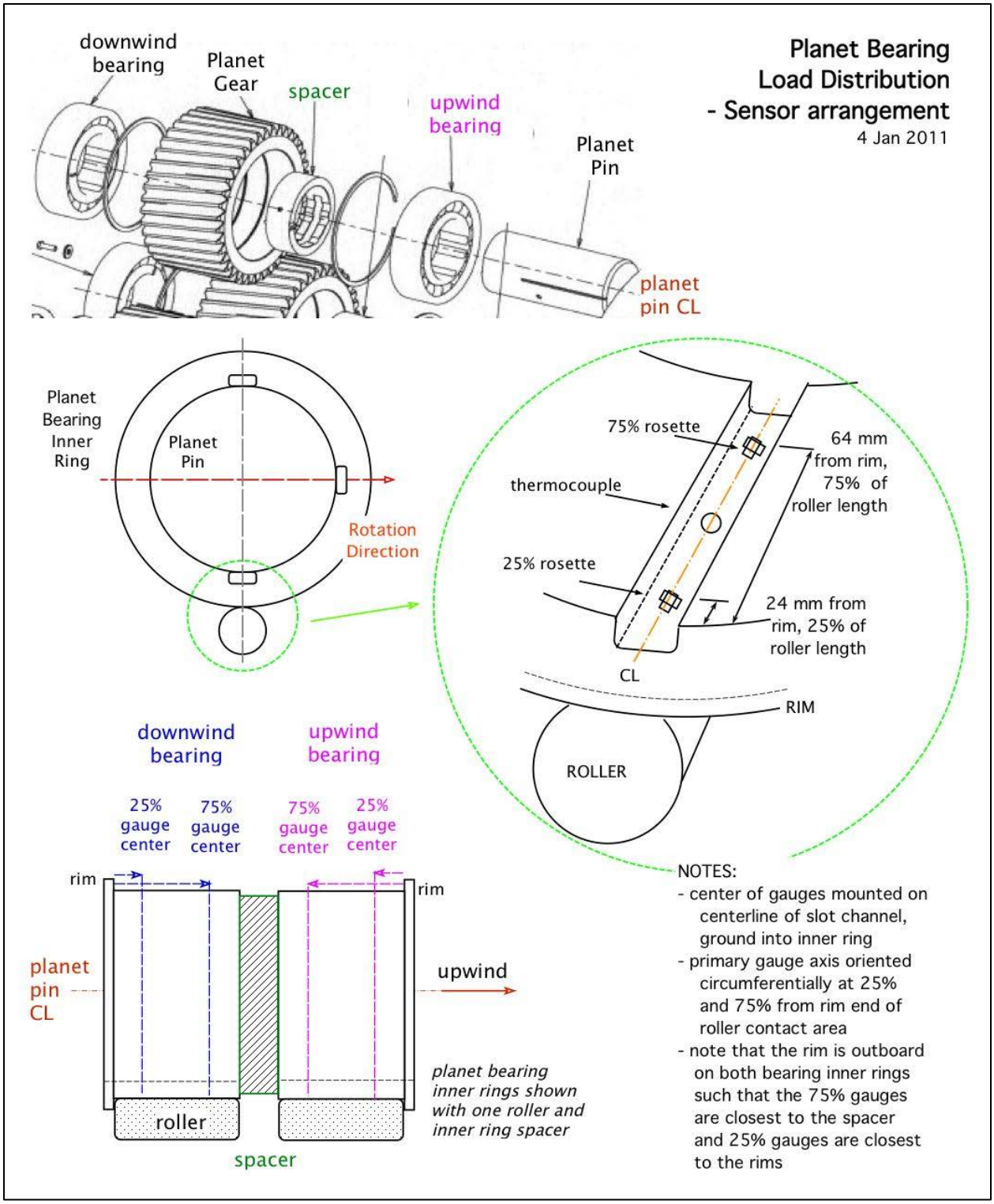

Figure B-21. Planet bearing radial load sensor arrangement

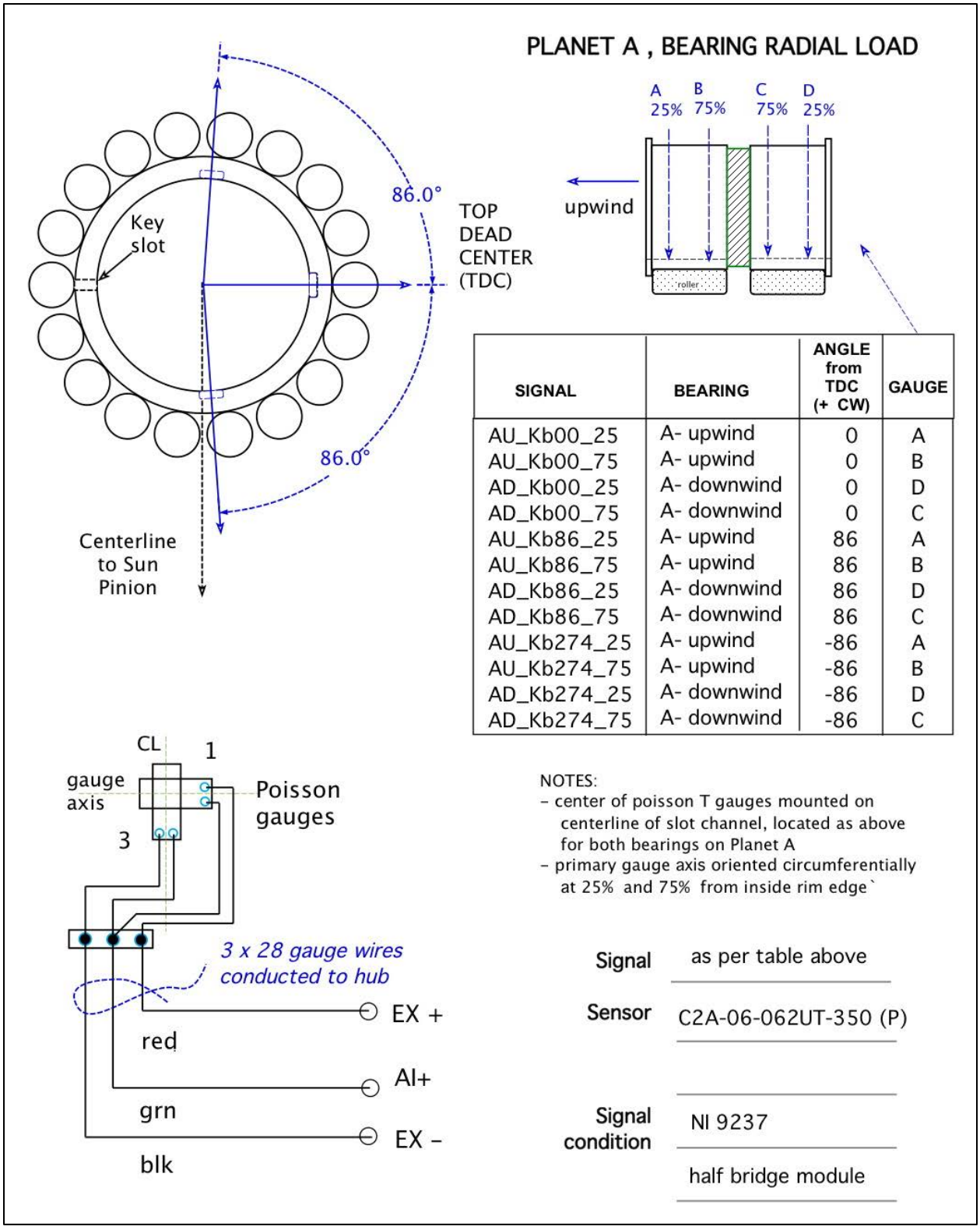

SIGNAL	BEARING	ANGLE from TDC (+ CW)	GAUGE
AU_Kb00_25	A- upwind	0	A
AU_Kb00_75	A- upwind	0	B
AD_Kb00_25	A- downwind	0	D
AD_Kb00_75	A- downwind	0	C
AU_Kb86_25	A- upwind	86	A
AU_Kb86_75	A- upwind	86	B
AD_Kb86_25	A- downwind	86	D
AD_Kb86_75	A- downwind	86	C
AU_Kb274_25	A- upwind	-86	A
AU_Kb274_75	A- upwind	-86	B
AD_Kb274_25	A- downwind	-86	D
AD_Kb274_75	A- downwind	-86	C

Figure B-22. Planet bearing A radial load

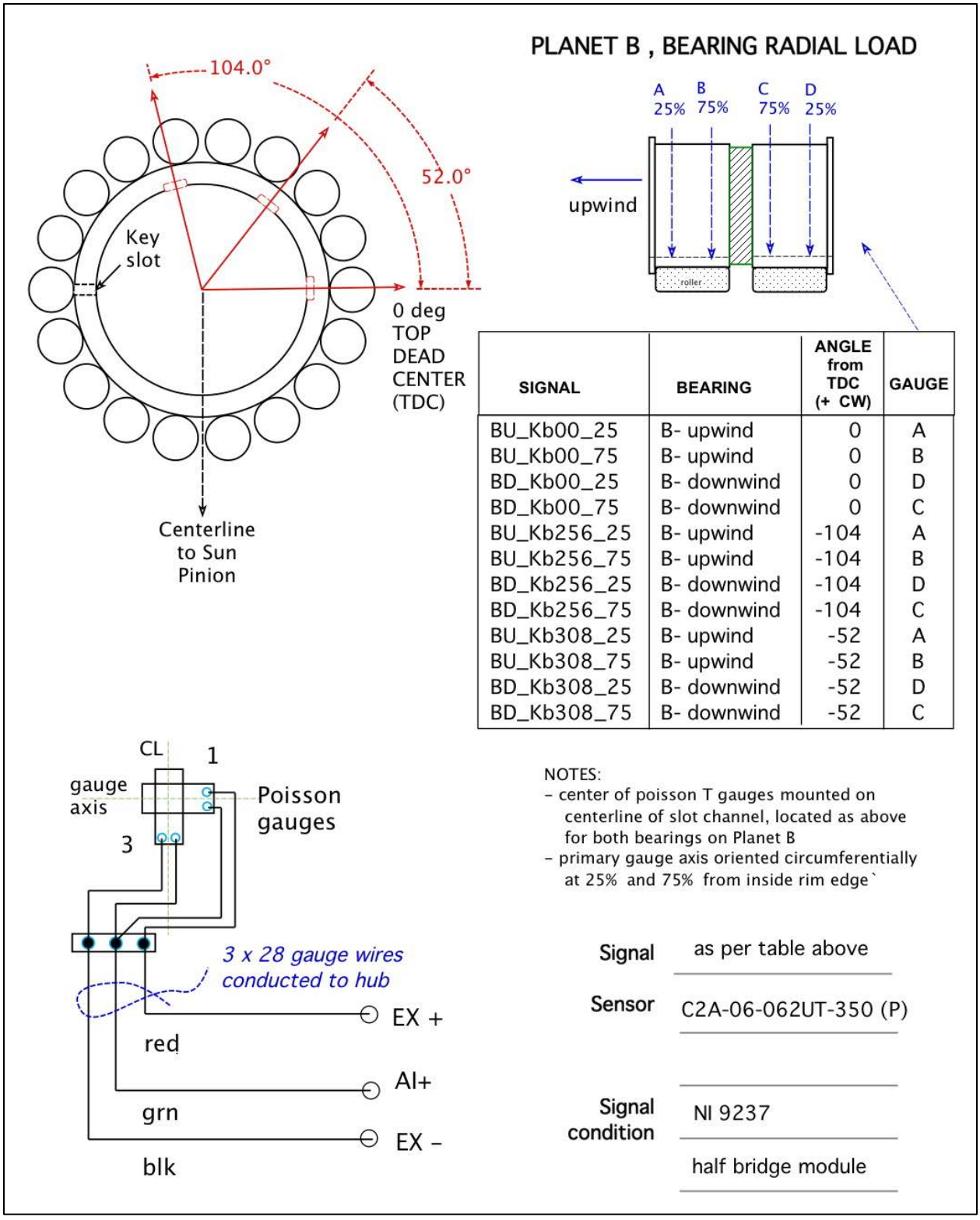

Figure B-23. Planet bearing B radial load

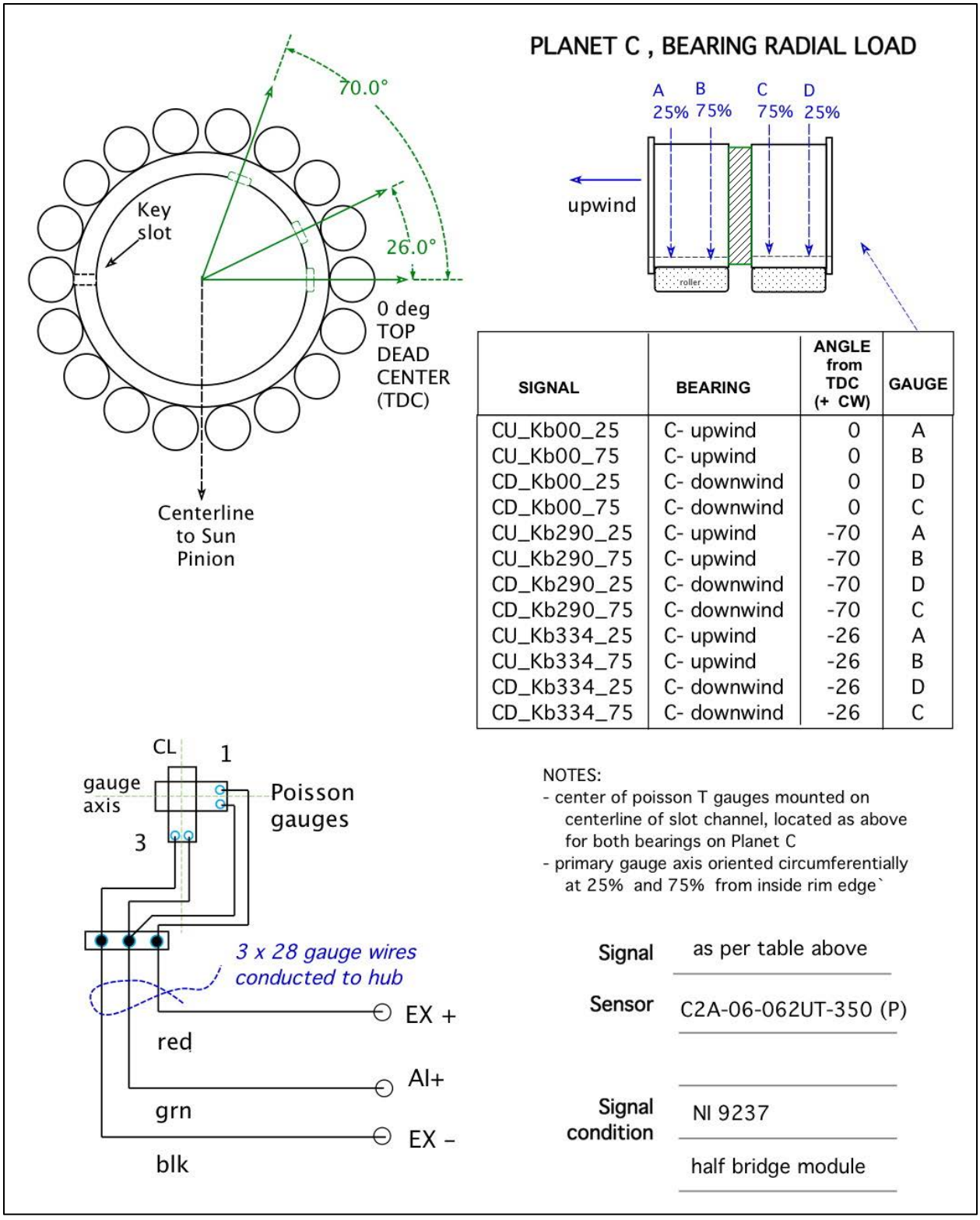

SIGNAL	BEARING	ANGLE from TDC (+ CW)	GAUGE
CU_Kb00_25	C- upwind	0	A
CU_Kb00_75	C- upwind	0	B
CD_Kb00_25	C- downwind	0	D
CD_Kb00_75	C- downwind	0	C
CU_Kb290_25	C- upwind	-70	A
CU_Kb290_75	C- upwind	-70	B
CD_Kb290_25	C- downwind	-70	D
CD_Kb290_75	C- downwind	-70	C
CU_Kb334_25	C- upwind	-26	A
CU_Kb334_75	C- upwind	-26	B
CD_Kb334_25	C- downwind	-26	D
CD_Kb334_75	C- downwind	-26	C

Figure B-24. Planet bearing C radial load

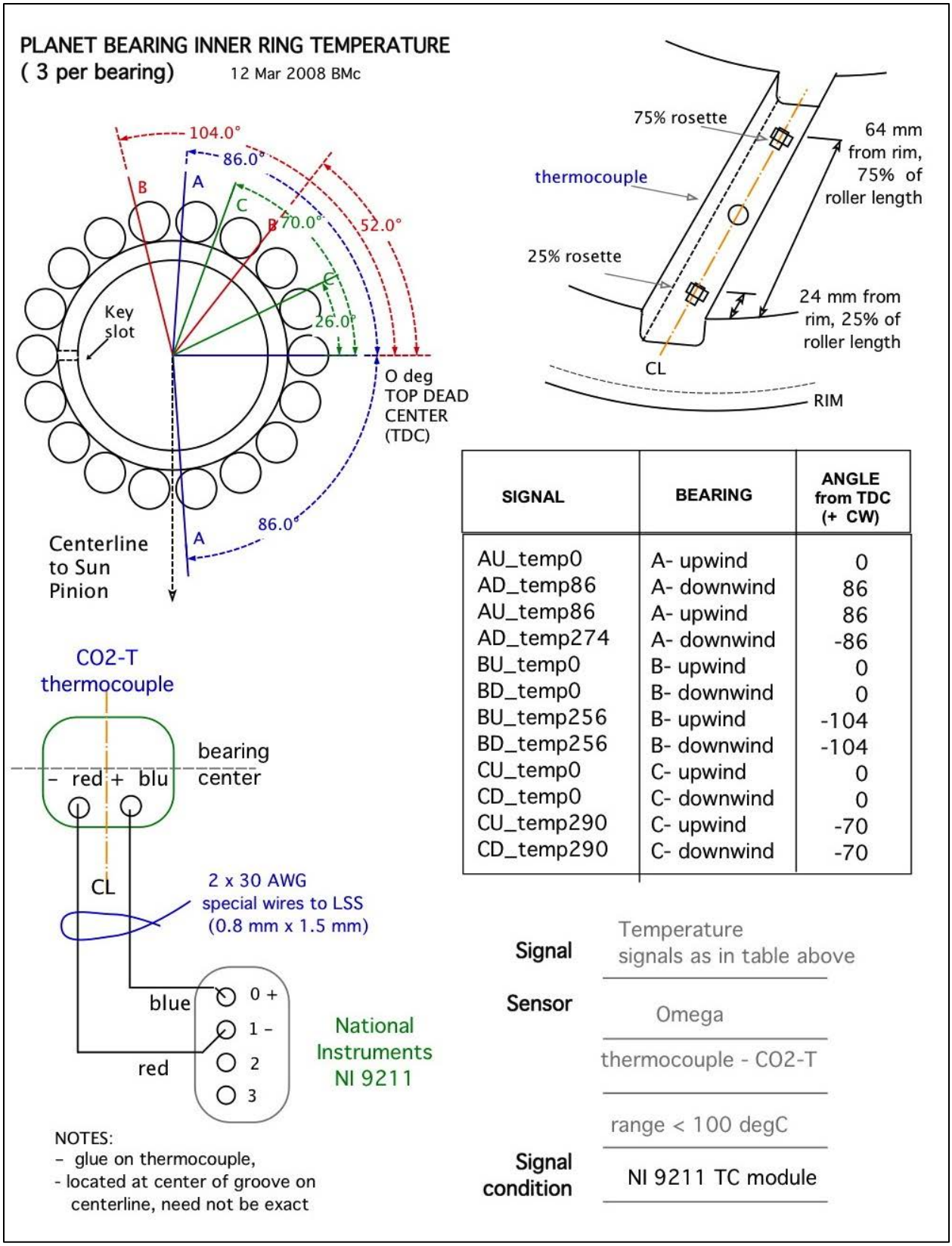

SIGNAL	BEARING	ANGLE from TDC (+ CW)
AU_temp0	A- upwind	0
AD_temp86	A- downwind	86
AU_temp86	A- upwind	86
AD_temp274	A- downwind	-86
BU_temp0	B- upwind	0
BD_temp0	B- downwind	0
BU_temp256	B- upwind	-104
BD_temp256	B- downwind	-104
CU_temp0	C- upwind	0
CD_temp0	C- downwind	0
CU_temp290	C- upwind	-70
CD_temp290	C- downwind	-70

Signal	Temperature signals as in table above
Sensor	Omega thermocouple - CO2-T
	range < 100 degC
Signal condition	NI 9211 TC module

Figure B-25. Planet bearing inner ring temperature

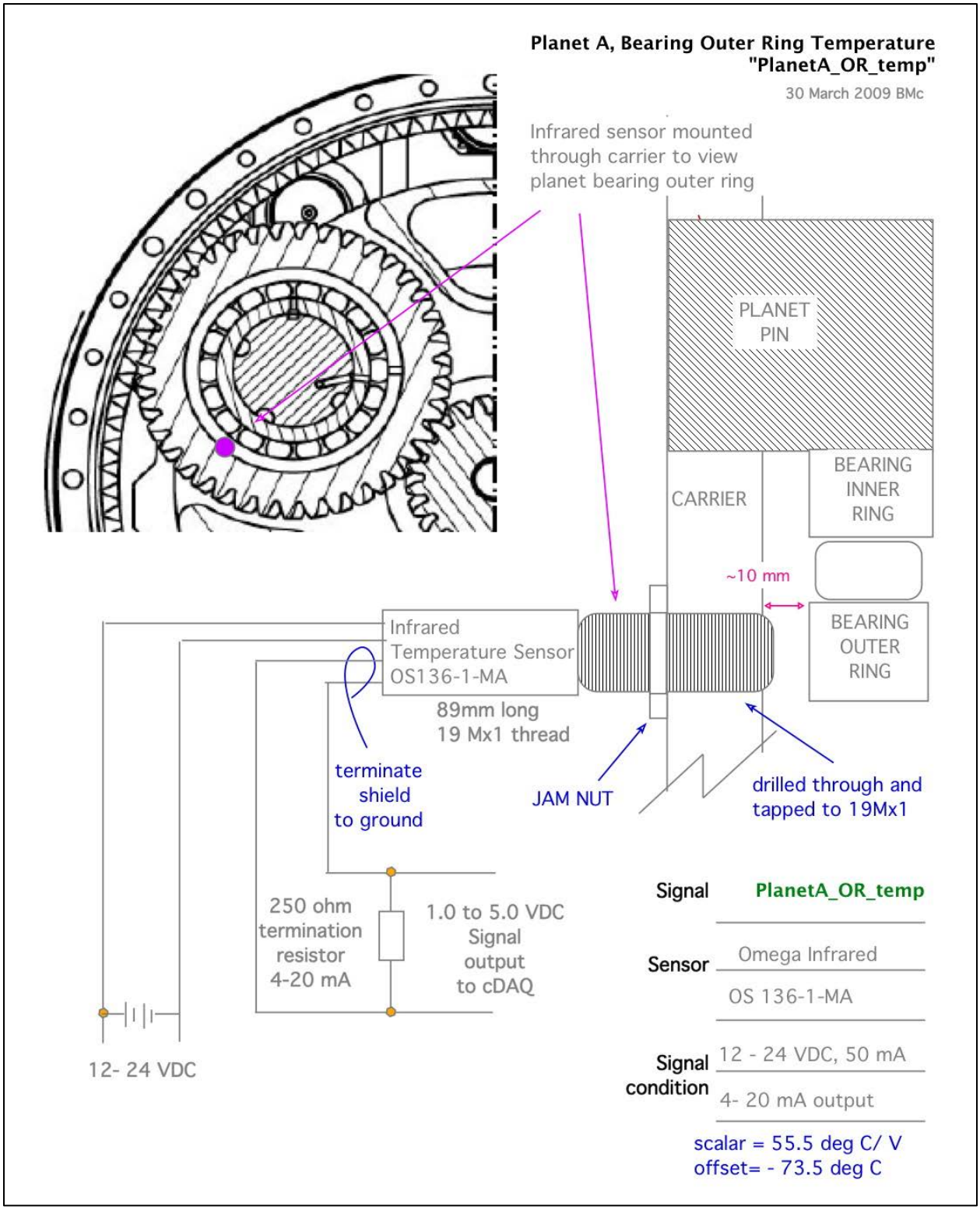

Figure B-26. Planet bearing outer ring temperature

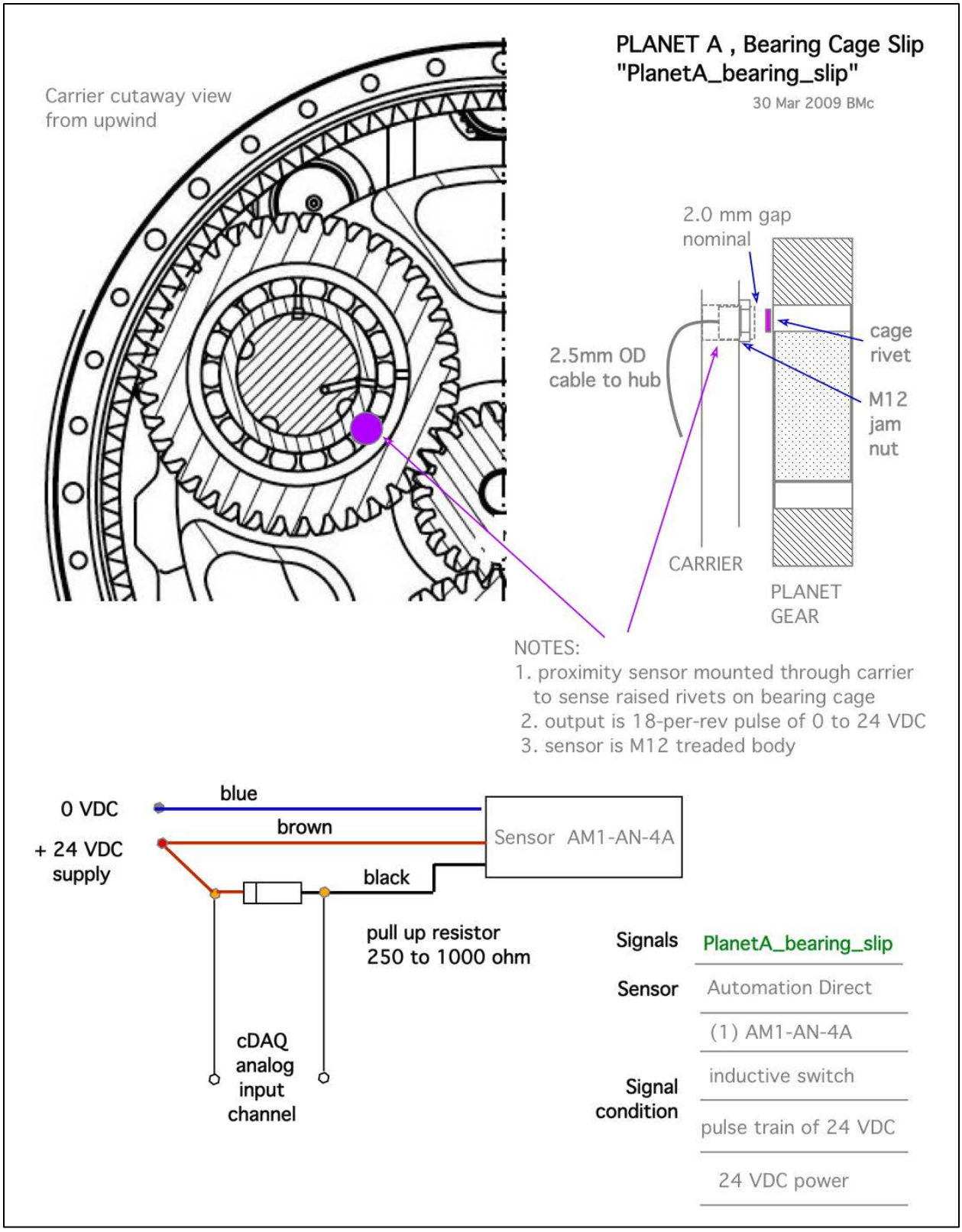

Figure B-27. Planet bearing slip

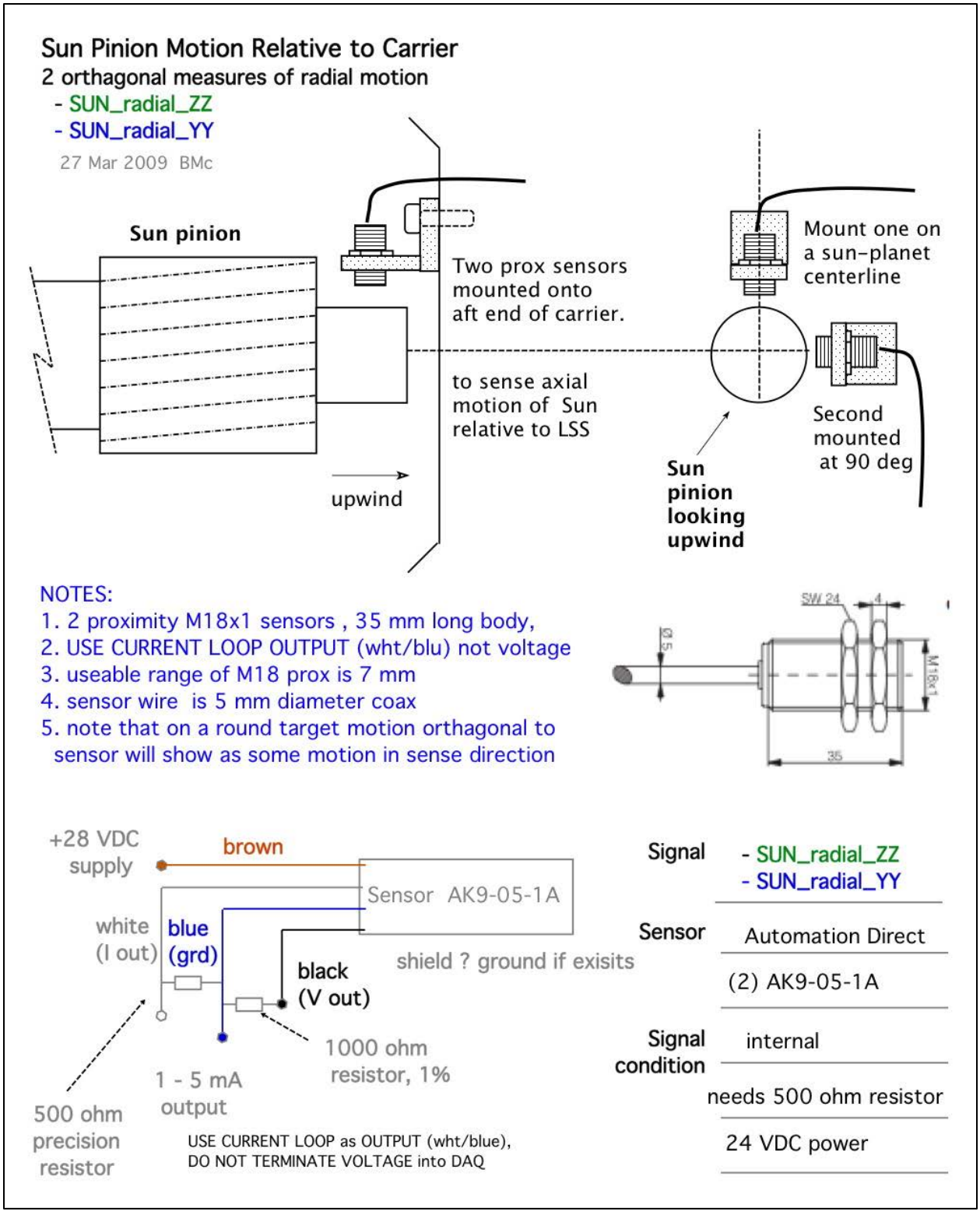

Figure B-28. Sun pinion radial motion

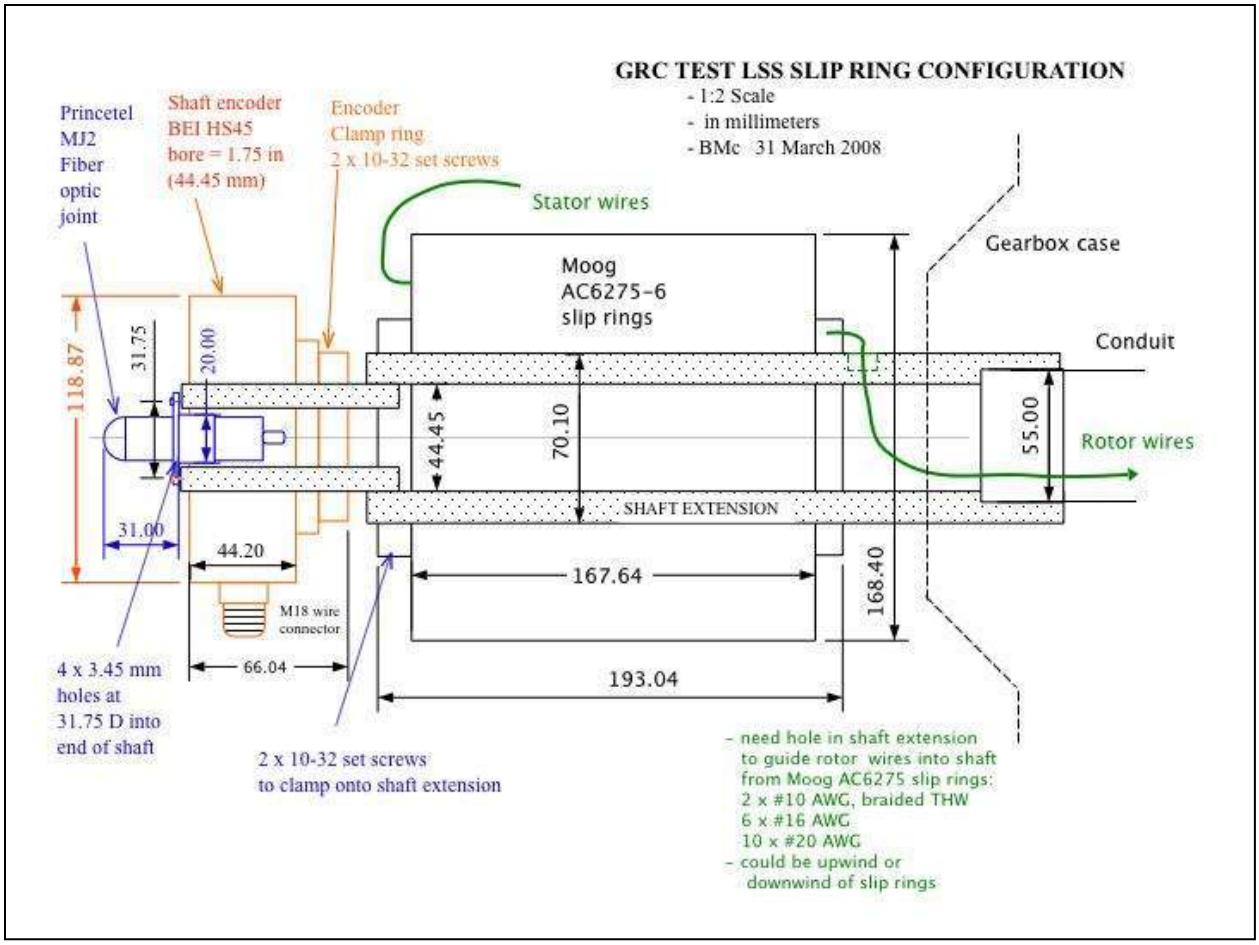

Figure B-29. Mainshaft aft-end slip ring assembly

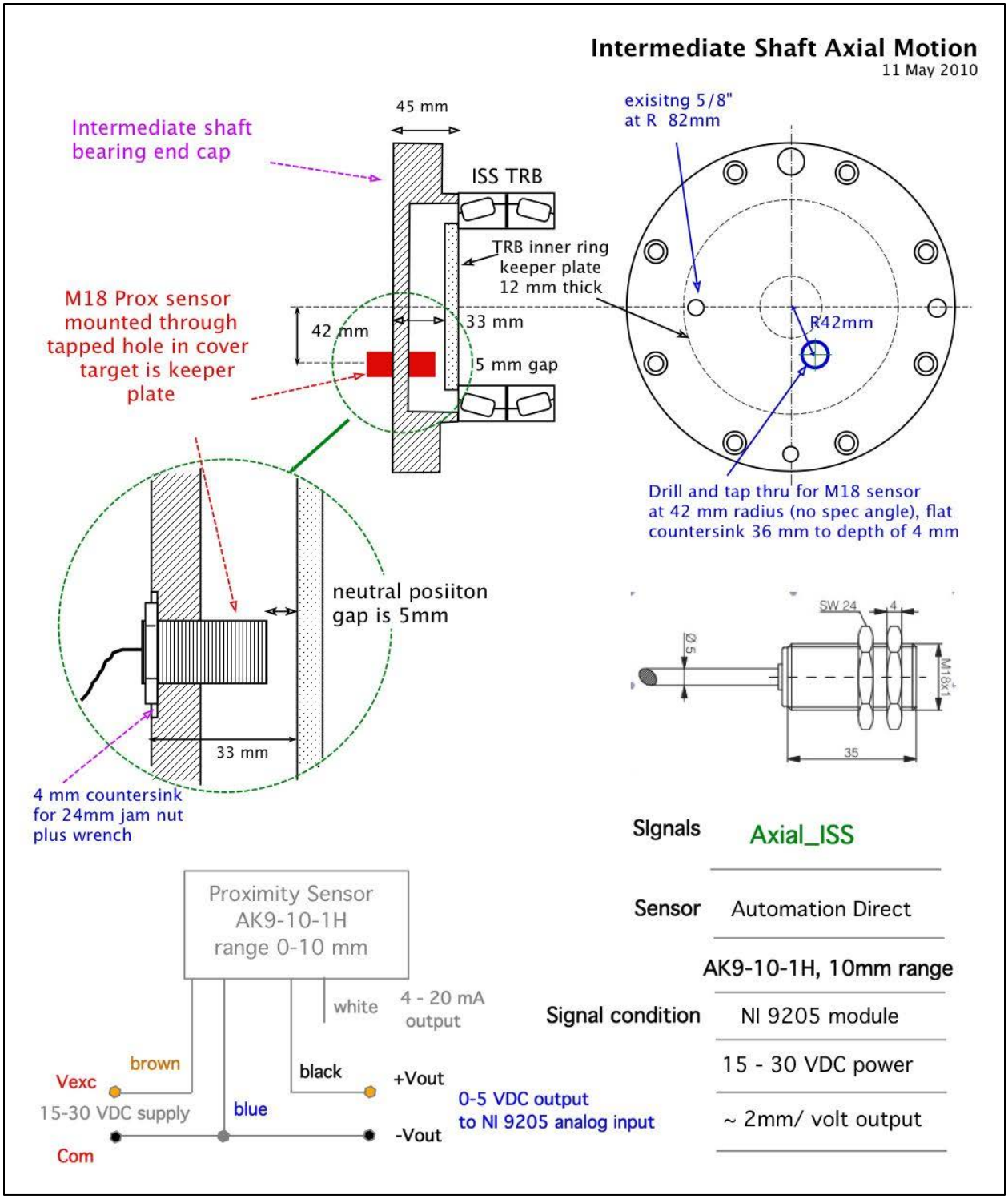

Figure B-30. Intermediate-shaft axial motion

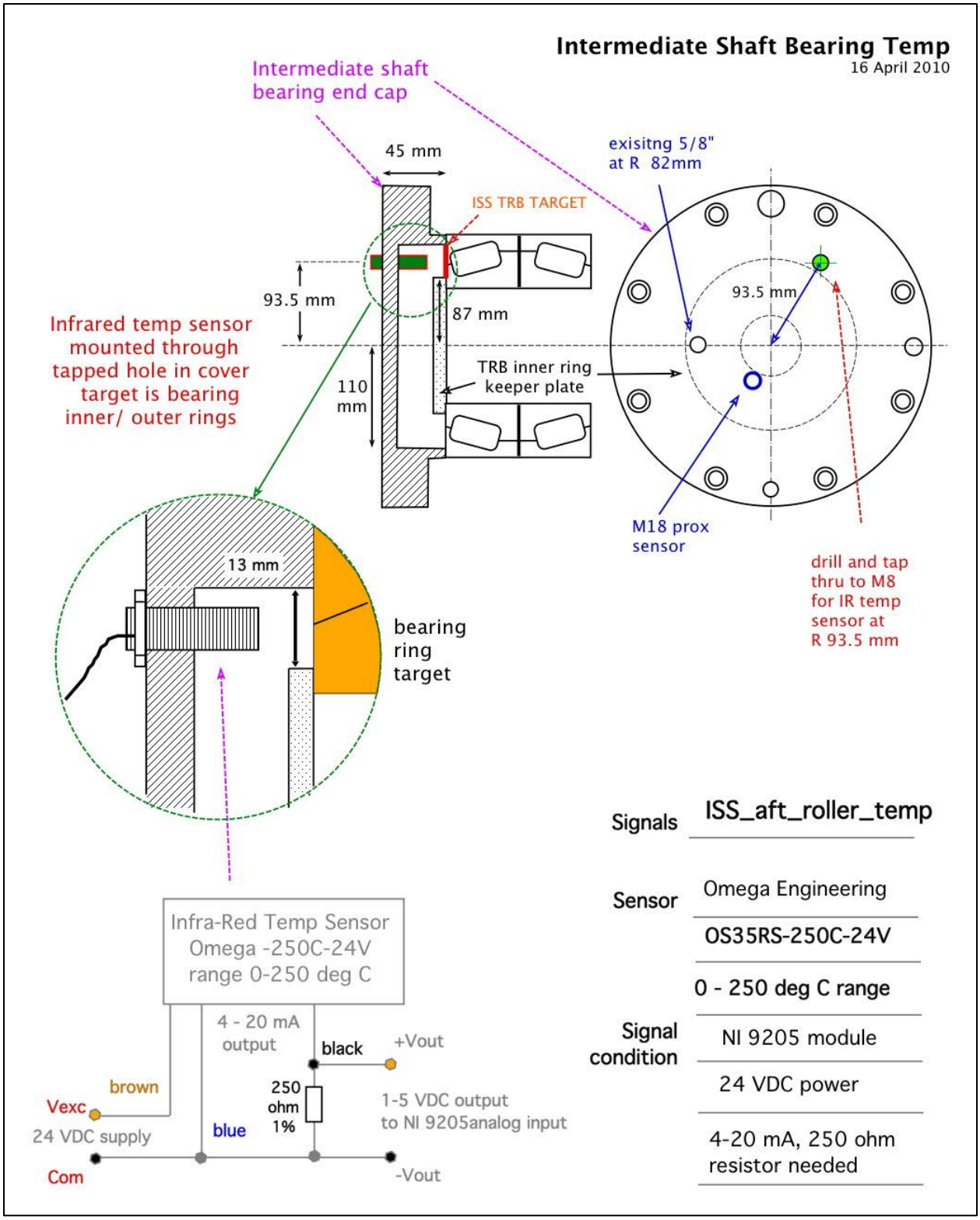

Figure B-31. Intermediate-shaft aft bearing temperature

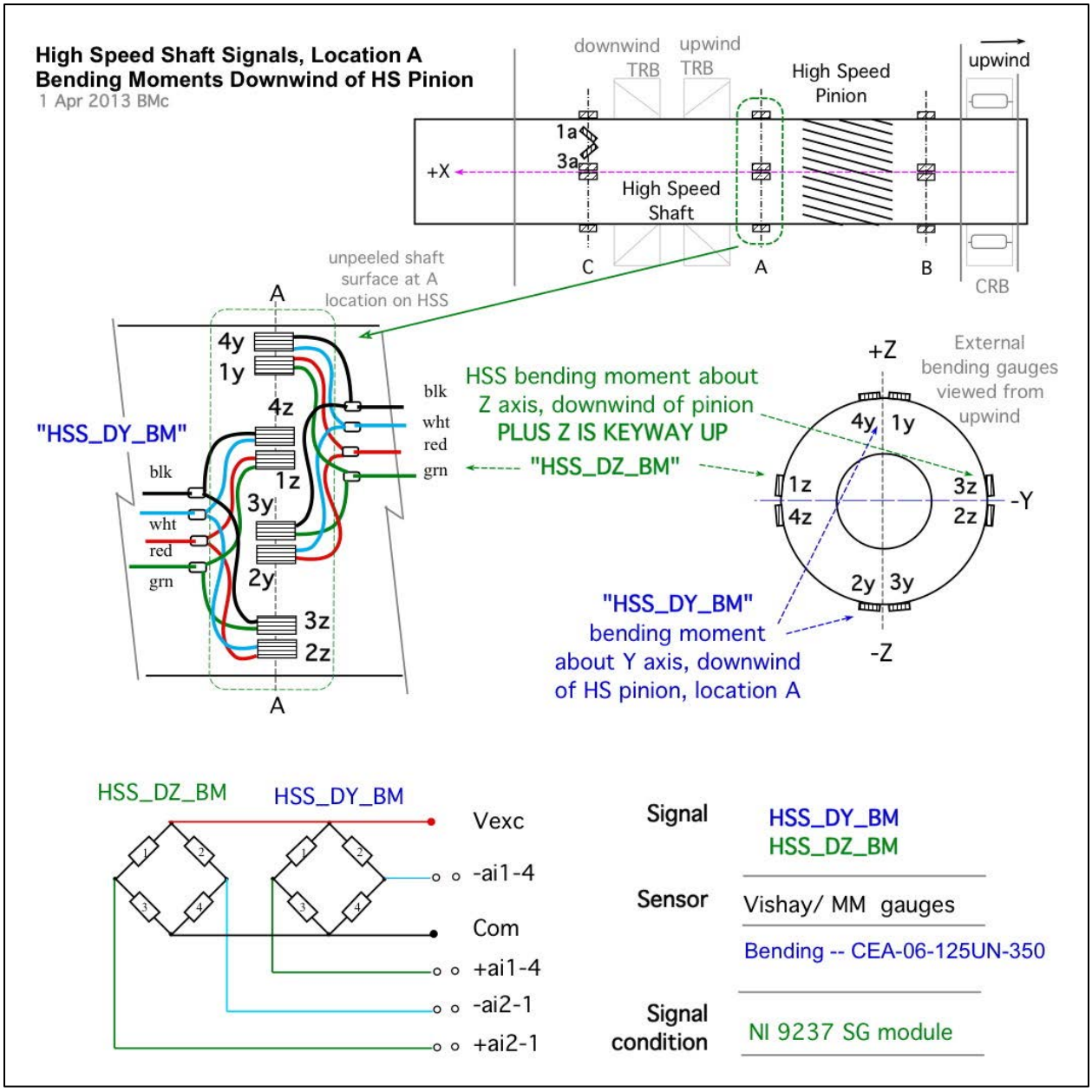

Figure B-32. High-speed shaft bending and torque at location A

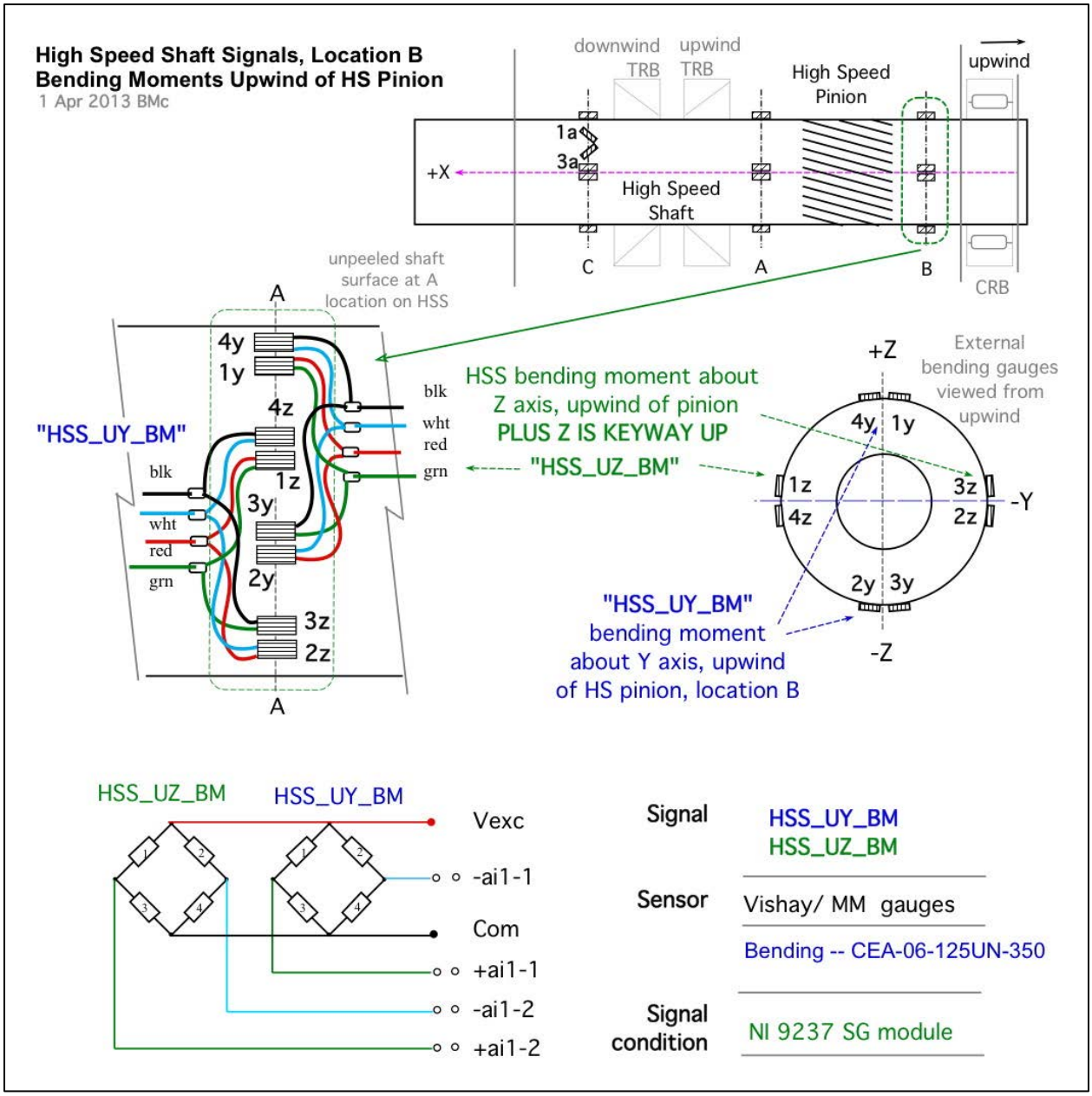

Figure B-33. High-speed shaft bending and torque at location B

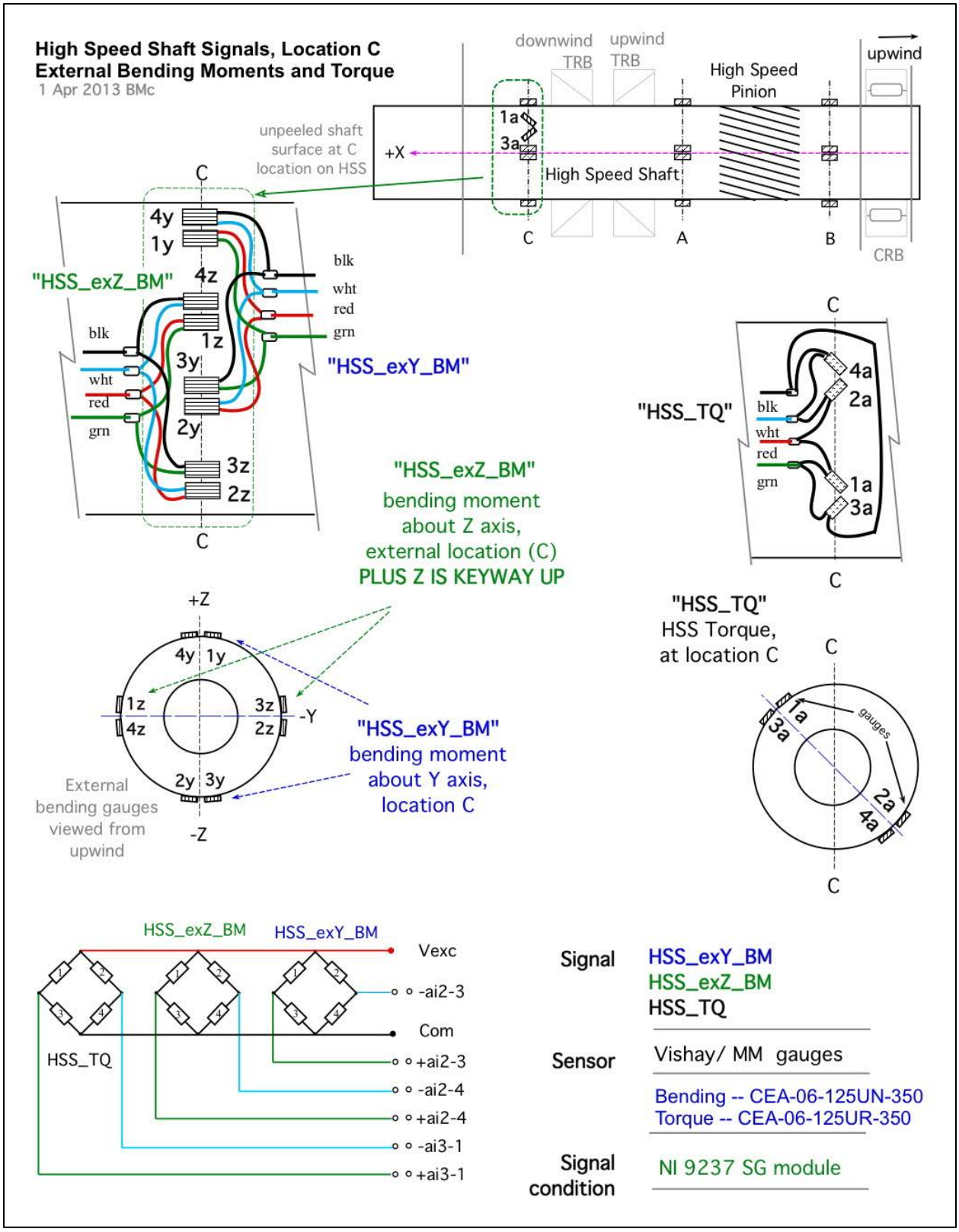

Figure B-34. High-speed shaft bending and torque at location C

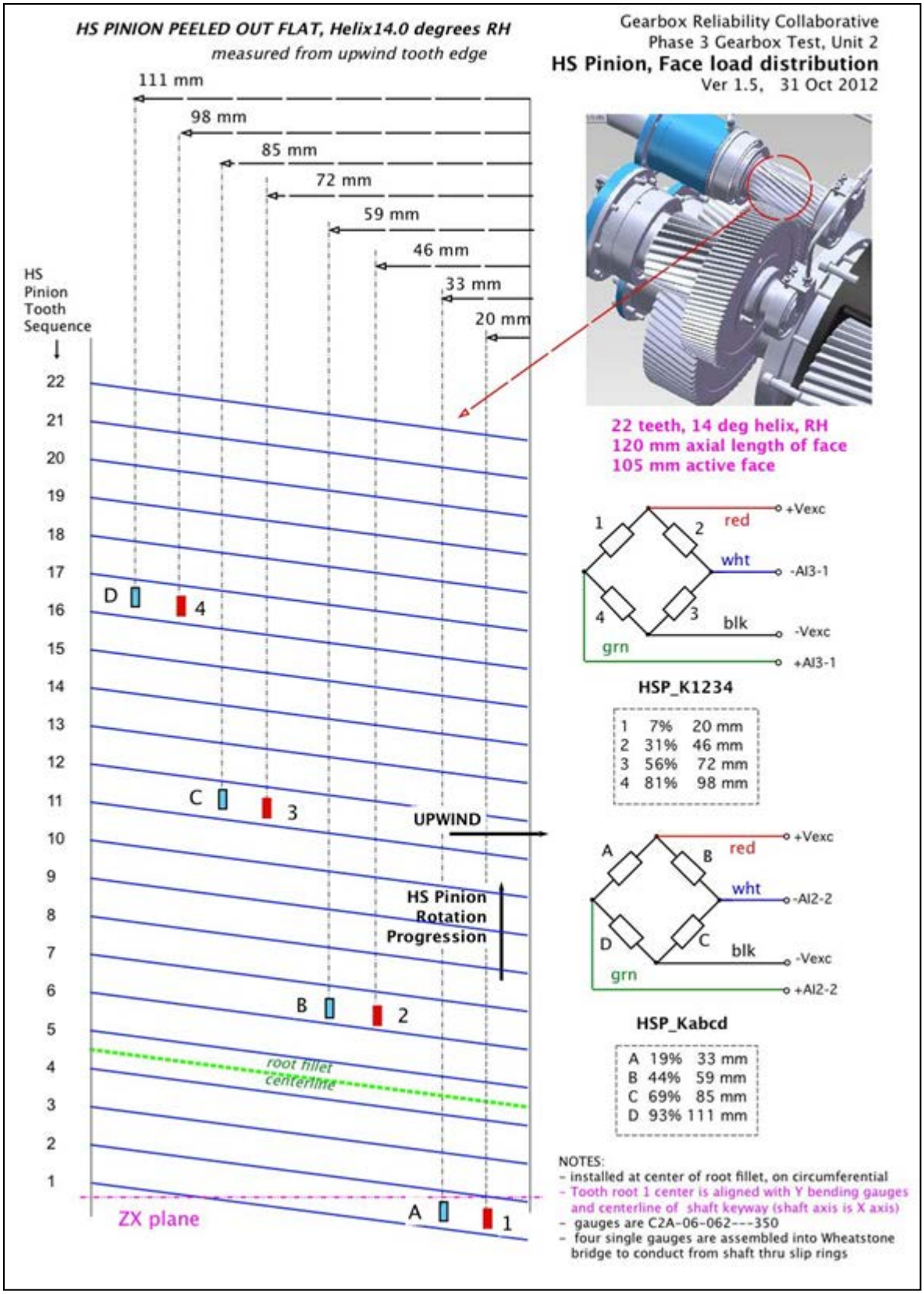

Figure B-35. High-speed shaft pinion face width load distribution

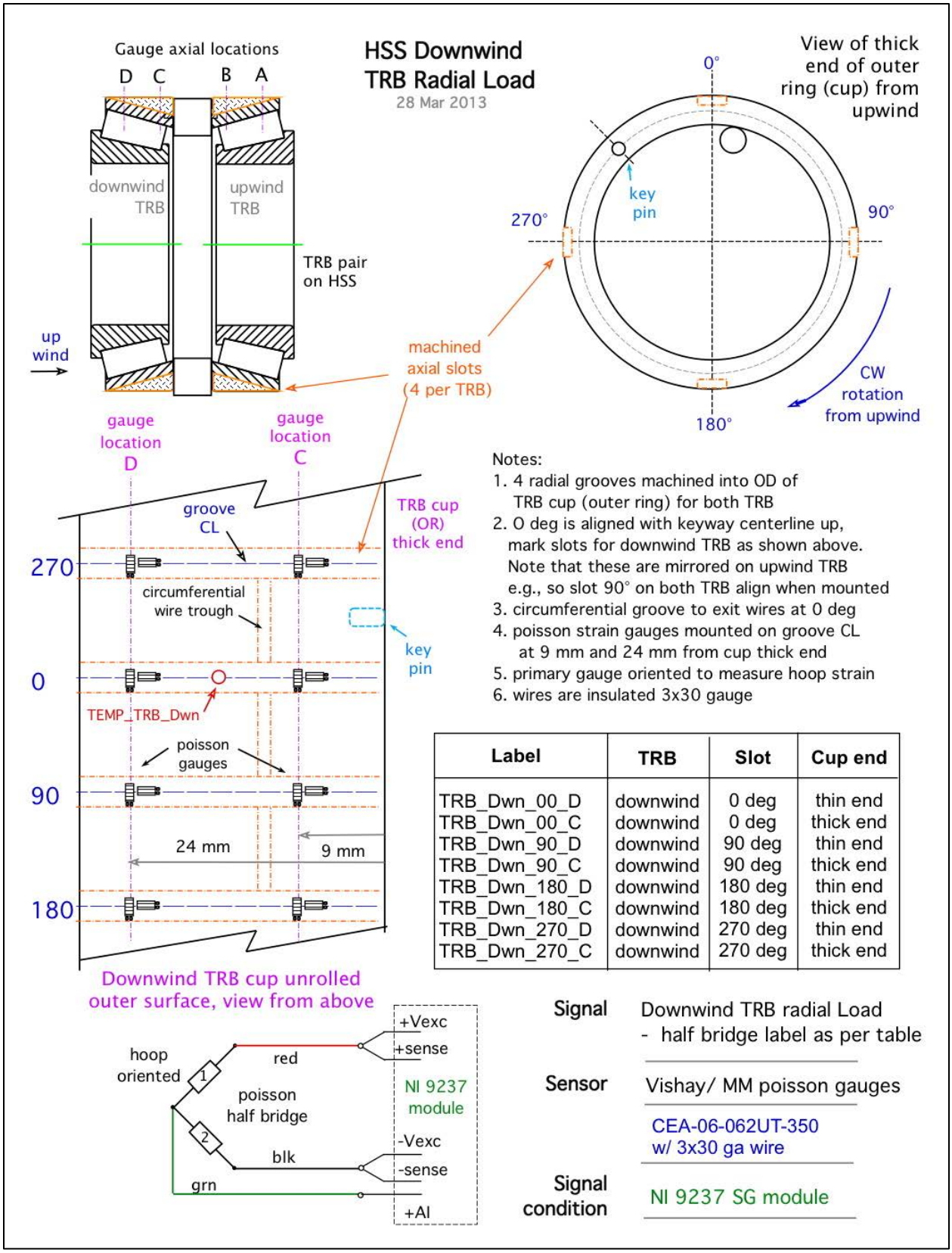

Label	TRB	Slot	Cup end
TRB_Dwn_00_D	downwind	0 deg	thin end
TRB_Dwn_00_C	downwind	0 deg	thick end
TRB_Dwn_90_D	downwind	90 deg	thin end
TRB_Dwn_90_C	downwind	90 deg	thick end
TRB_Dwn_180_D	downwind	180 deg	thin end
TRB_Dwn_180_C	downwind	180 deg	thick end
TRB_Dwn_270_D	downwind	270 deg	thin end
TRB_Dwn_270_C	downwind	270 deg	thick end

Figure B-36. High-speed shaft downwind tapered roller bearing strain

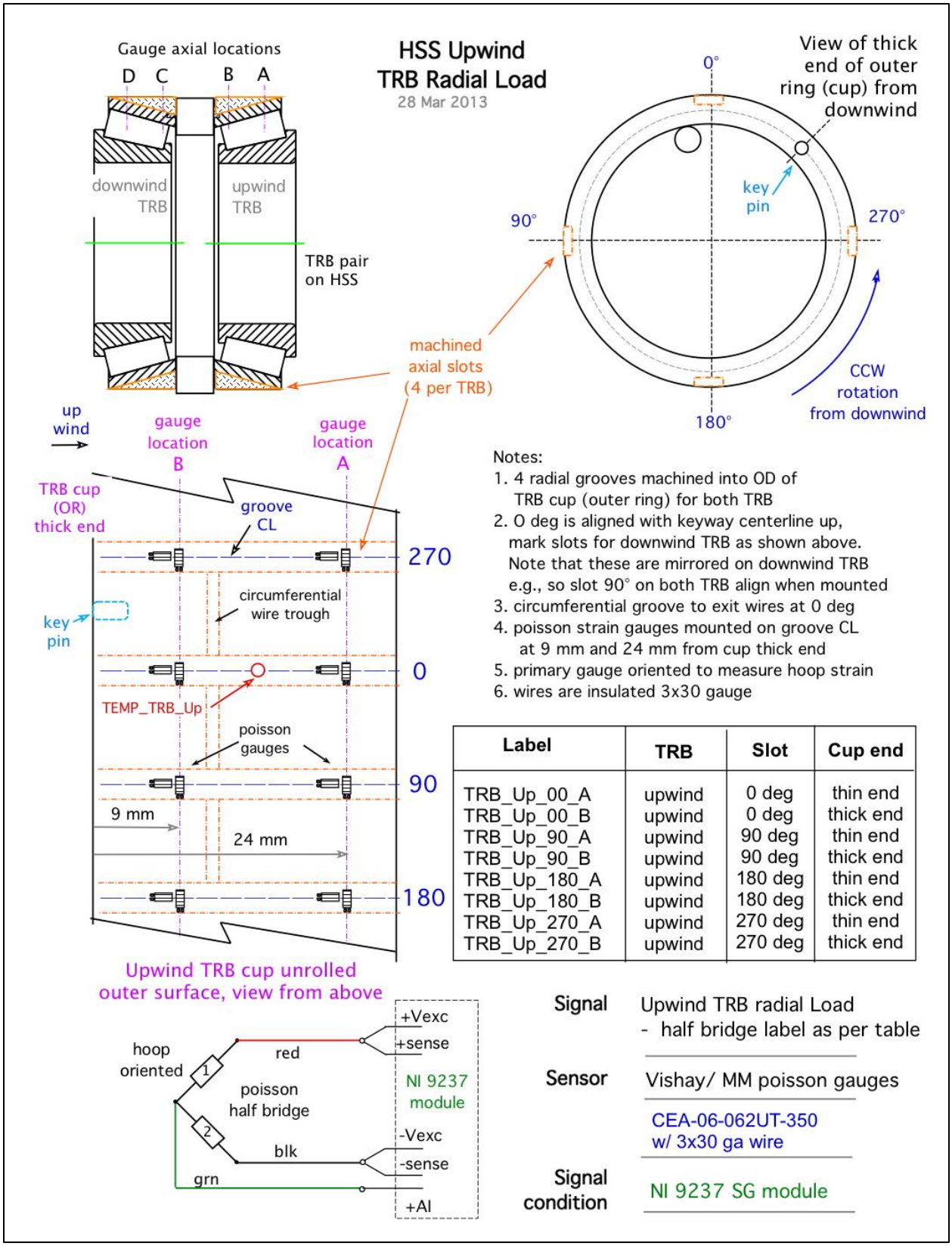

Label	TRB	Slot	Cup end
TRB_Up_00_A	upwind	0 deg	thin end
TRB_Up_00_B	upwind	0 deg	thick end
TRB_Up_90_A	upwind	90 deg	thin end
TRB_Up_90_B	upwind	90 deg	thick end
TRB_Up_180_A	upwind	180 deg	thin end
TRB_Up_180_B	upwind	180 deg	thick end
TRB_Up_270_A	upwind	270 deg	thin end
TRB_Up_270_B	upwind	270 deg	thick end

Figure B-37. High-speed shaft upwind tapered roller bearing strain

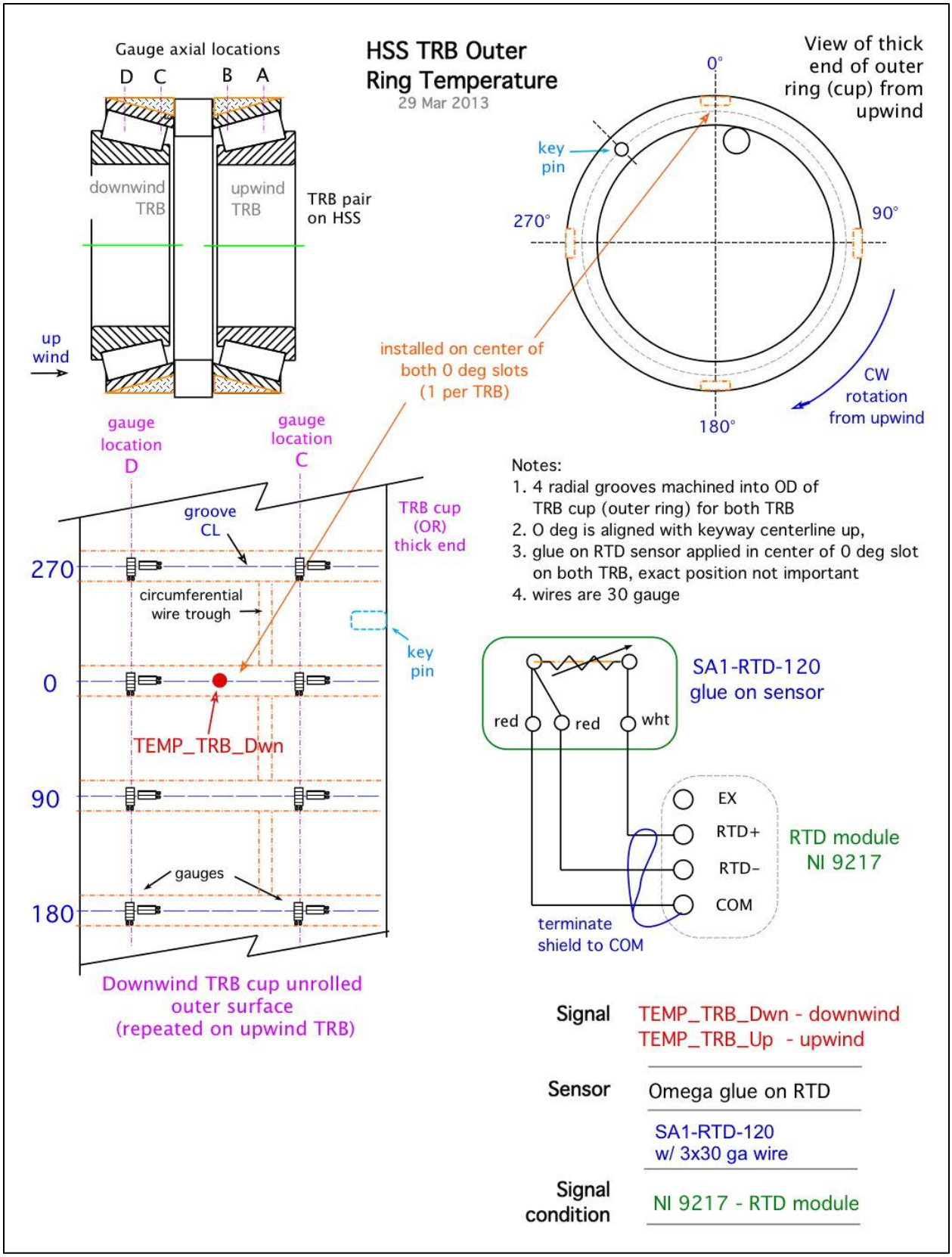

Figure B-38. High speed shaft tapered roller bearing outer ring temperature

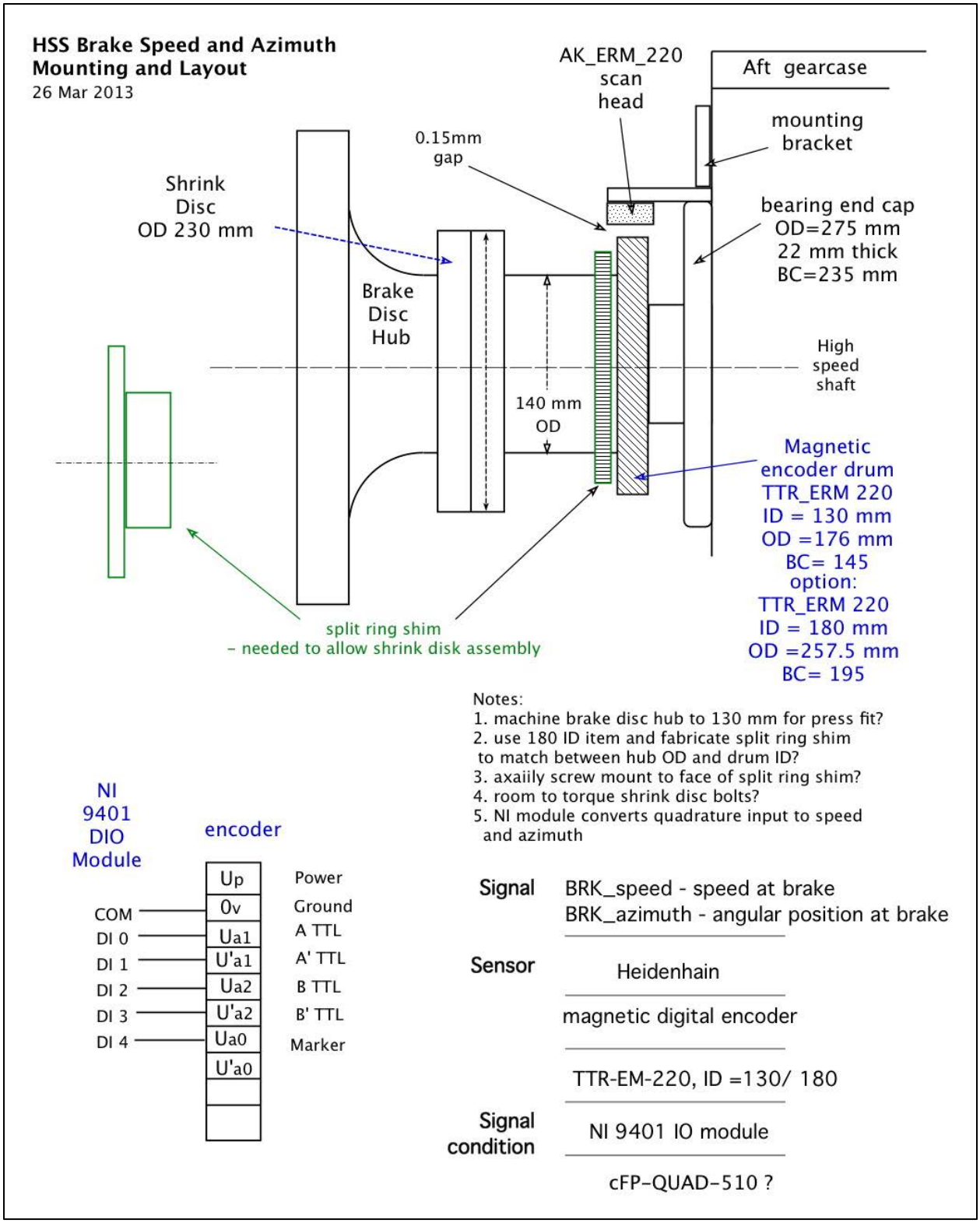

Figure B-39. Brake disk speed and azimuth

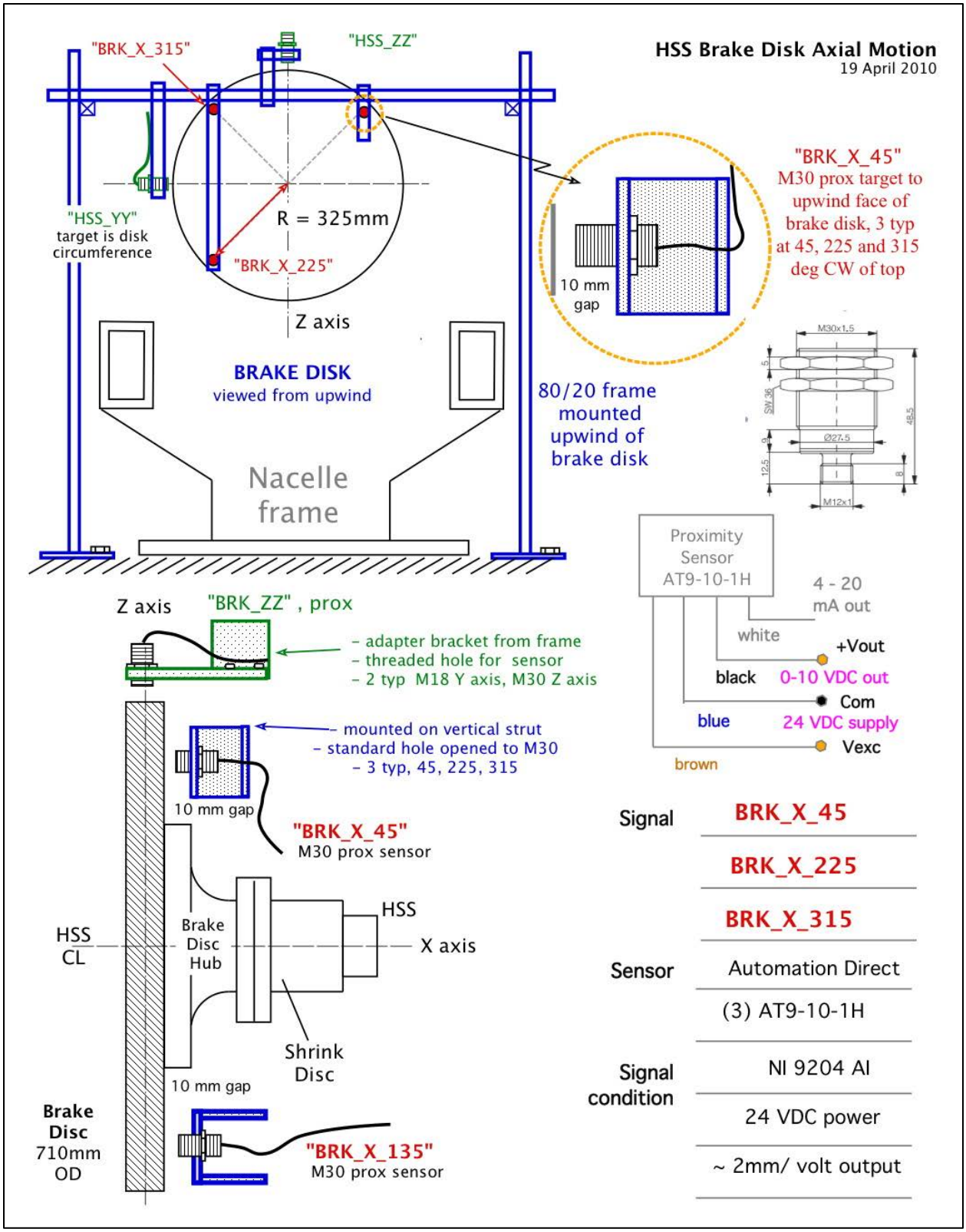

Figure B-40. Brake disk axial motion

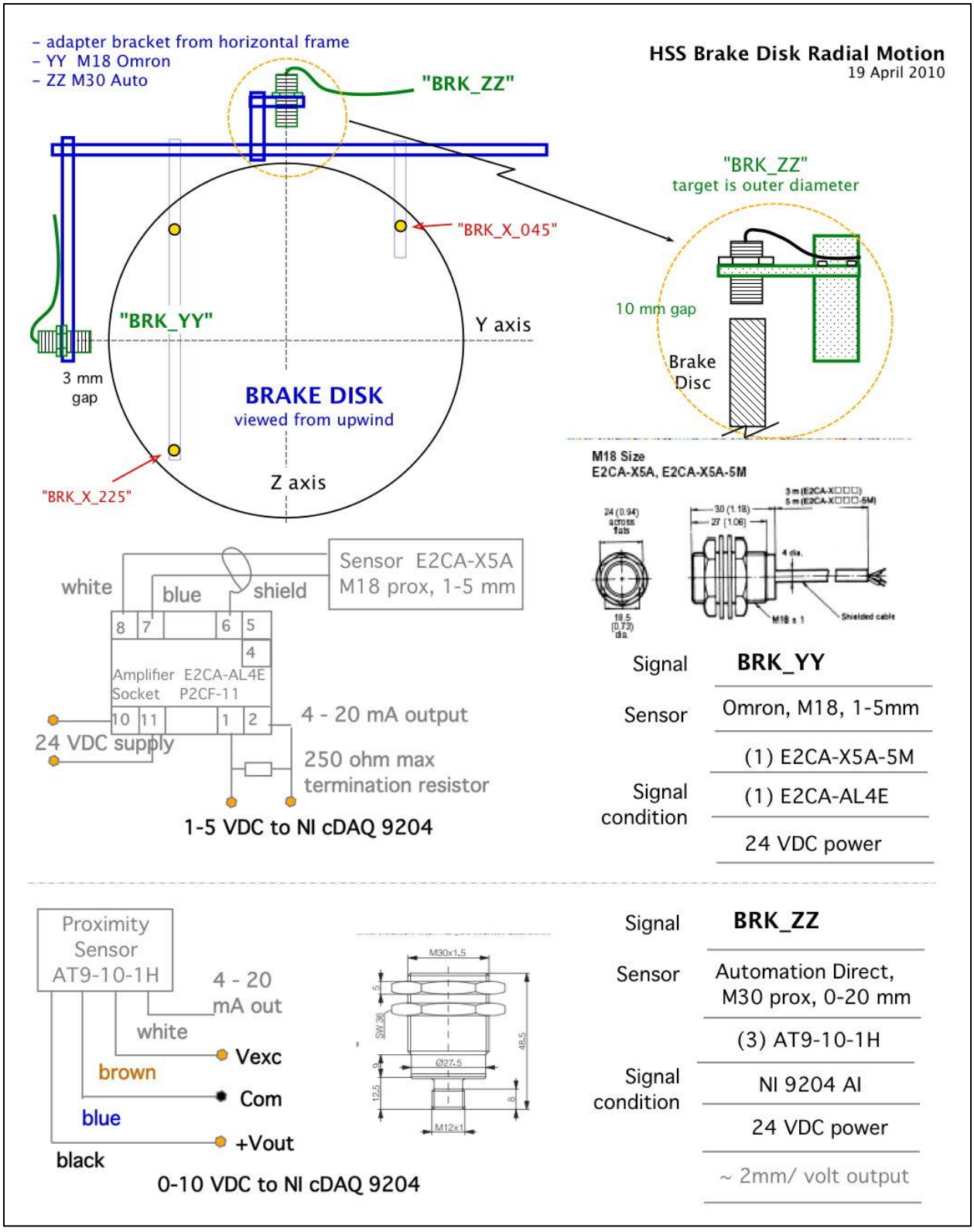

Figure B-41. Brake disk radial motion

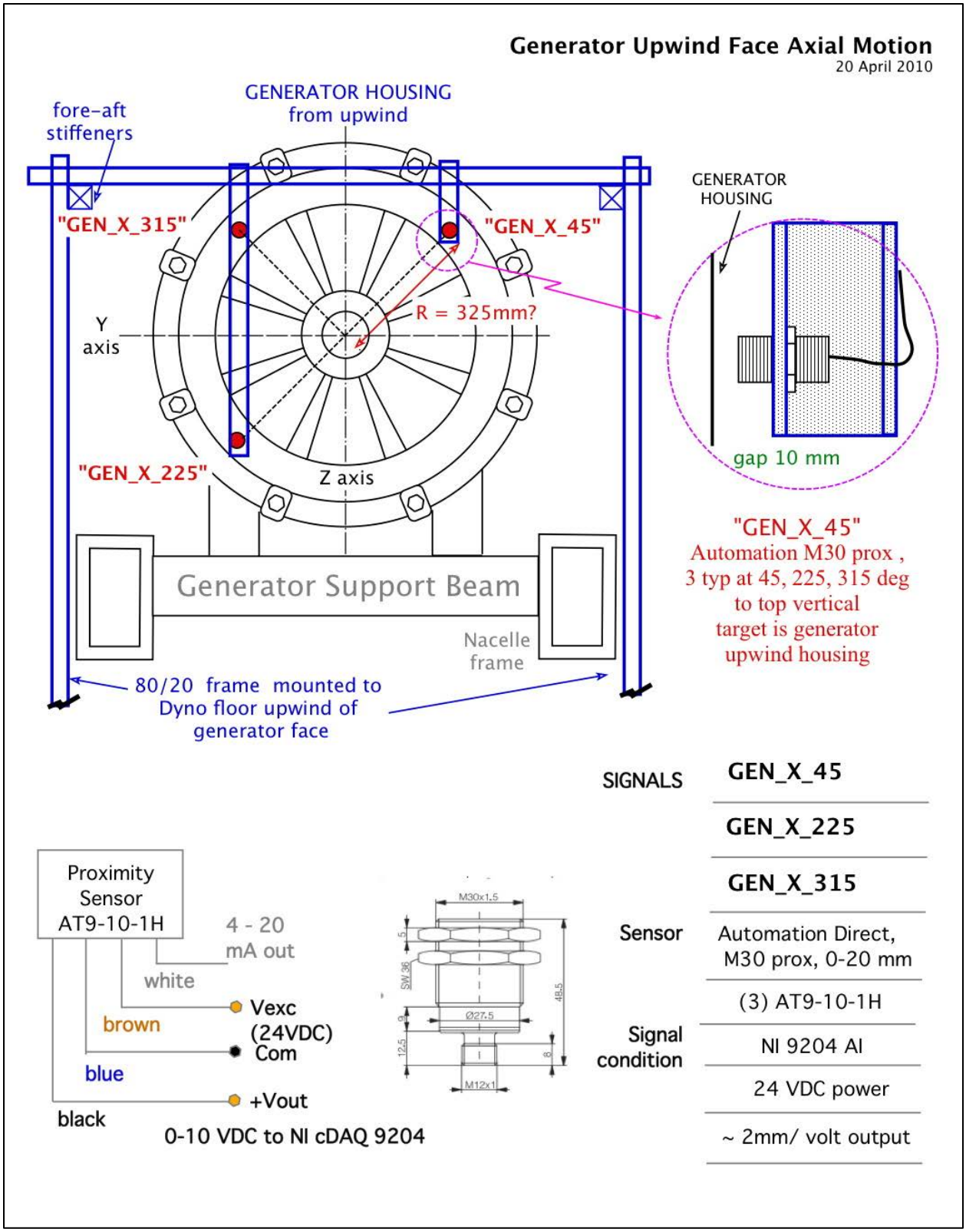

Figure B-42. Axial motion of generator upwind face

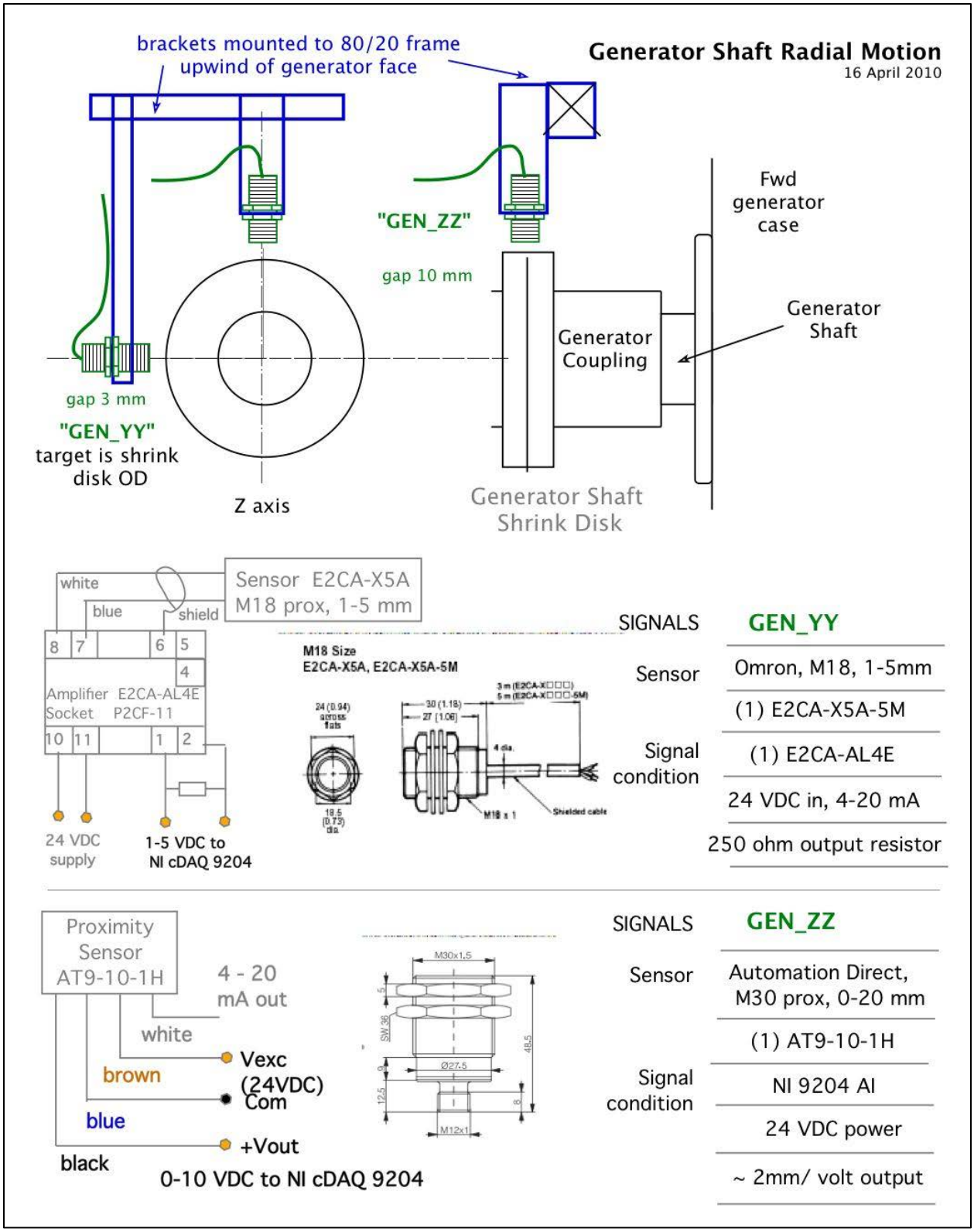

Figure B-43. Radial motion of generator input shaft

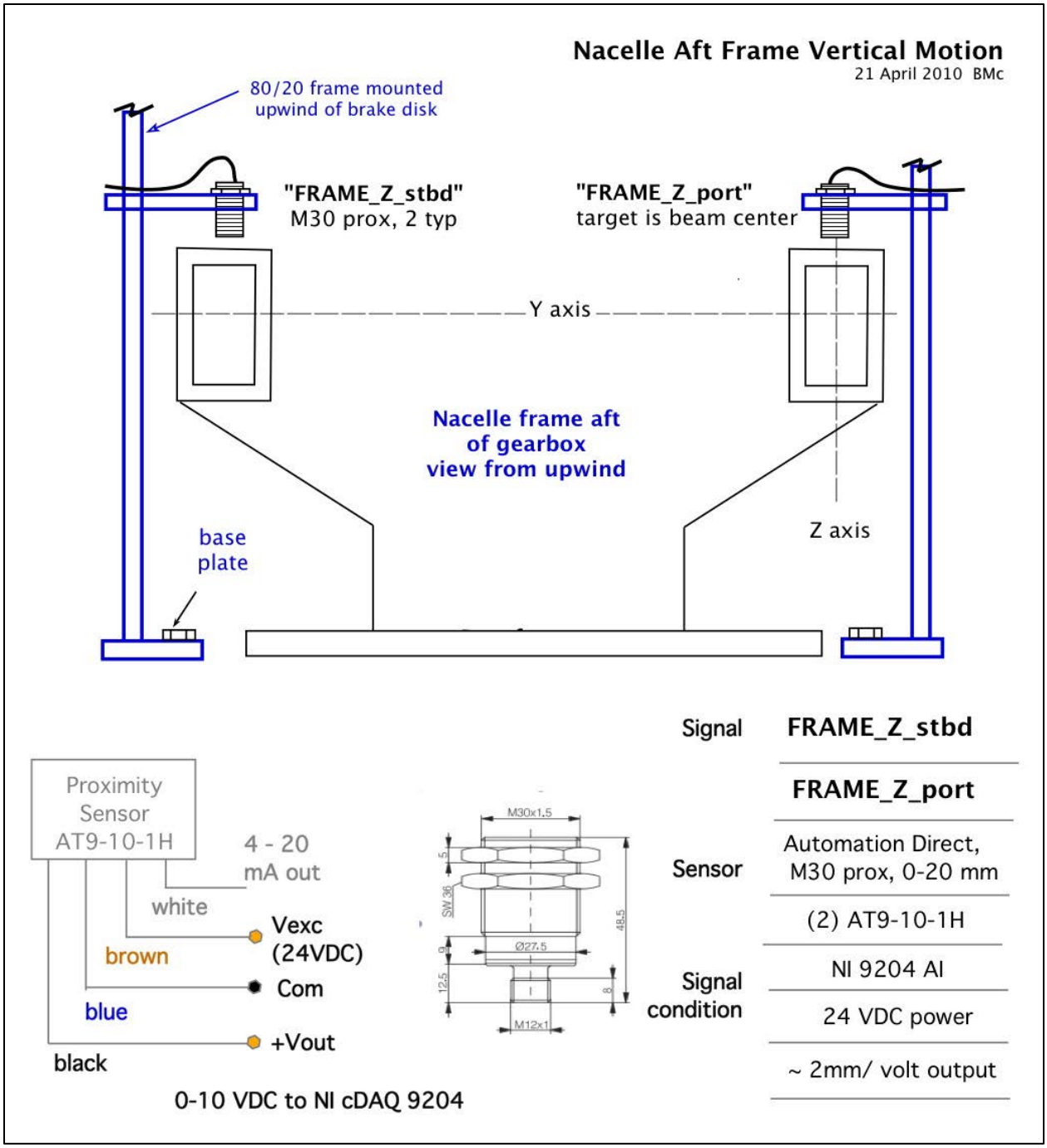

Figure B-44. Deflection of nacelle frame aft of gearbox

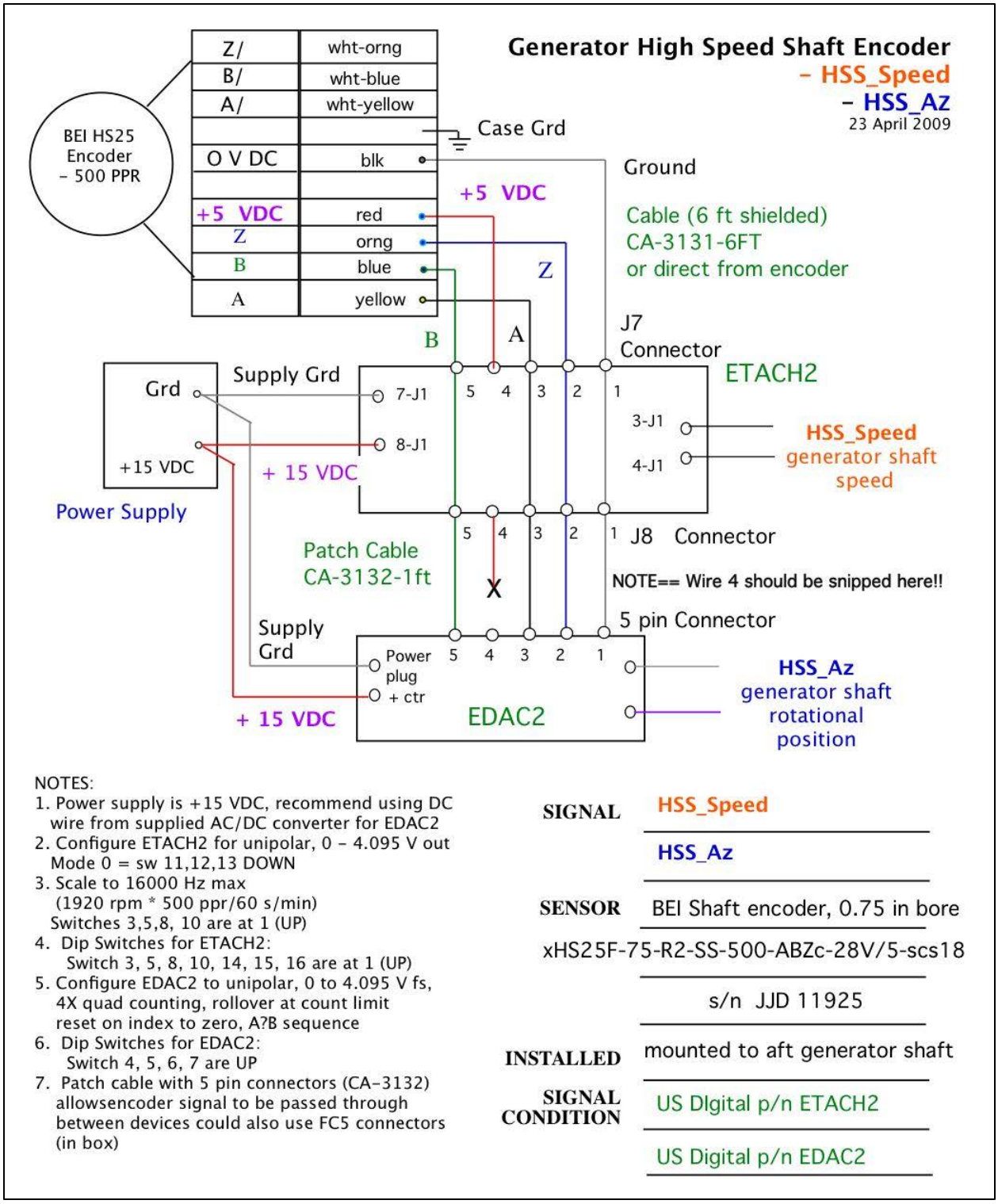

NOTES:
1. Power supply is +15 VDC, recommend using DC wire from supplied AC/DC converter for EDAC2
2. Configure ETACH2 for unipolar, 0 - 4.095 V out
   Mode 0 = sw 11,12,13 DOWN
3. Scale to 16000 Hz max
   (1920 rpm * 500 ppr/60 s/min)
   Switches 3,5,8, 10 are at 1 (UP)
4. Dip Switches for ETACH2:
   Switch 3, 5, 8, 10, 14, 15, 16 are at 1 (UP)
5. Configure EDAC2 to unipolar, 0 to 4.095 V fs, 4X quad counting, rollover at count limit reset on index to zero, A?B sequence
6. Dip Switches for EDAC2:
   Switch 4, 5, 6, 7 are UP
7. Patch cable with 5 pin connectors (CA-3132) allowsencoder signal to be passed through between devices could also use FC5 connectors (in box)

SIGNAL	HSS_Speed
	HSS_Az
SENSOR	BEI Shaft encoder, 0.75 in bore
	xHS25F-75-R2-SS-500-ABZc-28V/5-scs18
	s/n JJD 11925
INSTALLED	mounted to aft generator shaft
SIGNAL CONDITION	US DIgital p/n ETACH2
	US Digital p/n EDAC2

Figure B-45. Generator shaft speed and azimuth

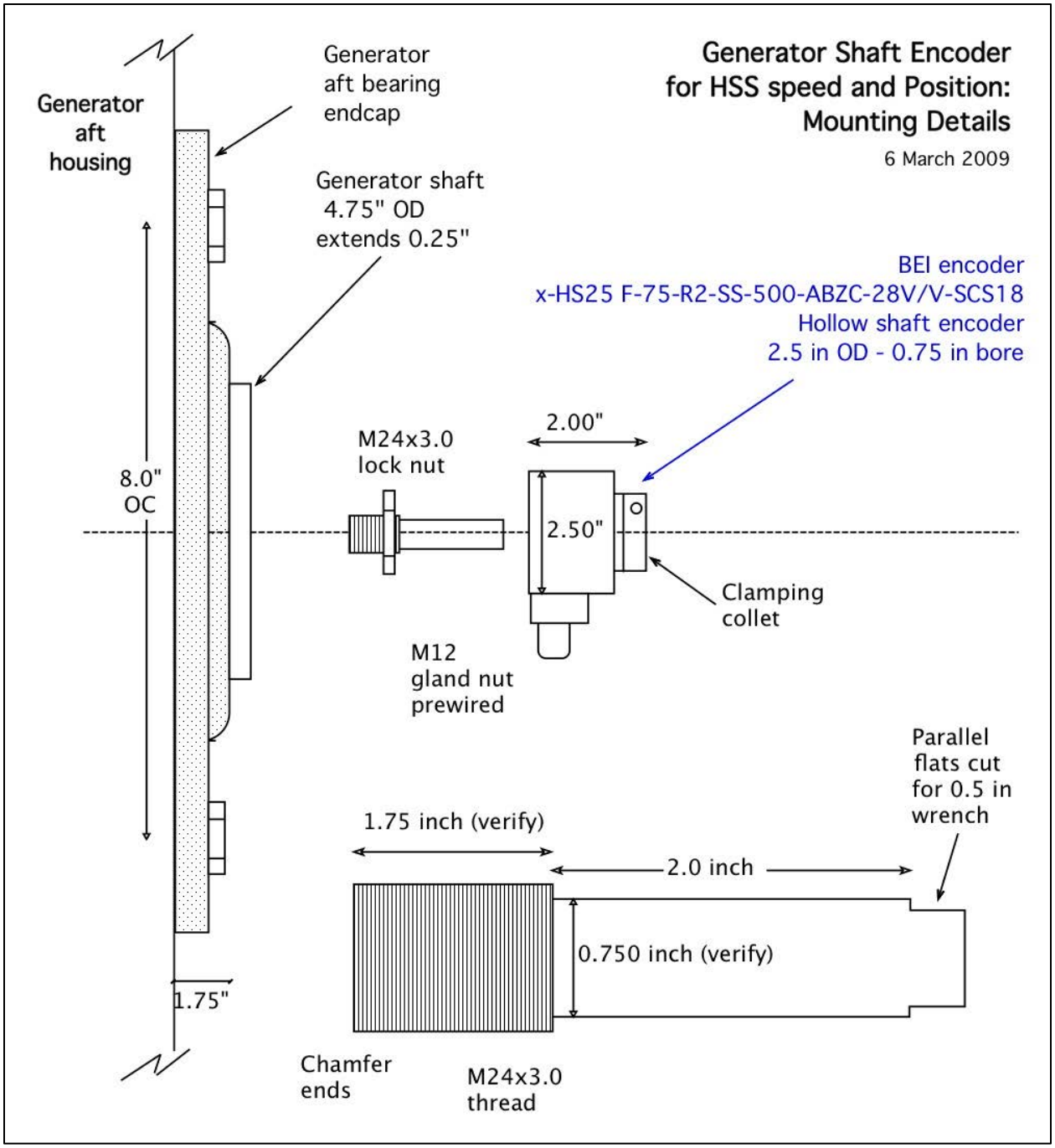

Figure B-46. Generator shaft encoder

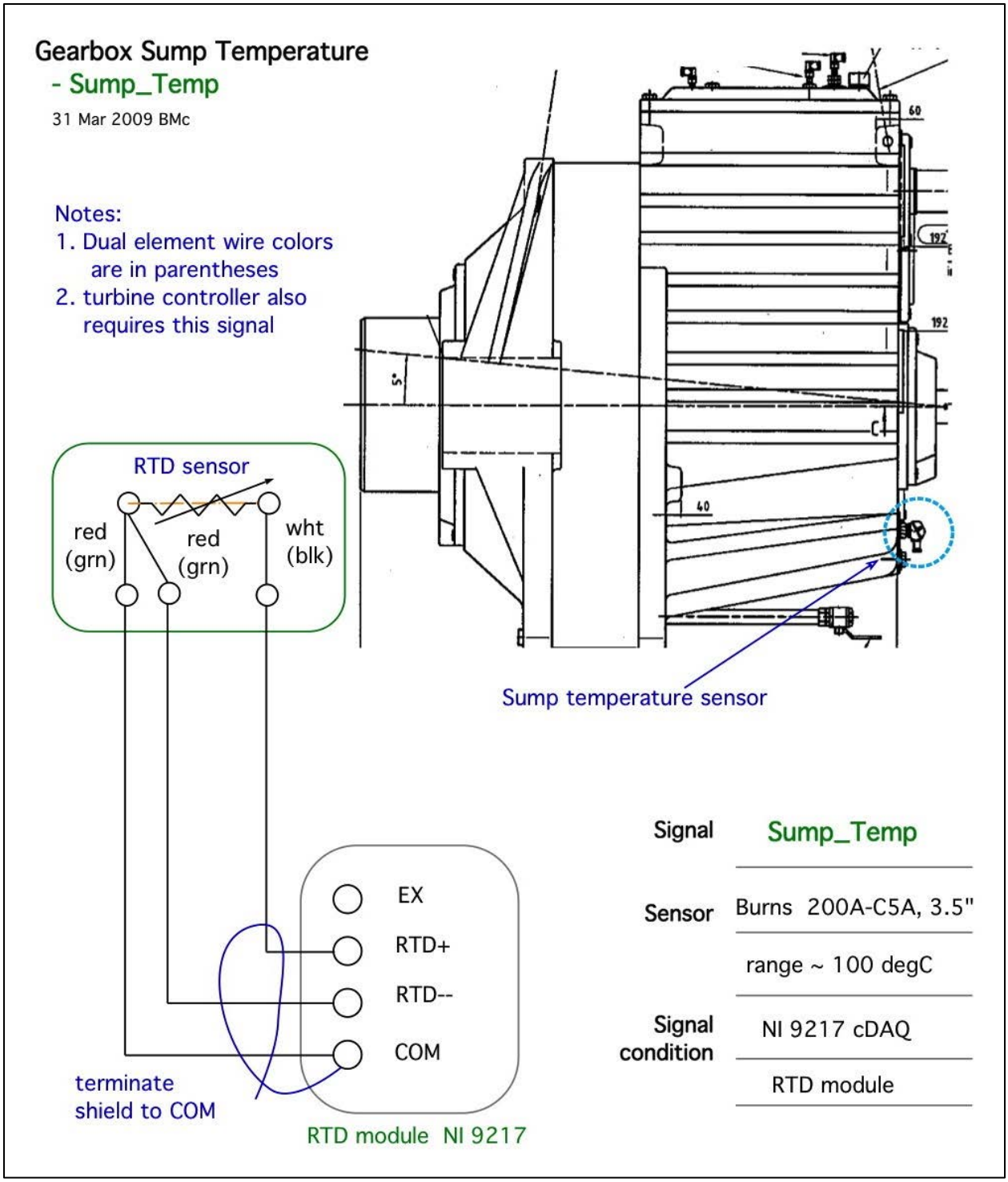

Figure B-47. Gearbox oil sump temperature

Appendix C. Sample Design Load Cases

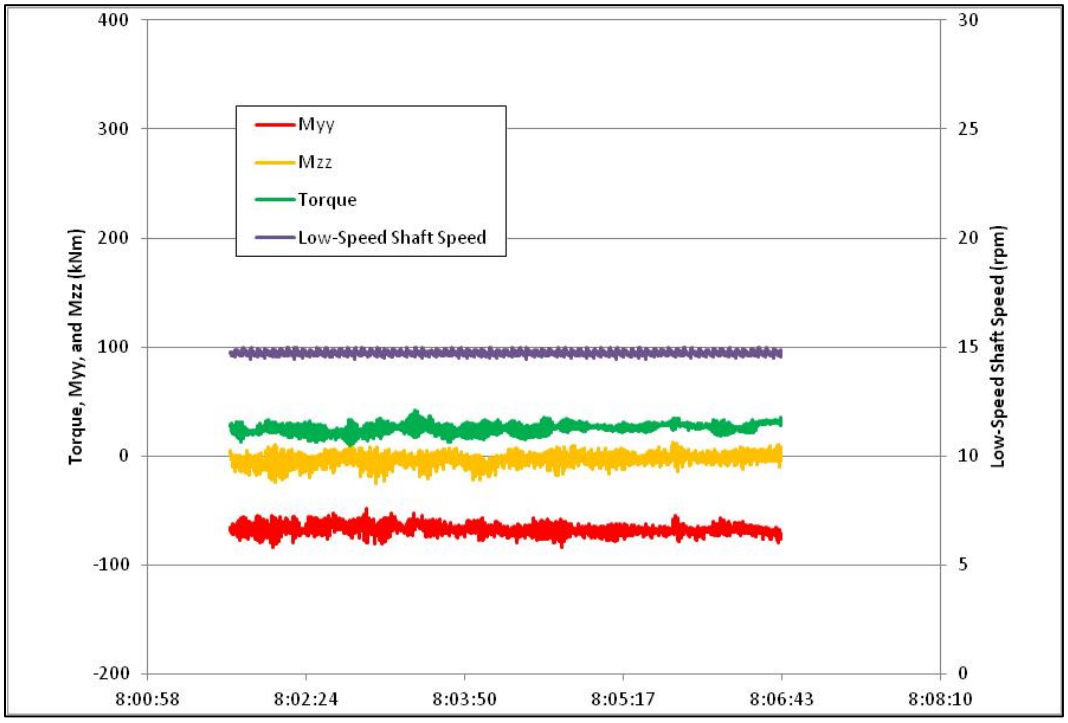

Figure C-1. Normal operation, V_{wind} = 5 m/s
(file: NO-05 2009-10-07-08-01-43.xlsx)

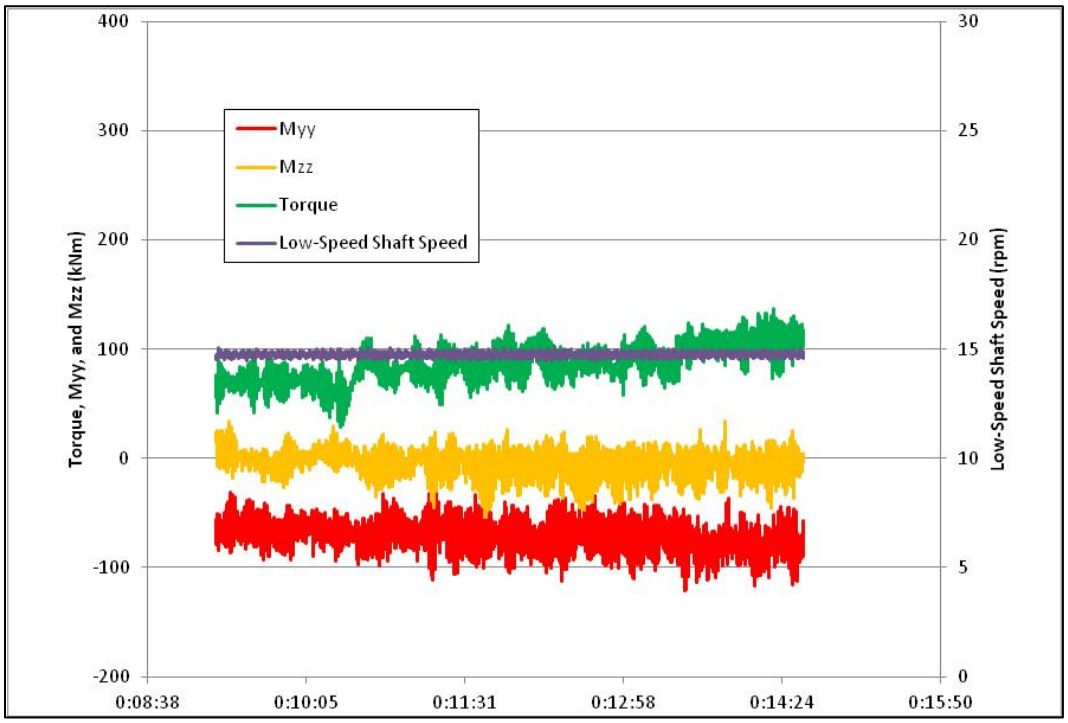

Figure C-2. Normal operation, V_{wind} = 10 m/s
(file: NO-10 2009-09-26-00-09-16.xlsx)

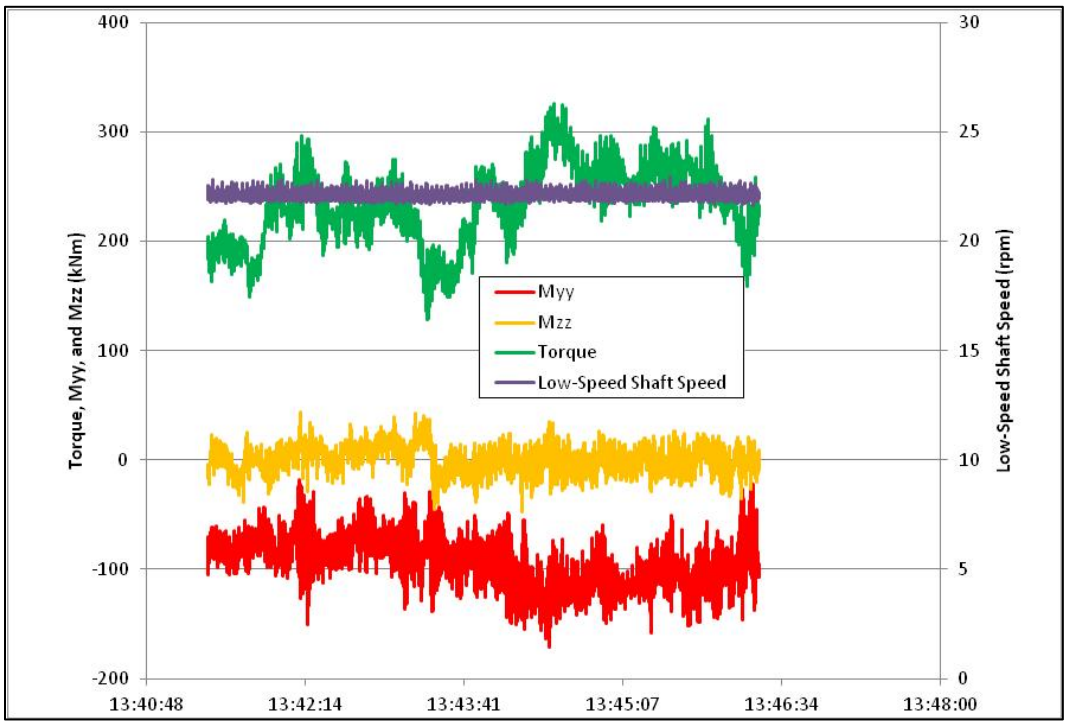

Figure C-3. Normal operation, V_{wind} = 15 m/s
(file: NO-15 2009-09-22-13-41-21.xlsx)

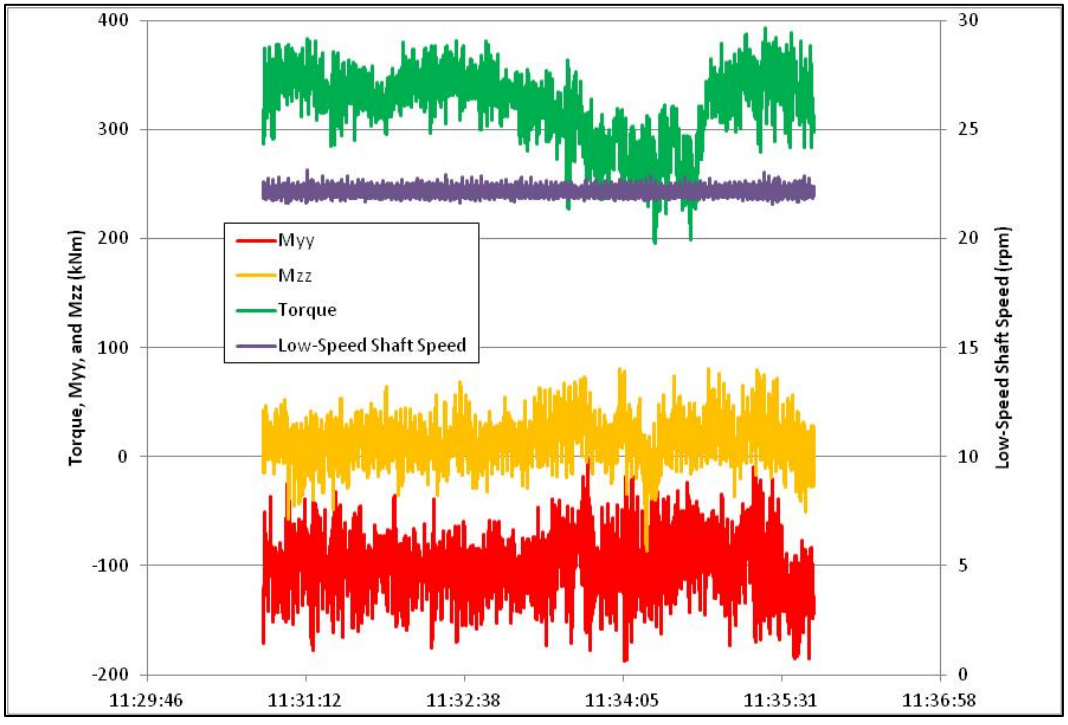

Figure C-4. Normal operation, V_{wind} = 20 m/s
(file: NO-20 2009-09-21-11-30-49.xlsx)

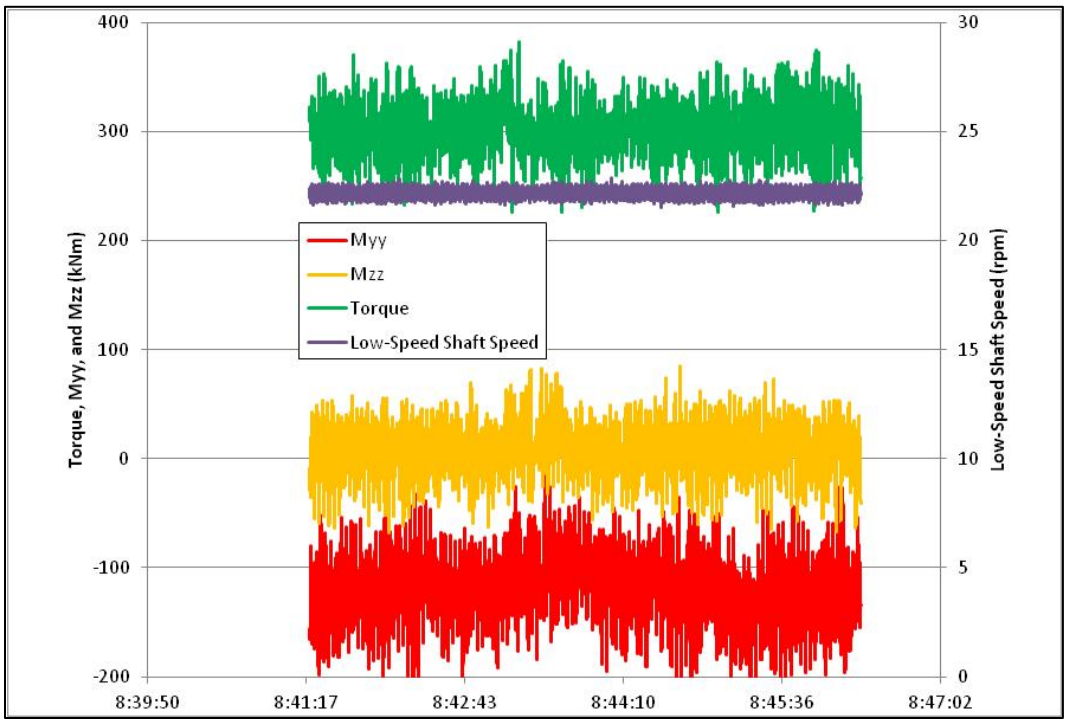

Figure C-5. Normal operation, V_{wind} = 25 m/s
(file: NO-25 2009-10-01-08-41-19.xlsx)

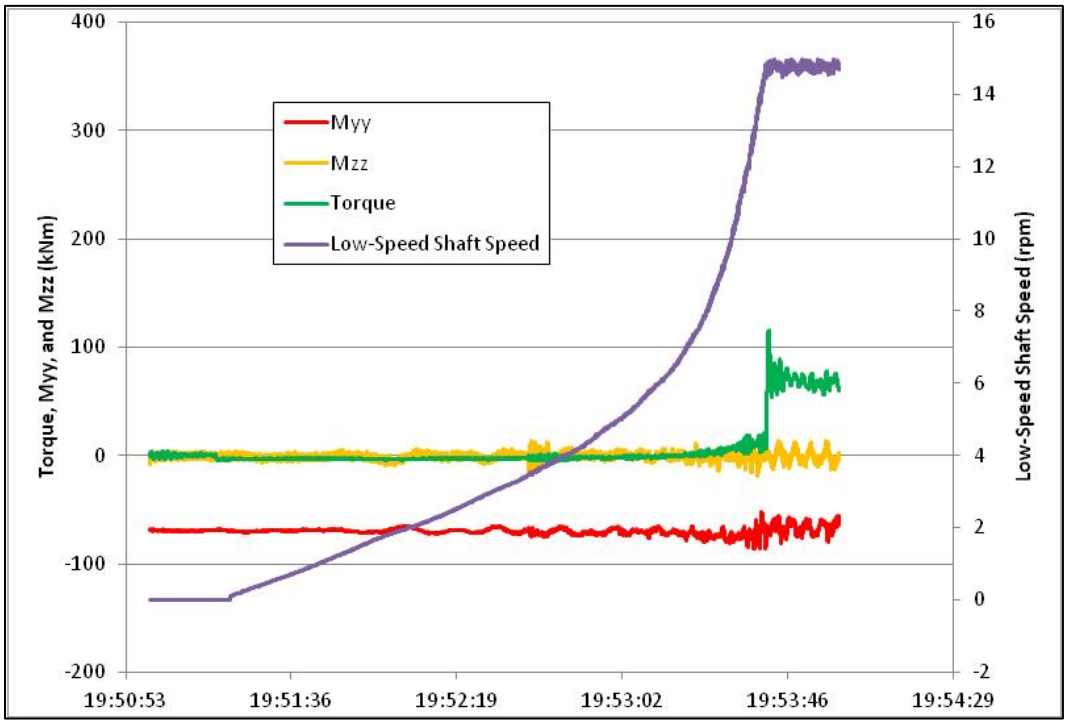

Figure C-6. Startup to low-speed generator
(file: Startup2 2009-09-21-19-50-59.xlsx)

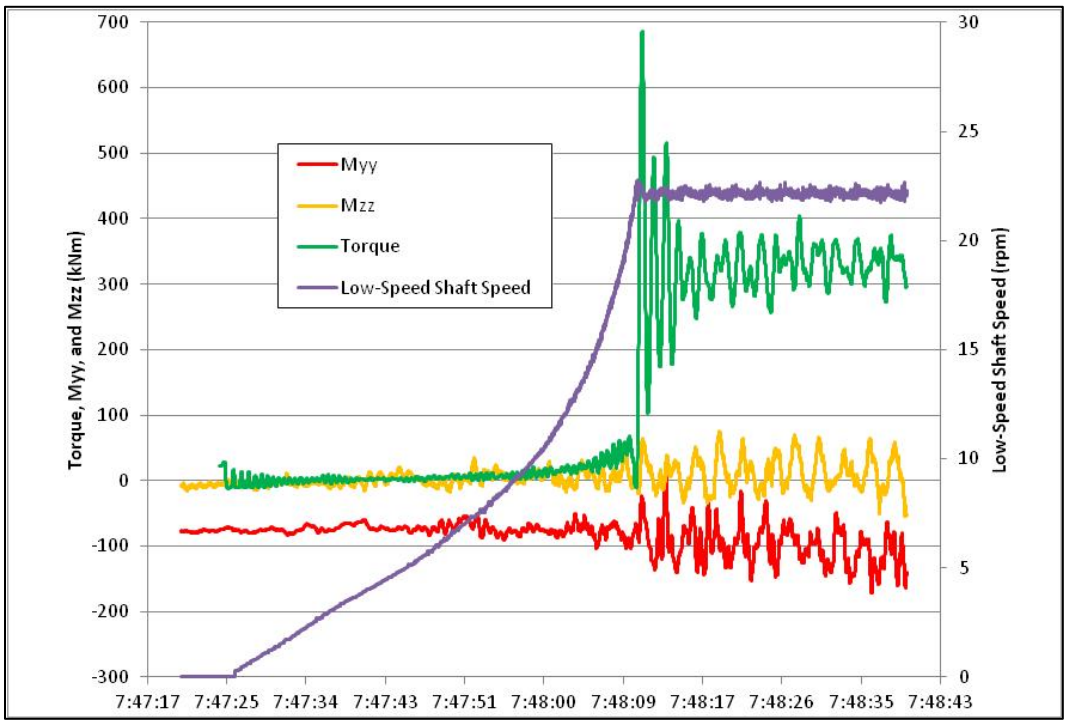

Figure C-7. Startup to high-speed generator
(file: Startup1 2009-09-21-07-40-45.xlsx)

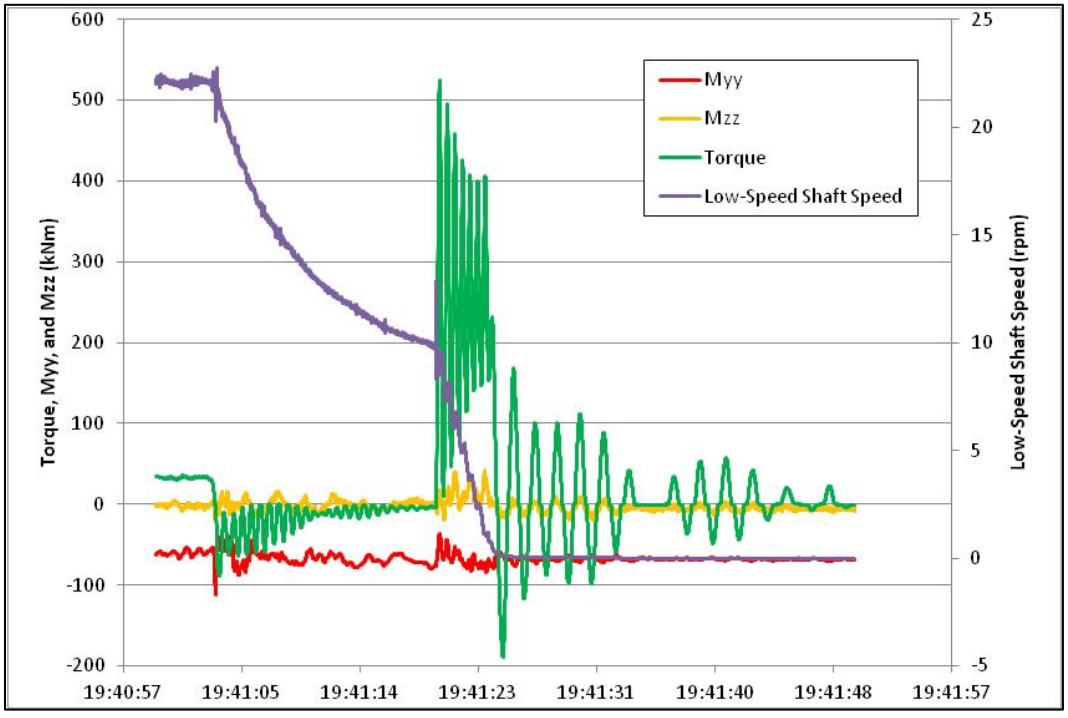

Figure C-8. Shutdown from high-speed generator
(file: Shutdown1 2009-09-21-19-40-59.xlsx)

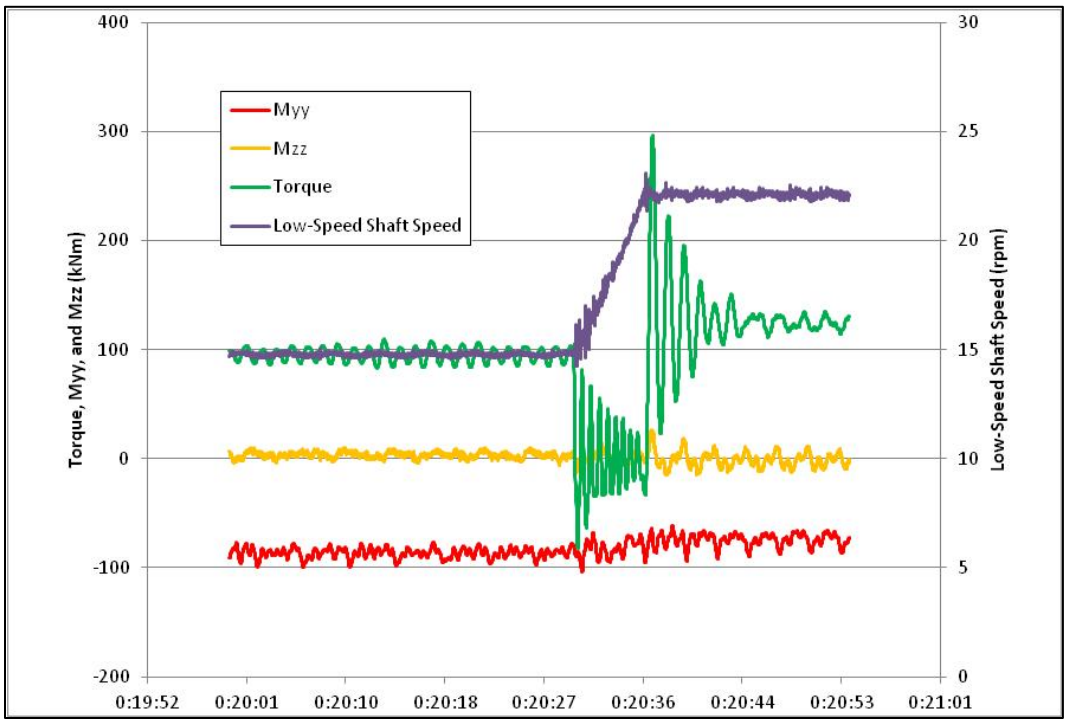

Figure C-9. Upshift
(file: Upshift 2009-09-26-00-19-17.xlsx)

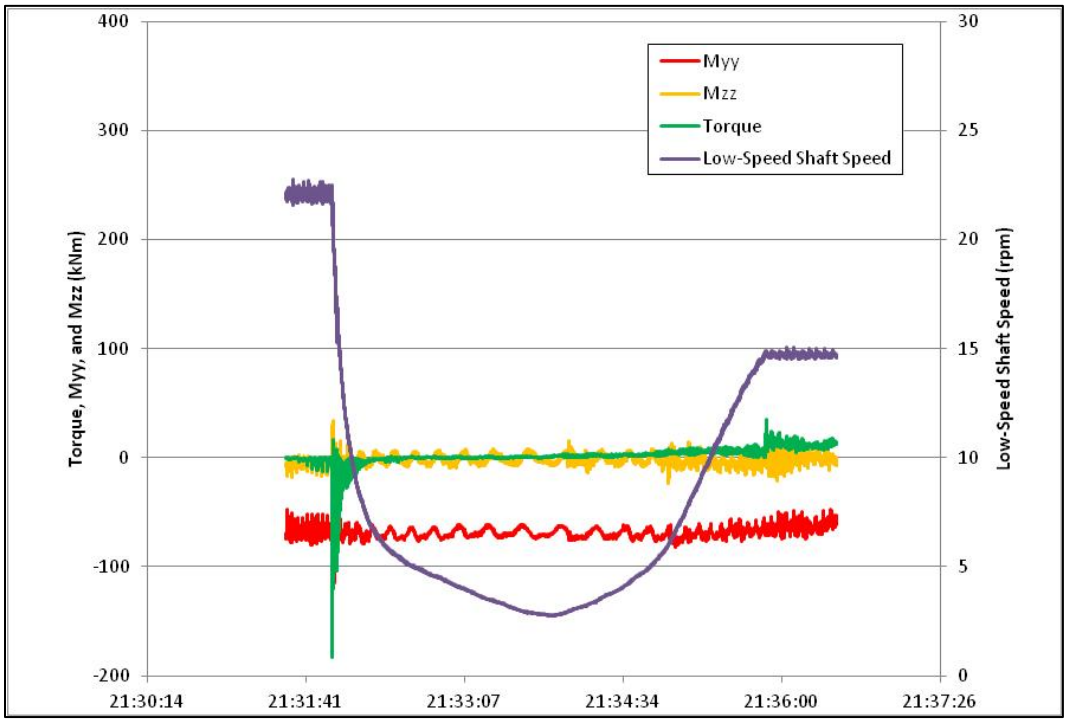

Figure C-10. Downshift
(file: Downshift 2009-09-22-21-31-30.xlsx)